POLITECNICO DI TORINO

Master's Degree in Aerospace Engineering

Politecnico di Torino

Master's Degree Thesis

Modeling of Propulsion Systems for Supersonic Civil Aircraft

Supervisors

Prof. Nicole VIOLA

Candidate

Francesco PICCIONELLO

October 2023

Abstract

This thesis elaborates an approach to evaluate the performance of low-bypass turbofan engines without afterburner for a low-boom supersonic aircraft operating at Mach 1.5 and the development of a propulsive database for the estimation of the CO_2 Metric Value of the novel SST.

The implemented method replicates a part of the engine design process: the novel engine is designed from the list of system requirements, the reference point is calculated and a graphical optimization is implemented in order to minimise the specific thrust fuel consumption as a figure of merit. Then, the Off-design is performed for different conditions by using two different methods: the Serial Nested Loop and the Matrix Iteration. The propulsive database is generated by using the two methods, and the related results are compared at the end of the discussion.

The engine model is developed by using the block diagram method: the engine is considered a system of components and subsystems, each of which is associated with its own model.

The Chemical Equilibrium is employed to develop a gas model that takes into account the variation of the Pressure Heat Coefficient with the temperature and the fuel-to-air ratio (Variable Specific Heat). However, a simplified gas model (Modified Specific Heat) is considered as well.

The nitro-oxides, carbon monoxide, unburned hydrocarbon emission indexes, and engine weight are also estimated using simplified formulas.

All models are implemented in MATLAB environment and the related results are validated by using GSP 11 commercial software.

The study contributes to the MORE&LESS project, providing methods to rapidly design novel supersonic propulsion concepts with improved environmental performance.

Acknowledgements

Ringrazio i miei genitori per avermi sostenuto e supportato in questi anni di studio, ringrazio mia sorella Karola e mio fratello Dario, i miei zii, i miei cugini, i miei nonni Santina, Carmela, Gaspare e Francesco, e i miei amici.

Uno speciale ringraziamento all'Ente regionale per il Diritto allo Studio Univeristario del Piemonte (EDISU) per avermi accolto nelle sue strutture e incentivato nello studio.

Ringrazio la professoressa Nicole Viola, la dottoressa Grazia Piccirillo, il dottor Oscar Gori per tutto l'aiuto nello sviluppo e nella stesura del lavoro di tesi.

"... We choose to go to the moon in this decade and do the other things, ***not because they are easy, but because they are hard****, because that goal will serve to organize and measure the best of our energies and skills, because that challenge is one that we are willing to accept, one we are unwilling to postpone and one which we intend to win and the others, too..."*

John F. Kennedy, Rice University, 12 September 1962

Table of Contents

List of Tables

List of Figures

Chapter 1

Introduction

1.1 The Supersonic Flight

1.1.1 A Brief History of Supersonic Civil Transport

A **supersonic transport (SST)** or a **supersonic airliner** is a civilian supersonic aircraft designed to transport passengers at speeds greater than the speed of sound. The first supersonic aircraft was the Bell X-1, an experimental aircraft developed in the United States during the 1940s, on October 14, 1947, US Air Force pilot Chuck Yeager became the first human to break the sound barrier in this aircraft. From 1947 onwards, different military aircraft were built for military purposes, notable examples include the Soviet Mikoyan-Gurevich MiG-19 and MiG-21, the British English Electric Lightning, the French Dassault Mirage III and the American North American F-100 Super Sabre and McDonnell F-101 Voodoo.

Figure 1.1: The Bell X-1: the first supersonic aircraft

Figure 1.2: Chuck Yager: The first human to break the sound barrier

In the next decades, different civilian supersonic programs were developed, the first was The U.S. Supersonic Transport (SST) program, which started in the 1960s and terminated in 1971 due to concerns regarding economic viability, sonic

boom and environmental issues, but simultaneously the soviet promoted their own one, which leads to the TU-144. But the most successful program was the British/French Concorde, which operated from 1976 to the 24th of October 2003, following the accident at Parigi-Le Bourget airport, in which 100 passengers and 9 persons of cabin crew died. In summary, the only SSTs to see regular service have been Concorde and the Tupolev Tu-144.

Figure 1.3: The Concorde

Figure 1.4: The soviet Tu-144

1.1.2 The Future SST Programs

Today different programs are developing for the future of the SST. The most famous reported program is **the Boom Overture**, the largest aircraft currently under development and thus most similar to Concorde. Several others are smaller and therefore potentially appealing to private and executive operators as well as airlines for premium use.

One of the largest other proposed aircraft is from US-based **Exosonic**. It is in the early stages of developing a 70-seat jet operating at Mach 1.7. It has a contract with the US Air Force to investigate the use of the aircraft for VIP or Presidential transport.

Spike Aerospace and its **S-512** proposal have been around since 2014. This is a 12 to 18-passenger aircraft, operating at Mach 1.6 with low sonic boom features. One of its design differences is a windowless cabin (with screen projections instead), designed to make the engineering simpler. Boston-based Spike originally aimed to have an aircraft flying in 2018, but the deadline continues to move.

Virgin Galactic has proposals for a supersonic jet, carrying up to 19 passengers at Mach 3. This was unveiled in 2020 and has support from Boeing and Rolls-Royce. This is separate from the company's orbital program.

The **Aerion Corporation** has proposed its own business jet: the **Aerion AS-2**. This aircraft is able to transport 12-passenger aircraft aimed for Mach 1.6 with a supersonic natural laminar flow wing for a minimum projected range of 8,800 km.

Figure 1.5: Boom: The overture

Figure 1.6: The Aerion AS-2

1.1.3 The main challenges of Supersonic Transport

The supersonic flight presents various challenges that companies and airliners have to face. These concern both engineering and economic aspects. The main engineering issues involve:

- **Sonic Boom**: the FAA[1] prohibits supersonic flight over the United States of America because of its great impact on humans, animals and buildings, this induces the airlines to operate over the ocean, as was for the Concorde operations.
- **Wave Drag**: a particular phenomenon that happens during the flight operating close to Mach 1 is the wave drag formation which increases the total aerodynamic drag of the aircraft.
- **The propulsion system**: the engine must be designed in other to have the best performance possible during the flight, however, due to the wide operating speeds, that is a very challenging point. During the development of concepts and programs, generally, some requests for proposals of "innovative" engines were advanced, using variable thermodynamic cycles (Ref. [1]).
- **Jet noise**: Extreme jet velocities used during take-off caused Concorde and Tu-144s to produce significant take-off noise. Communities near the airport were affected by high engine noise levels, which prompted some regulators to disfavor the practice.
- **Skin friction**: At supersonic speeds, an aircraft adiabatically compresses the air in front of it. The increased temperature of the air heats the aircraft which

[1]Federal Aviation Administration - https://www.faa.gov/

must be designed in order to face the high range of temperatures using not only aluminum but "special" materials such as stainless steel and titanium, increases the costs of manufacture.

- **Environmental Impact**: The International Council on Clean Transportation (ICCT) estimates an SST would burn 5 to 7 times as much fuel per passenger. The ICCT shows that a New York to London supersonic flight would consume more than twice as much fuel per passenger than in subsonic business class, six times as much as for economy class and three times as much as subsonic business for Los Angeles to Sydney. Designers can either meet existing environmental standards with advanced technology or lobby policymakers to establish new standards for SSTs.

1.2 The Propulsion System

A propulsion system for aeronautics consists of a source of mechanical power and a propulsor [2]. Generally, this system performs the **thrust generation** as a main function, but it also provides electrical or pneumatic power for the aircraft systems (if required).

Most aircraft engines are either piston engines or gas turbines, although a few have been rocket-powered and in recent years many small UAVs have used electric motors. The main focus of this thesis work is on the **gas turbine** engine, which the typical architecture consists of a compressor, a chamber and a turbine. The original air-breathing gas turbine jet engine was the turbojet. It was a concept brought to life by two engineers, Frank Whittle in England UK and Hans von Ohain in Germany.

Modern turbofans are a development of the turbojet: they are basically turbojets that include a new section called the fan stage. Rather than using all their exhaust gases to provide direct thrust like a turbojet, the new **turbofan engines** extract some of the power from the exhaust gases inside the engine and use it to power the fan stage. The fan stage accelerates a large volume of air through a duct, bypassing the engine core (the actual gas turbine component of the engine) and expelling it at the rear as a jet, creating thrust. A proportion of the air that comes through the fan stage enters the engine core rather than being ducted to the rear and is thus compressed and heated; some of the energy is extracted to power the compressors and fans, while the remainder is exhausted at the rear. This high-speed, hot-gas exhaust blends with the low-speed, cool-air exhaust from the

[2]the term "propulsor refers to a device that converts the power generated by the engine into propulsive force

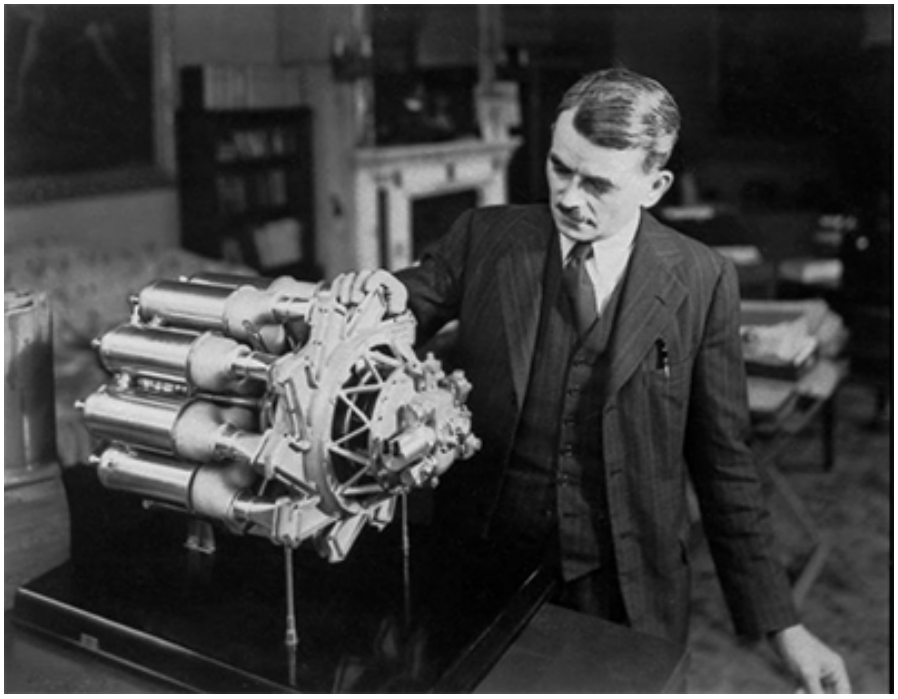

Figure 1.7: Sir Frank Whittle, the inventor of the turbojet

fan stage and both contribute to the overall thrust of the engine. Depending on what proportion of cool air is bypassed around the engine core, a turbofan can be called low-bypass, high-bypass, or very-high-bypass engines. Low bypass engines were the first turbofan engines produced and provided the majority of their thrust from the hot core exhaust gases, while the fan stage only supplements this. These engines are still commonly seen on military fighter aircraft because they have a smaller frontal area which creates less ram drag at supersonic speeds leaving more of the thrust produced by the engine to propel the aircraft. Their comparatively high noise levels and subsonic fuel consumption are deemed acceptable in such an application, whereas although the first generation of turbofan airliners used low-bypass engines, their high noise levels and fuel consumption mean they have fallen out of favor for large aircraft. High bypass engines have a much larger fan stage and provide most of their thrust from the duct air of the fan; the engine core provides power to the fan stage and only a proportion of the overall thrust comes from the engine core exhaust stream.

Over the last several decades, there has been a move towards very high bypass engines, which use fans far larger than the engine core itself, which is typically a modern, high-efficiency two or three-spool design. This high efficiency and power is what allows such large fans to be viable and the increased thrust available (up to 75,000 lbs per engine in engines such as the Rolls-Royce Trent XWB or General

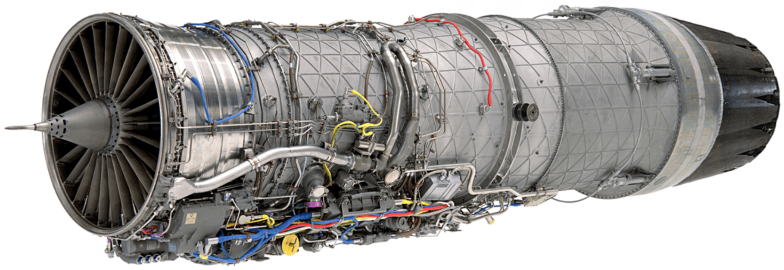

Figure 1.8: A low-bypass turbofan: The F100 PW229

Electric GENx), have allowed a move to large twin-engine aircraft, such as the Airbus A350 or Boeing 777, as well as allowing twin-engine aircraft to operate on long over water routes, previously the domain of 3-engine or 4-engine aircraft.

1.3 Purpose and Methodology

The main purpose of this thesis work is to generate a propulsive database for a low-boom supersonic business jet in order to estimate the carbon dioxide emissions during a hypothetical mission, as will be discussed in Sec. 5.2. The process is quite complex and it is developed through the illustrated steps in Fig. 1.9.

Figure 1.9: The main steps of the proposed methodology

The starting point of the entire analysis is the list of requirements related to the propulsion systems. These requirements are derived from the previous analysis of the aircraft design, concerning the configuration, the mission profile, the aerodynamics and the initial sizing of the other SST systems. The mission profile is derived by using the ASTOS software and, hence, it was possible to evaluate the required thrust of the aircraft during all phases of the reference mission.

Next, the most appropriate engine configuration is selected by evaluating the reference literacy and from the list of requirements as well. In order to design a novel engine that satisfies all requirements, a mathematical model is adopted. Therefore all parameters are selected in order to properly match the requirements.

The last two final steps concern the database generation and the CO_2 Metric Value calculations. The development of the propulsive database is performed by running several Off-design simulations, in which the three main independent

variables are varied. Finally, the thesis concludes by describing the CO_2 Metric Value calculations, which refer to the quantity of carbon dioxide produced by the novel SST. The formulation adopted is the same for the subsonic aircraft since, today, there is no ad-hoc aeronautical legislation that establishes the restrictions in terms of produced emissions for civil supersonic transports. Considering the absence of accompanying documentation, the MORE&LESS research project is conceived, with its ultimate goal being to facilitate the development of future legislation by analysing and developing different cases of study operating[3] in the supersonic regime. Moreover, this study has given significant support to the **MORE&LESS European project** and the working team, since it proposes a methodology for the characterisation of the propulsion system of the SSTs. This calculation is performed by using a formula developed for subsonic applications and reported in the **ICAO Annex 16 Volume III**. The final results will support the research team for the development of *legislation proposals* for the future civil supersonic transport in Europe.

1.4 The MORE&LESS Project

MORE&LESS (**MDO** and **RE**gulations for **L**ow boom and **E**nvironmentally **S**ustainable **S**upersonic aviation), answering the EC call "Towards global environmental regulation of supersonic aviation" (LC-MG-1-15-2020), aims to support Europe in shaping global environmental regulations for future supersonic aviation: recommendations are established on the basis of the outcomes of extensive high-fidelity modeling activities and test campaigns that merge into the multidisciplinary optimization framework to assess the holistic impact of supersonic aviation onto environment.

1.5 Aircraft Engine Design and Approaches to System Modeling

Aircraft engine design is a highly complex process that often requires several years of development. There is no "universal" roadmap for the entire process, but it is possible to summarise the main steps by the flowchart shown in Fig. 1.11.

This flowchart was developed by Professors J.D. Mattingly and G.C. Oates (Ref. [2]). As shown, they emphasize the iterative nature of the entire process. Generally, the starting point is the **Request for Proposal (RFP)**, which is a requirements document describing the desired performance of the aircraft/engine system.

[3]The case of study is a supersonic aircraft developed by the research team

Figure 1.10: MORE&LESS: MDO and REgulations for Low-boom and Environmentally Sustainable Supersonic aviation

The initial stages of the process are replicated and improved for this thesis work, as will be described in the next chapters. The main differences between the general design process and this work concern propulsive database generation for the **ASTOS** software and the estimation of carbon dioxide emission. The database is generated by running several Off-design simulations by varying flight conditions and throttle ratios. Therefore, the most important aspect in the early phases of the process is the **engine thermodynamics model**, which enables the evaluation of system performance in terms of thrust, thrust fuel consumption, air mass flow rate, emission indexes and other parameters.

The proposed modeling approaches outlined in this thesis, as described in the flowchart, encompass both On-design and Off-design analysis for the **Turbofan Mixed Flows**, which is considered the most appropriate engine for the reference case of study (see Sec. 5.3). Moreover, the **Turbofan with separated exhaust**, **single spool Turbojet** and **dual-spool Turbojet** are also modeled for future works (see Appendix C, D, E).

For the Off-design analysis, two approaches are implemented: **Matrix iteration** which uses component maps, and the **Serial Nested Loop**, developed by J.D. Mattingly (Ref. [2]). The first approach is commonly used in commercial software such as GasTurb and GSP 11. It involves solving the cycle problem using the Newton-Raphson method and scaling existing maps of some components to find efficiencies, pressures and corrected mass flow rates. The main limitation of this method is related to the assumption that the specific component of the new engine has a "similar" and "proportional" map to an existing one.

The second approach introduces some additional simplifications related to turbine operating conditions, component efficiencies and pressures, which are considered constants. This allows to solve the cycle without the need of component maps.

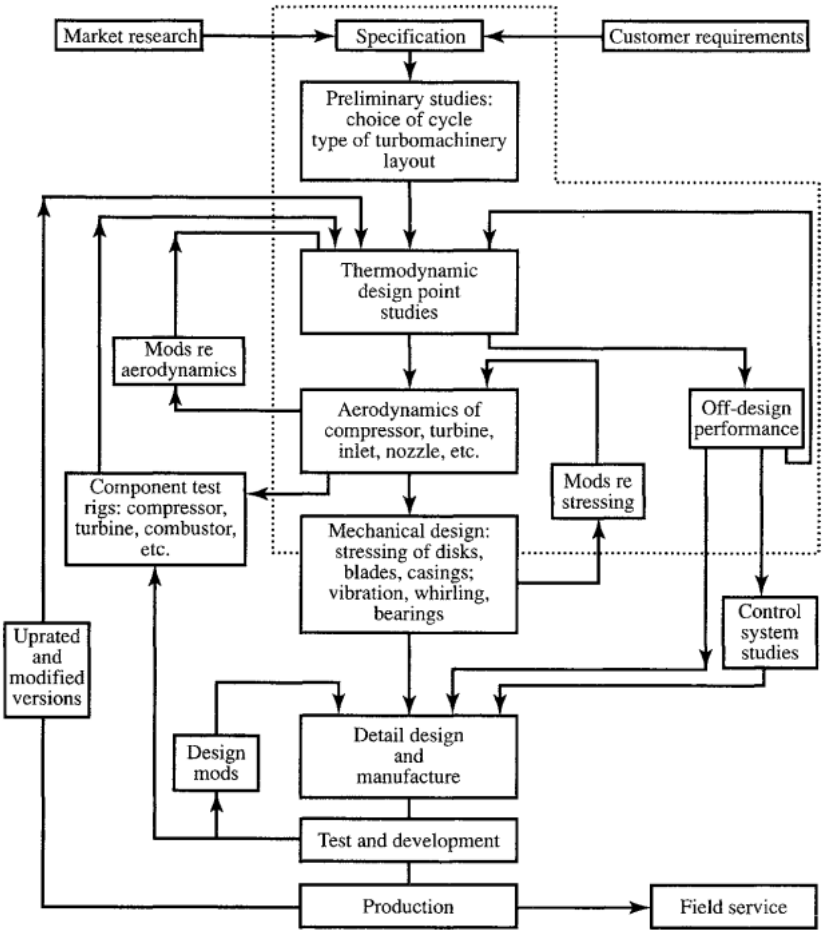

Figure 1.11: Gas turbine engine design process

These simplifications are reasonable across various engine operating conditions but may be less accurate during descending and landing phases, characterised by low-power settings. The conclusion reached through the database development is to use the second method for the initial iterations due to its simplicity in implementation and, then, improve that by using the Matrix Iteration. Therefore, in this thesis work, both methods are used and analysed, with a focus on their advantages and limitations.

Chapter 2

Gas Model

2.1 Introduction and Purpose

An accurate cycle calculation must incorporate a realistic description of gas properties. This entails considering the variation of the **constant pressure coefficient** concerning pressure and temperature. This section will discuss the methodology used in the thesis work to model the thermodynamic state of the gas. The proposed approach is replicated by different engine programs, such as **GasTurb** (Ref. [3]) and **GPS 11** (Ref. [4]), to obtain an accurate gas model.

2.2 The Half-Ideal Gas

The state of a thermodynamic system is fully described by two state variables. If the enthalpy (J/kg) is considered, it is possible to express it as a function of temperature and pressure

$$h = f(T, P) \tag{2.1}$$

Eq. 2.1 can be rewritten in differential form as

$$dh = \left(\frac{\partial h}{\partial T}\right)_{P=const} dT + \left(\frac{\partial h}{\partial P}\right)_{T=const} dP \tag{2.2}$$

According to our references Ref. [3] and Ref. [2], the working fluid in a gas turbine can be modeled as a **half-ideal perfect gas**, which implies that the gas obeys the following properties

$$C_p = f(T)$$

$$C_p \neq f(P)$$

$$\left(\frac{\partial h}{\partial P}\right)_{T=const} = 0$$

Here, C_p represents the **Constant Pressure Heat**, defined as

$$C_p = \left(\frac{\partial h}{\partial T}\right)_{P=const} \tag{2.3}$$

In general, the hypothesis of the half-ideal gas model is valid for temperatures above 200 K up to 2220 K for air and air-fuel mixtures. In the case of the **ideal Gas Model**, C_p is constant, leading to:

$$\left(\frac{\partial h}{\partial P}\right)_{T=const} = 0 \tag{2.4}$$

Returning to the more general and accurate case of half-ideal specific heat, the final expression for enthalpy can be obtained from Eq. 2.3:

$$dh = \left(\frac{\partial h}{\partial T}\right)_{P=const} dT = C_p(T)\ dT \tag{2.5}$$

$$h(T) = \int_{T_{ref}}^{T} C_p(T) dT \tag{2.6}$$

Here, T_{ref} is the *reference temperature*, which can be selected arbitrarily but must be consistent with the reference temperature of the *fuel heating value (FVH)*. The Eq. 2.6 demonstrates that the enthalpy function depends on the variation of C_p. The problem at this point is to find an appropriate expression for it.

2.3 The Variable Specific Heat Model

2.3.1 Chemical Equilibrium

The expression of the constant pressure coefficient may be derived from the Chemical Equilibrium data that is based on the Chemical Equilibrium assumption. Considering the following reaction

$$N_A A + N_B B \rightleftharpoons N_C C + N_D D \tag{2.7}$$

the chemical equilibrium, essentially, is a condition in which the forward rate of reaction of reactants A and B equals the backward rate of reaction of products C and D. It corresponds to the minimum value of the Gibbs function ($G = H - TS$) for the entire mixture as shown in Fig. 2.1.

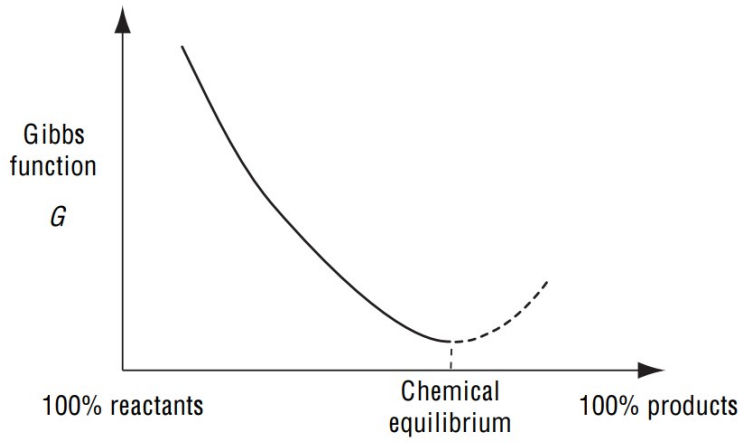

Figure 2.1: Chemical equilibrium: Gibbs function

This condition has a great limitation: the result does not consider the rate of changes in mole numbers nor the integrated values that may exist at specific moments caused by the small residence of fluid in some engine components. So, the condition of small time of residence does not allow to reach the chemical equilibrium. More complex models could be developed and implemented to reproduce these conditions as exposed in chapter 9 of Ref. [2], generally, they are used for the detailed design of the chamber. However, supposing the Chemical Equilibrium reactions are really useful and simple ways for the performance prediction of novel engines during a conceptual phase with a good agreement to experimental results.

2.3.2 Chemical Equilibrium Algorithm

The most commonly used method for the determination of specific heat and other thermodynamic quantities is the **Chemical Equilibrium Algorithm (CEA)**. From the **NASA Glenn thermochemical database** Ref. [5] and by using the *CEA run*, a free computer program, it is possible to calculate, for a mixture of air and a generic hydrocarbon ($C_{12}H_{23}$) with a given fuel-to-air ratio f, the specific heat of the fuel and air mixture as

$$C_p = \frac{C_{p,air} + f \cdot C_{p,prod}}{1 + f} \tag{2.8}$$

Both specific heat coefficients are e given by a seven-order polynomial

$$C_p = A_0 + A_1 T + A_2 T^2 + A_3 T^3 + A_4 T^4 + A_5 T^5 + A_6 T^6 + A_7 T^7 \tag{2.9}$$

So the polynomial coefficients are calculated through the polynomial fitting of CEA data and finally, they are listed in Tab. 2.1.

Table 2.1: Polynomial coefficients for pure air and products

Air Alone		**Air and Fuel**	
A_0	1.5020051×10^{-1}	A_0	7.3816638×10^{-2}
A_1	$-5.15366879 \times 10^{-5}$	A_1	1.2258630×10^{-3}
A_2	6.5519486×10^{-8}	A_2	$-1.3771901 \times 10^{-6}$
A_3	$-6.7178376 \times 10^{-12}$	A_3	$9.96886793 \times 10^{-10}$
A_4	$-1.5128259 \times 10^{-14}$	A_4	$-4.2051104 \times 10^{-13}$
A_5	$7.6215767 \times 10^{-18}$	A_5	$1.0212913 \times 10^{-16}$
A_6	$-1.4526770 \times 10^{-21}$	A_6	$-1.3335668 \times 10^{-20}$
A_7	$1.0115540 \times 10^{-25}$	A_7	$7.2678710 \times 10^{-25}$
h_{ref}	-1.7558886 Btu/lbm	h_{ref}	30.58153 Btu/lbm
ϕ_{ref}	0.0454323 Btu/lbm	ϕ_{ref}	0.6483398 Btu/lbm

Using Eq. 2.6, it is possible to calculate the enthalpy for the pure air or for the products as

$$h = h_{\text{ref}} + A_0 T + \frac{A_1}{2} T^2 + \frac{A_2}{3} T^3 + \frac{A_3}{4} T^4 + \frac{A_4}{5} T^5 + \frac{A_5}{6} T^6 + \frac{A_6}{7} T^7 + \frac{A_7}{8} T^8 \tag{2.10}$$

And for a gas mixture

$$h = \frac{h_{\text{air}} + f \cdot h_{\text{prod}}}{1 + f} \tag{2.11}$$

Other important parameters are pressure and entropy in the case of the half-ideal gas model. Considering the differential equation for Gibbs entropy Ref. [2], they are evaluated considering

$$Tds = dh - RT \cdot \frac{dP}{P} \tag{2.12}$$

where R represents the gas constant of the mixture. It is possible to rewrite Eq. 2.12 to relate the change in entropy with pressure as follows

$$ds = \frac{dh}{T} - R\frac{dP}{P} \Rightarrow$$

$$\Delta s = s_2 - s_1 = \int_1^2 \frac{dh}{T} - R\ln\left(\frac{P_2}{P_1}\right) \Rightarrow$$

$$\Delta s = s_2 - s_1 = \int_1^2 \frac{C_p(T)}{T}dT - R\ln\left(\frac{P_2}{P_1}\right)$$

Therefore, the entropy variation is given by

$$s_2 - s_1 = \phi_2 - \phi_1 - R\ln\left(\frac{P_2}{P_1}\right) \tag{2.13}$$

here, ϕ is defined as the **entropy function**, particularly

$$\phi \doteq \int_{T_{ref}}^{T} \frac{C_p(T)}{T}dT \tag{2.14}$$

and it becomes

$$\phi = \phi_{\text{ref}} + A_0\ln(T) + \frac{A_1}{2}T^2 + \frac{A_2}{3}T^3 + \frac{A_3}{4}T^4 + \frac{A_4}{5}T^5 + \frac{A_5}{6}T^6 + \frac{A_6}{7}T^7 + \frac{A_7}{8}T^8 \tag{2.15}$$

For a gas mixture:

$$\phi = \frac{\phi_{\text{air}} + f\phi_{\text{prod}}}{1+f} \tag{2.16}$$

For convenience, it is possible to define *reduced pressure* as

$$P_r \doteq \exp\left(\frac{\phi - \phi_{\text{ref}}}{R}\right) \tag{2.17}$$

The *reduced pressure* is a useful parameter for modeling engine components. For example, during the compressor's On-design analysis (see Sec. 3.3.2), the polytropic efficiency is considered constant, allowing to relate the overall pressure ratio as follows

$$\phi_{t3} - \phi_{t2} = \frac{R}{e_c}\ln\left(\frac{P_{t3}}{P_{t2}}\right)$$
$$\pi_c \doteq \frac{P_{t3}}{P_{t2}} = \exp\left(e_c\frac{\phi_{t3} - \phi_{t2}}{R}\right)$$

Which can be rewritten in terms of reduced pressure

$$\pi_c = \left(\frac{P_{rt3}}{P_{rt2}}\right)^{e_c} \tag{2.18}$$

2.3.3 The Mass Flow Rate Parameter

A very useful expression is the **Mass Flow Rate Parameter (MFP)**, which is the result of the combination of the mass flow rate per area unit with the perfect gas law, the Mach number definition, the speed of the sound and the equations for the total temperature and pressure

$$\text{MFP} \doteq \frac{\dot{m}\sqrt{T_t}}{P_t A} = M\sqrt{\frac{\gamma}{R}\left(1 + \frac{\gamma - 1}{2}M^2\right)} \tag{2.19}$$

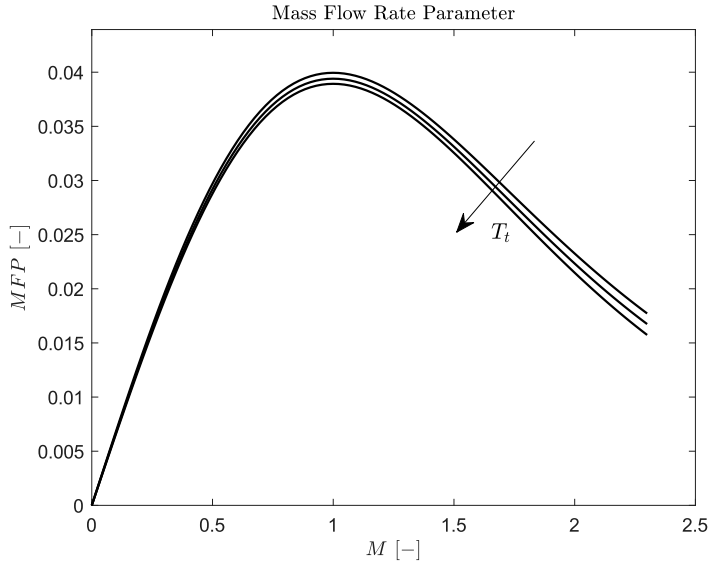

Figure 2.2: Mass Flow Rate Parameter variation, $f = 0.060$, $T_t = 500, 1000, 2000\ K$

This expression is primarily used for the mixer model in Sec. 3.7.2 and for the nozzle in Sec. 3.8. Two routines: **MASSFP** and **RGCOMPR** are developed and implemented in the MATLAB codes, allowing the calculation of the Mach number, pressure and temperature ratios (P_t/P, T_t/T), in the case of the Variable Specific Heat gas model.

2.3.4 The FAIR Routine

The previous section has presented the mathematical equations of the half-ideal gas model, all of which are implemented in a subroutine called **FAIR**, in MATLAB Environment. This subroutine is fundamental to accurately predict the engine performance of the model used in this thesis work. Particularly, it allows the evaluation of the entire gas state with one of the following inputs: temperature (T), enthalpy (h), or reduced pressure (P_r). Also, the fuel-to-air ratio (f) of the mixture must be given, otherwise, if the gas is air alone, it is possible to set it equal to zero. The outputs include:

- R: the universal gas constant of the mixture
- C_p: the constant pressure specific heat of the mixture
- γ: the ratio of the constant specific heat at constant pressure over the constant specific heat at constant volume of the mixture
- a: the speed of sound of the mixture
- T: the temperature of the mixture (if unknown)
- h: the enthalpy of the mixture (if unknown)
- ϕ: the entropy function
- s: the entropy of the mixture
- P_r: the reduced pressure of the mixture (if unknown)

In cases where enthalpy or pressure is the input, a nonlinear system must be solved to obtain the temperature and other quantities. The solution of the system can be obtained using the *fzero* function in MATLAB with a selected tolerance of 10^{-14}.

The routine has been validated using the table in Appendix D of Ref. [6]. The results obtained using MATLAB match those in the table, both in the International System Unit and the Imperial unit systems.

The Fig. 2.3 and Fig. 2.4 illustrate the variation of the constant pressure heat C_p and the ratio of specific heats γ, respectively. These results are computed using "FAIR" for a fuel-to-air ratio ranging from 0 (pure air mixture) to the stoichiometric value $f_{st} = 0.0685$ for a generic hydrocarbon fuel $C_{12}H_{23}$. The temperature range considered is from 220 K to 2000 K. As observed, both parameters change significantly with temperature and air mixture, especially when the temperature rises above 500 K.

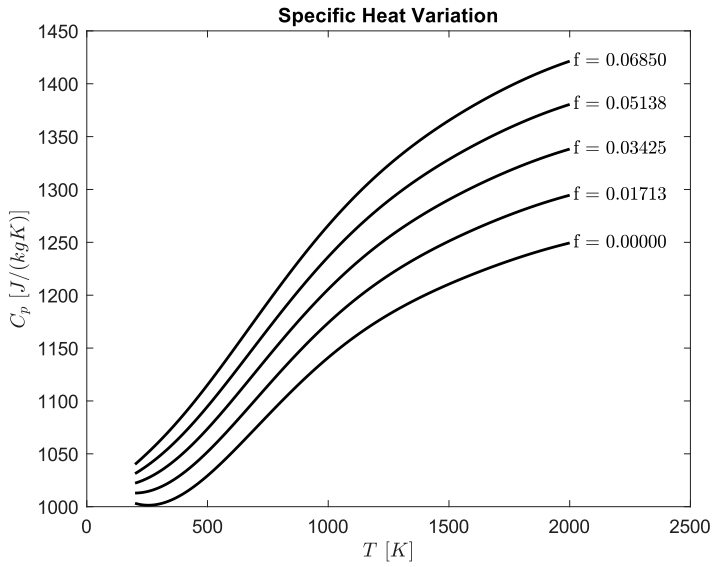

Figure 2.3: Specific heat C_p vs. temperature for a generic $C_{12}H_{23}$ hydrocarbon and air combustion products

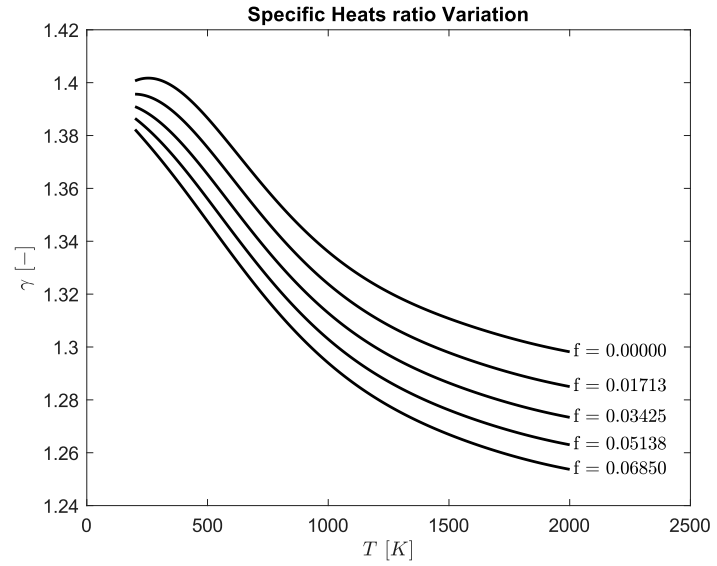

Figure 2.4: Ratio of specific heats γ vs. temperature for a generic $C_{12}H_{23}$ hydrocarbon and air combustion products

It is possible to observe that an increase in the C_p variation leads to a variation of enthalpy, which means the related thermodynamic work and power will be

affected by an error. Another important consideration is the chosen fuel for the analysis. Generally, typical propellants used in aeronautical propulsion do not vary from each other in terms of specific heat, so it is possible to justify the use of a generic hydrocarbon composition to simulate the performance of a jet engine, neglecting the real chemical composition. The case is different if alternative fuels such as bio-fuel or hydrogen mixtures are considered. According to the references, the procedure to obtain the polynomial coefficient does not differ from the exposed one and the equations are still valid in the proposed range.

2.4 The Modified Specific Heat Model

Another gas model used in thesis work is the **Modified Specific Heat**. This consists of a manual assignation of the C_p and γ values to the average ones. The values are obtained from a simplification of the Variable Specific Heat gas model. Assuming the gas as **Calorically Perfect Gas**, which means

$$C_p(T) = C_p \tag{2.20}$$

$$C_v(T) = C_v \tag{2.21}$$

$$\gamma(T) = \gamma \tag{2.22}$$

This assumption leads to a great simplification in calculations, particularly for the enthalpy variation that may be evaluated from Eq. 2.6

$$h_2 - h_1 = C_p \cdot (T_2 - T_1) \tag{2.23}$$

Also the entropy calculation changes too

$$s_2 - s_1 = C_p \cdot ln\left(\frac{T_2}{T_1}\right) - R \cdot ln\left(\frac{P_2}{P_1}\right) \tag{2.24}$$

Thus, the pressure ratio is obtained from 2.24.

$$\frac{T_2}{T_1} = \left(\frac{P_2}{P_1}\right)^{(\gamma-1)/\gamma} \cdot exp\left(\frac{s_2 - s_1}{C_p}\right) \tag{2.25}$$

Another assumption related to the gas state through the ducts is to consider the process as isentropic, which leads to

$$\frac{T_2}{T_1} = \left(\frac{P_2}{P_1}\right)^{(\gamma-1)/\gamma} \tag{2.26}$$

Our experience establishes that the exposed model for engine calculations is valid in a strict range of temperatures and mixture settings, in perfect agreement with Ref. [7]. To evaluate the related error the specific heat coefficient is calculated for three temperature values 220 K, 500 K, 800 K, and the fuel-to-air equal to zero ($f = 0$). The mixture is pure air, a condition that will occur in the inlet, compressors and fan. The results are shown in table 2.2, and as it is possible to see, if the average value $C_p = 1002\ J/(kg \cdot K)$ is considered it will cause a maximum error of +9.58%, that is unacceptable since it will generate a great error in enthalpy calculation. The same consideration could be reported for the ratio of specific heats γ (see Tab. 2.3).

Table 2.2: Specific Heat Variation for pure air

T	220 K	500 K	800 K
C_p	1002 $J/(kg \cdot K)$	1029 $J/(kg \cdot K)$	1098 $J/(kg \cdot K)$
ϵ	0.00%	+2.69%	+9.58%

Table 2.3: Specific Heats ratio Variation for pure air

T	220 K	500 K	800 K
γ	1.40 $J/(kg \cdot K)$	1.39 $J/(kg \cdot K)$	1.35 $J/(kg \cdot K)$
ϵ	0.00%	−0.71%	−3.57%

After the combustion, the temperature will increase significantly and in some applications with turbine air cooling systems, today it is able to reach above 2000 K. Assigning an average value to C_p and γ, is very challenging because the two values are depended on temperature and fuel-to-air ratio. According to the current literacy (Ref. [8] and Ref. [9]), the general assigned values are

$$C_p' = 1184\ J/(kg \cdot K) \tag{2.27}$$

$$\gamma' = 1.33 \tag{2.28}$$

now it is possible to compare the two assigned values with the ones obtained with the Variable Specific Heat Model. Therefore, four temperature values are set 600 K, 1000 K, 1300 K and 1800 K, the fuel-to-air ratio is assigned to three different values for lean mixtures and rich mixtures. The results are shown in table 2.4.

Table 2.4: Specific Heat Variation for air mixtures

T	600 K	1000 K	1300 K	1800 K
$f = 0.0171$ C_p $[J/(kg \cdot sec)]$	1075	1173	1226	1280
ϵ [%]	−9.20	−0.93	+3.55	+8.11
$f = 0.0343$ C_p $[J/(kg \cdot sec)]$	1099	1205	1263	1322
ϵ [%]	−7.18%	+1.77%	+6.67%	+11.7%
$f = 0.0685$ C_p $[J/(kg \cdot sec)]$	1145	1266	1332	1403
ϵ [%]	−3.29	+6.93	+12.5	+18.5

To conclude this section, the used gas model is exposed, underlying the most important aspect that has to be taken into account in a gas model: the Constant Pressure Heat Variation with temperature. This must be as accurate as possible since the related error will affect the enthalpy calculations and as a consequence the engine performance. A significant impact of the C_p variation is on the **Uninstalled Thrust-specific to fuel Consumption (TSFC)**, which strongly depends upon the fuel-to-air ratio and so to enthalpy calculations related to the **Temperature Inlet Turbine**. The Modified Specific Heat Gas model has the great vantage to be really less expensive in terms of computational costs and easy to implement, but could generate a significant error in performance predictions (especially as described on TSFC), quoting Ref. [7], about MSH:

«This is the least accurate method and it should only be used in illustrative calculations for teaching purposes, or for crude estimation»

the model has to be used only in a strict range of operative temperatures. The Variable Specific Heat model has no limitations in operative uses but requires a great computational cost caused by the non-linear equations that increase the simulation's time.

Chapter 3

Aircraft Engine Components Modeling

3.1 Standard Atmosphere

The external pressure and temperature vary with the flight altitudes, affecting the engine's performance. In this thesis work, the **International Standard Atmosphere** has been adopted in order to establish a relationship between the aircraft flight level and air thermodynamic state (P_0, T_0). The model is implemented in the MATLAB environment, developing a function called "ISA". To visualise the static temperature and static pressure, multiple simulations are performed and the related results are shown in Fig. 3.1 and Fig. 3.2.

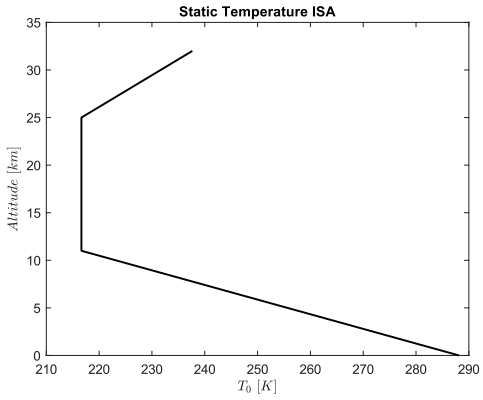

Figure 3.1: ISA: Temperature Variation with the altitude

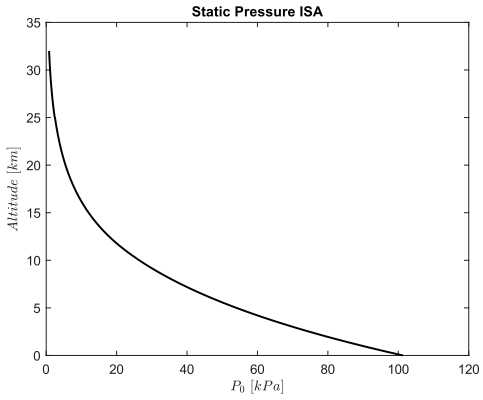

Figure 3.2: ISA: Pressure Variation with the altitude

Considering the **Variable Specific Heat (VSH)** as the gas model (see Sec. 2.3), the static environment enthalpy (h_0) is evaluated using the "FAIR" routine, having the external static temperature T_0, evaluated from ISA model as input. Then, the total enthalpy of the airflow environment h_{t0} is calculated by

$$h_{t0} = h_0 + \frac{1}{2}\left(M_0 \cdot a_0\right)^2 \tag{3.1}$$

where M_0 is the flight Mach number and a_0 is the speed of sound calculated by "FAIR" too. Next, it is possible to determine the gas state of the environment using h_{t0} as the input. Besides some negligible terms, the computation provides outputs such as P_{rt0} and T_{t0}, then the ratios τ_r and π_r are evaluated as follows

$$\tau_r = \frac{h_{t0}}{h_0} \tag{3.2}$$

$$\pi_r = \frac{P_{rt0}}{P_{r0}} \tag{3.3}$$

The transformation of the environment is nearly isentropic, so the total pressure P_{t0} can be determined using the following equation

$$P_{t0} = \frac{P_{rt0}}{P_{r0}} \cdot P_0 \tag{3.4}$$

By using the **Modified Specific Heat (MSH)** model (see Sec. 2.4), the calculation of the gas state of the environment is straightforward. Given the average values of γ and C_p, which are typically assumed to be 1.400 and $1004\,\mathrm{J/(kg \cdot K)}$ respectively, the exposed equations can be rewritten as follows

$$T_{t0} = T_0\left(1 + \frac{\gamma - 1}{2} \cdot M_0^2\right) \tag{3.5}$$

$$P_{t0} = P_0\left(1 + \frac{\gamma - 1}{2} \cdot M_0^2\right)^{\frac{\gamma}{\gamma - 1}} \tag{3.6}$$

$$\tau_r = \frac{T_{t0}}{T_0} \tag{3.7}$$

$$\pi_r = \frac{P_{t0}}{P_0} \tag{3.8}$$

In summary, the two different gas models are implemented in the MATLAB environment in order to solve the gas state of the environment air stream. Firstly, knowing the flight altitude, given by the user as an independent variable, the ISA function is executed, then with the external temperature T_0 and pressure P_0, the

total enthalpy h_{t0} and pressure P_{t0} are evaluated using equations from Eq. 3.5 to Eq. 3.8 in the case of MSH as the gas model or from Eq. 3.1 to Eq. 3.4 in the case of VSH model.

3.2 Inlet

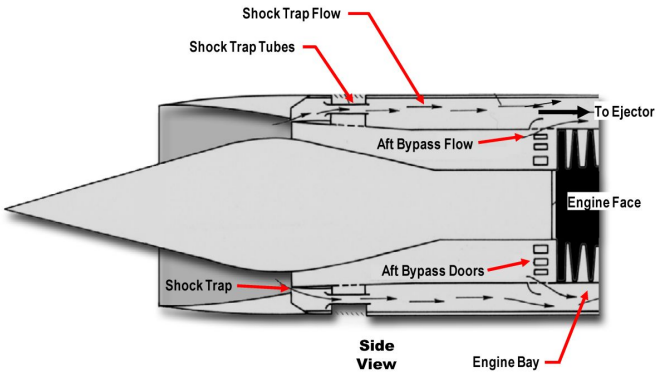

Figure 3.3: A typical architecture of a supersonic inlet

Inlets are installed in the engines, aiming to bring the free stream air into the compressors working in concert with compressors to give the overall pressure ratio of the engine cycle

$$\frac{P_{t3}}{P_0} = \frac{P_{t0}}{P_0}\frac{P_{t2}}{P_{t0}}\frac{P_{t3}}{P_{t2}} = \pi_r \pi_d \pi_c \tag{3.9}$$

$\pi_r \pi_d$ is the inlet's pressure ratio and π_c represents the engine's Overall Pressure Ratio (OPR). The **Military specification MIL-E-5008B** has been adopted in this thesis work to estimate the inlet's adiabatic efficiency η_R and total pressure ratio π_d variation with the flight Mach Number M_0. The model is really simple to implement and allows to evaluate performances without intake geometry. According to the specification, it is possible to calculate the pressure drop as

$$\pi_d = \pi_{d,max} \cdot \eta_R \tag{3.10}$$

$$\eta_R = \begin{cases} 1, & M_0 \leq 1 \\ 1 - 0.075(M_0 - 1)^{1.35}, & 1 < M_0 \leq 5 \\ \frac{800}{M_0^4 + 935}, & M_0 > 5 \end{cases} \tag{3.11}$$

Thus, it is possible to compute the inlet's output state

$$\tau_d = \frac{h_{t2}}{h_{t0}} = 1 \Rightarrow h_{t2} = h_{t0} \tag{3.12}$$

$$\pi_d = \frac{P_{t2}}{P_{t1}} \Rightarrow P_{t2} = \pi_d \cdot P_{t1} \tag{3.13}$$

The term η_R is related to shock waves, $\pi_{d,max}$ to the inlet's wall friction, this second term is selected considering the **Engine Level of Technology** and engine's category shown in Fig. 3.24. The model can be used during all On-design and Off-design simulations for both subsonic and supersonic applications. In Fig. 3.4 total pressure survey of different supersonic aircraft is presented, instead in Fig. 3.5 MIL-E-5008B Standard Model is performed using the MATLAB code. In both images, it is possible to observe the increase of total pressure drop with the Mach number due to shock waves.

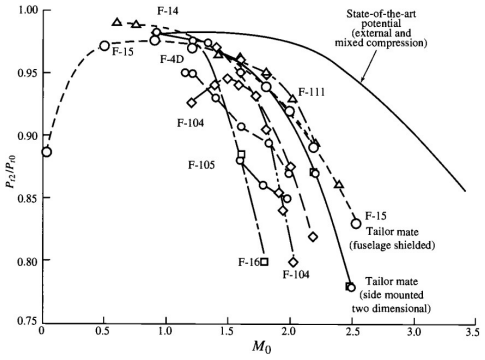

Figure 3.4: Total Pressure ratio Survey

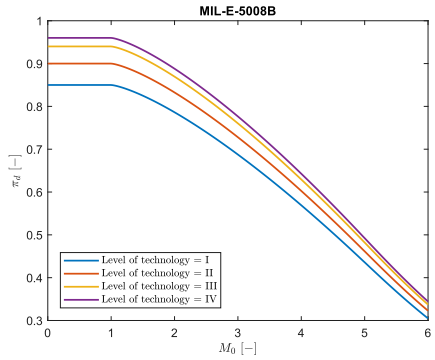

Figure 3.5: MIL-E-5008B for different levels of technology (considering C category)

3.3 Compressor

3.3.1 Introduction and Purpose

In this section, the main governing equations and functions of compressors will be described. Since the thesis work is principally focused on supersonic applications, only the axial compressor will be analysed, neglecting the centrifugal ones, which are used essentially in turboprop and turboshaft engines. The compressor's design is a very hard procedure, it requires multiple iterations carrying different engineering aspects such as thermal, aerodynamics, structural and vibrations. Furthermore,

each compressor must be designed to work in correlation with other engine elements, particularly with turbines. As explained in the introduction the main goal of the thesis is to develop a propulsive database for a supersonic business jet during a conceptual design phase, thus it will take into account only the thermodynamics of the component. Both gas models (Variable Specific Heat and Modified Specific Heat) are applied to the compressor and fan. The On-design and Off-design analysis will be considered as well.

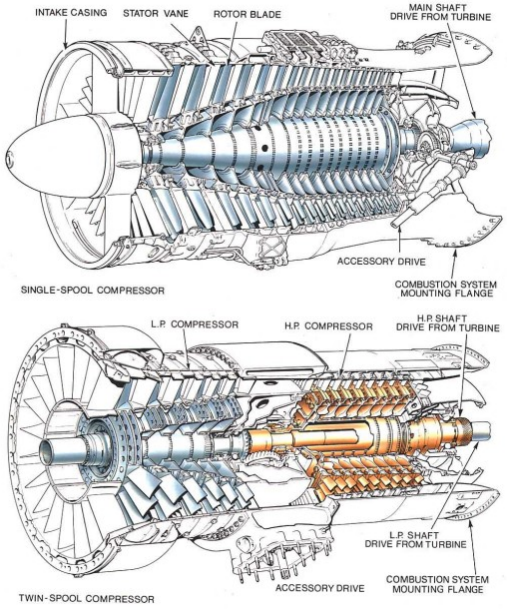

Figure 3.6: Typical architecture of axial compressors

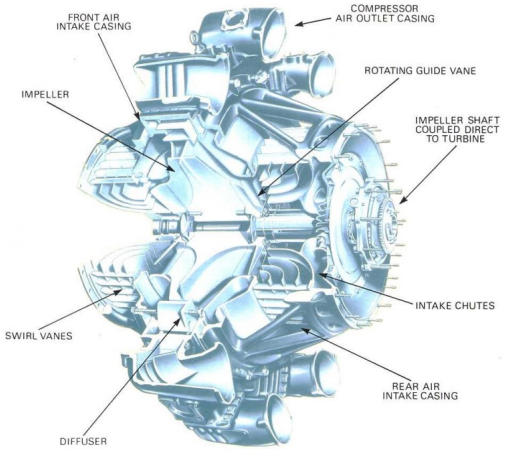

Figure 3.7: Typical architecture of centrifugal compressors

3.3.2 The Compressor Model

The compressor could be considered adiabatic, with a high degree of approximation. To measure the compressor's performance, the **isentropic efficiency** η_c is used, defined as

$$\eta_c \doteq \frac{\text{ideal work of compression for given } \pi_c}{\text{actual work of compression for given } \pi_c} \tag{3.14}$$

The main hypothesis of the compressor thermodynamic model related to the adiabatic process ($Q_e = 0$) reduces the first law of thermodynamics as

$$W_i + \cancelto{0}{Q_e} = \Delta h_t \Rightarrow W_c = h_{t3} - h_{t2} \tag{3.15}$$

For ideal work, an isentropic (adiabatic and reversible) transformation will be considered, so the ideal compressor work is given by

$$W_{c,ideal} = h_{t3i} - h_{t2} \tag{3.16}$$

By combining Eq. 3.15 and Eq. 3.16 the compressor isentropic efficiency as defined in Eq. 3.17 is obtained as

$$\eta_c = \frac{h_{3i} - h_{t2}}{h_{t3} - h_{t2}} \tag{3.17}$$

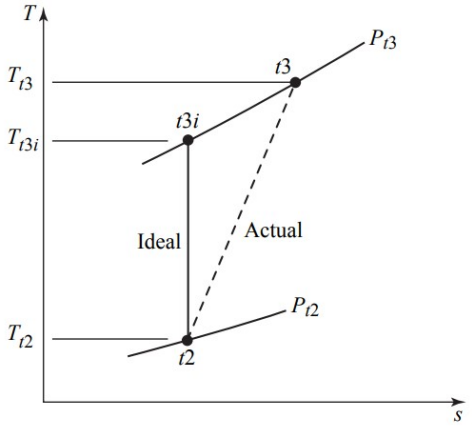

Figure 3.8: Actual and Ideal compressor processes

In the case of a calorically perfect gas (Modified Specific Heat Gas Model), the Eq. 3.17 can be rewritten as

$$\eta_c = \frac{h_{t3i} - h_{t2}}{h_{t3} - h_{t2}} = \frac{c_p\,(T_{t3i} - T_{t2})}{c_p\,(T_{t3i} - T_{t2})} = \frac{T_{t3i} - T_{t2}}{T_{t3} - T_{t2}} \tag{3.18}$$

The parametric performance analysis generally, is executed knowing the compressor ratio π_c, or if more than one compressor stage is installed, it is necessary to specify the ratio related to the specific component. Generally, the engine **Overall Engine Pressure Ratio (OPR or π_c)** is defined as the product of the compressors' pressure ratios. Based on this, it is possible to write

$$\pi_c \doteq \frac{P_{t3}}{P_{t2}} \tag{3.19}$$

The main aim at this point is to relate the total pressure ratio to the total enthalpy or temperature. Considering firstly the MSH model it is possible to relate the total temperature in ideal conditions to the pressure ratio of the compressor by using isentropic equations

$$\tau_{ci} = \frac{T_{t3i}}{T_{t2}} = \left(\frac{P_{t3}}{P_{t2}}\right)^{\frac{\gamma-1}{\gamma}} = \pi_c^{\frac{\gamma-1}{\gamma}} \tag{3.20}$$

Therefore isentropic efficiency will reduce

$$\eta_c = \frac{\pi_c^{\frac{\gamma-1}{\gamma}} - 1}{\tau_c - 1} \tag{3.21}$$

Considering an engine with more than one stage compressor, the equations from Eq. 3.19 to Eq. 3.21 are still valid, with the only change

$$\pi_s \doteq \frac{\text{Total Pressure Output}}{\text{Total Pressure Input}} = \frac{P_{t,f}}{P_{t,i}} \tag{3.22}$$

And as defined previously the Overall Pressure Ratio can be calculated as

$$\text{OPR} = \pi_c \doteq \prod_{j=1}^{N} \pi_{s,j} \tag{3.23}$$

Where N, is the total number of compressor stages. To solve the compressor On-design, it is necessary to know η_c or τ_c (that implies T_{t3} is known), however, it is possible to introduce the **Compressor Polytropic Efficiency** e_c, in order to calculate τ_c directly. This last one is defined as

$$e_c \doteq \frac{\text{ideal work of compression for a differential pressure change}}{\text{actual work of compression for a differential pressure change}} \tag{3.24}$$

So it is possible to relate τ_c to e_c, in the case of the calorically perfect gas or Modified Specific Heat gas model, as follows

$$e_c \doteq \frac{dw_i}{dw} = \frac{dh_{ti}}{dh_t} = \frac{dT_{ti}}{dT_t} \tag{3.25}$$

For ideal compression, $T_{ti} = P_{ti}^{\frac{\gamma-1}{\gamma}}$ x constant is valid, so it is possible to write

$$\frac{dT_t}{T_t} = \frac{\gamma-1}{\gamma}\frac{dP_t}{P_t} \tag{3.26}$$

$$e_c = \frac{dT_{ti}}{dT_t} = \frac{dT_{ti}/T_t}{dT_t/T_t} = \frac{\gamma-1}{\gamma}\frac{dP_t/P_t}{dT_t/T_t} \tag{3.27}$$

Assuming e_c constant

$$\frac{dT_t}{T_t} = \frac{\gamma - 1}{\gamma e_c} \frac{dP_t}{P_t} \tag{3.28}$$

Integrating between states $t2$ and $t3$

$$ln\left(\frac{T_{t3}}{T_{t2}}\right) = \frac{\gamma - 1}{\gamma e_c} ln\left(\frac{P_{t3}}{P_{t2}}\right) \Rightarrow \tau_c = \pi_c^{\frac{\gamma-1}{\gamma e_c}} \tag{3.29}$$

Finally, it is possible to calculate the adiabatic efficiency as

$$\eta_c = \frac{\pi_c^{\frac{\gamma-1}{\gamma}} - 1}{\tau_c - 1} = \frac{\pi_c^{\frac{\gamma-1}{\gamma}} - 1}{\pi_c^{\frac{\gamma-1}{\gamma e_c}} - 1} \tag{3.30}$$

According to Ref. [6], Eq. 3.30 accurately predicts the relationship between the isentropic efficiency of a compressor and the related compressor ratio for a given polytropic efficiency. The Fig. 3.9, shows the variation of η_c, for different e_c and, as it is possible to observe, the adiabatic efficiency decreases with π_c increase. Many commercial software such as GasTurb or GSP 11, allow to specify as input the adiabatic efficiency or polytropic efficiency. In all developed MATLAB codes of this thesis work, the second one is the input, since it is possible to relate the level of technology in a simple manner.

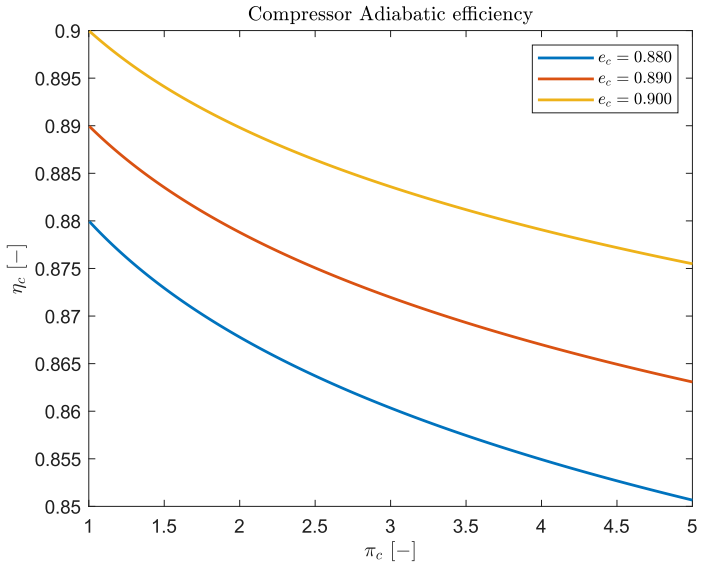

Figure 3.9: Compressor's adiabatic efficiency variation vs Overall Pressure Ratio

The exposed analysis is valid for a calorically perfect gas, therefore by applying the Modified Specific Heat Model. In the case of Variable Specific Heat, Eq. 3.24 can be written as

$$e_c = \frac{dh_{ti}}{dh_t} = \frac{dh_{ti}/T_t}{dh_t/T_t} \tag{3.31}$$

Using the Gibbs equation in differential form it is possible to write

$$\frac{dh_{ti}}{T_t} = R\,\frac{dP_t}{P_t} \tag{3.32}$$

Thus, replacing the ratio dh_{ti}/T_t in Eq. 3.31, it is possible to obtain

$$e_c = R\,\frac{dP_t/P_t}{dh_t/T_t} \tag{3.33}$$

Considering constant polytropic specific heat and integrating from $t2$ and $t3$

$$\phi_{t3} - \phi_{t2} \doteq \int_{t2}^{t3} \frac{dh_{ti}}{T_t} = \frac{R}{e_c} ln\left(\frac{P_{t3}}{P_{t2}}\right) \tag{3.34}$$

Where ϕ_t is the entropy function as defined in sec. 2.3. Therefore the compressor pressure ratio π_c can be written as

$$\pi_c = \frac{P_{t3}}{P_{t2}} = exp\left(e_c \frac{\phi_{t3} - \phi_{t2}}{R}\right) = \left(\frac{P_{rt3}}{P_{rt2}}\right)^{e_c} \tag{3.35}$$

Knowing the reduced pressure from precedent station P_{rt2}, compressor ratio π_c and polytropic efficiency e_c, the compressor output state is given by

$$P_{rt3} = \pi_c^{1/e_c} \cdot P_{rt2} \tag{3.36}$$

$$P_{rt3i} = \pi_c \cdot P_{rt2} \tag{3.37}$$

Now it is possible to call "FAIR" twice by using P_{rt3} as the entrance to calculate h_{t3} and P_{rt3i} per h_{t3}, and therefore the compressor isentropic efficiency η_c can be calculated as

$$\eta_c = \frac{h_{t3i} - h_{t2}}{h_{t3} - h_{t2}} \tag{3.38}$$

Concluding, the compressor On-design, the corrected mass flow rate $\dot{m}_c$ is calculated by using the definition

$$\dot{m}_c = \frac{\dot{m}\sqrt{T_{t2}/T_{ref}}}{P_{t2}/P_{ref}} = \frac{\dot{m}\sqrt{\theta_2}}{\delta_2} \tag{3.39}$$

The reference pressure P_{ref} and temperature T_{ref} are defined as the pressure and the temperature of the air at sea level conditions. The corrected mass flow rate is strictly related to the **Mass Flow Rate Parameter (MFP)** and so on to the entry Mach number. Generally, the corrected mass is used for the scaling map procedure as described in the next sections.

3.3.3 The Compressor Map Scaling

A compressor map typically consists of a contour plot with lines of pressure ratio versus corrected mass flow over a range of corrected spool speeds. Additionally, it includes constant efficiency contour lines and corrected speed numbers, usually scaled to a reference point. Realistic compressor maps are essential for accurately predicting engine performance, as emphasized in Ref. [10].

It is important to underline that creating a compressor map is a challenging task because it requires a thorough understanding of the compressor's geometry. Unfortunately, the lack of this crucial information often compels users to adopt simplified models or procedures to estimate compressor performance and, consequently, the entire engine's performance, particularly during the preliminary conceptual design phase or when responding to a request for proposal (Ref. [2]).

The subsequent phase of engine model development is critical, as it involves the entire algorithm and all procedures required to solve the Off-design problem. One potential solution is to avoid the use of the compressor map and assume that all adiabatic components remain constant. However, this simplification alone is insufficient to solve the engine cycle without maps. To address this limitation, it is necessary to assume choked flow conditions in the turbines. This allows for the creation of a customised algorithm (Serial Nested Loop) for Off-design simulations, although with certain operational limitations. This approach is adopted by J.D. Mattingly Ref. [2] and the upcoming sections will delve deeper into this method.

The second procedure involves scaling a compressor map from an existing one using a reference point. This relies on an assumption because it entails generating a map that does not exist in reality. Many commercial software, such as GasTurb (Ref. [11]) and GSP 11 (Ref. [4]), employ this method. A comprehensive physical explanation supporting the use of this technique can be found in Ref. [12] and Ref. [10]. In this case, the file maps used for the work are imported from GSP 11 open-source software.

The scaled new map is generated from the scaling factors. By denoting the reference point (On-design point) in terms of pressure ratio, corrected mass flow rate, adiabatic efficiency and the corrected number of speed of the compressor with subscripts "r", if the original map is known, its reference point is denoted with an asterisk "*", so it is possible to evaluate

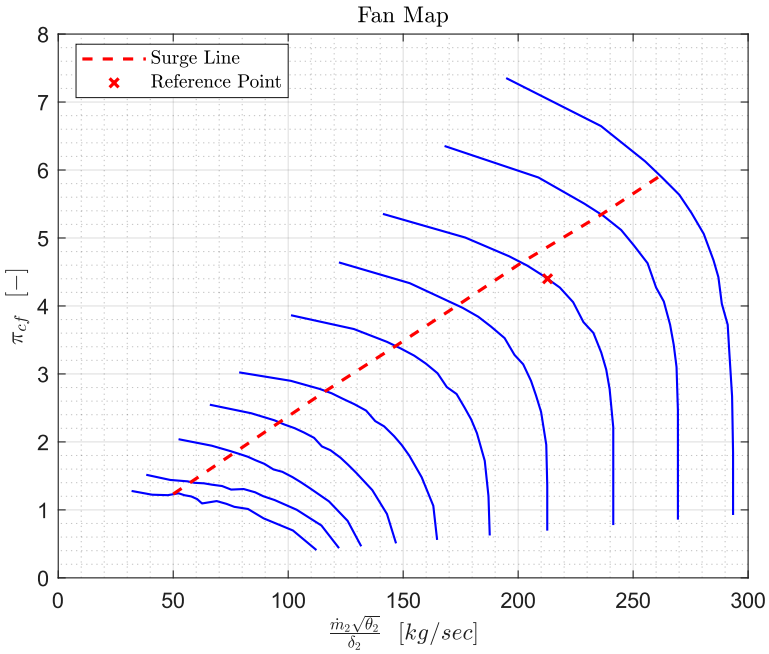

Figure 3.10: Example of compressor map

$$\pi = \frac{\pi - 1}{\pi^* - 1} \cdot (\pi_r - 1) + 1 \tag{3.40}$$

$$\eta_c = \frac{\eta_c}{\eta_c^*} \cdot \eta_{c,r} \tag{3.41}$$

$$\frac{\dot{m}\sqrt{\theta}}{\delta} = \frac{\frac{\dot{m}\sqrt{\theta}}{\delta}}{\left(\frac{\dot{m}\sqrt{\theta}}{\delta}\right)^*} \cdot \left(\frac{\dot{m}\sqrt{\theta}}{\delta}\right)_r \tag{3.42}$$

3.3.4 The Compressor Map Interpolation

The compressor map interpolation is articulated into three main steps having the compressor ratio π_c and the ratio of corrected number of speeds $\%N_c$ in input, the adiabatic efficiency η_c and corrected mass flow rate $\dot{m}_c$ as outputs using the beta-parameter (see Ref. [12]). The first step of data interpolation is the *increment number of speeds* evaluation, obtained as follows

$$\Delta N_c = \frac{N_{c\ guess} - N_c(i)}{N_c(i+1) - N_c(i)}$$

The interpolated index i, is the result of the condition

$$N_{c\ guess} \geq N_c(i) \ \wedge \ N_{c\ guess} < N_c(i+1) \tag{3.43}$$

So, the routine will vary i, from the first value in the map to the last one until the relation Eq. 3.43 is satisfied. If $N_{c\ guess}$ is greater than the maximum or lower than the minimum, the routine releases an error and the iteration will be stopped, since there is no physical solution to the problem.

The second step is to add the ΔN_C increment to the pressure ratio vector, corrected mass flow rate vector and the adiabatic efficiency vector, which are selected because they are associated with $N_c(i)$.

$$\{\pi_{interp}\} = \{\pi(i)\} + \Delta N_c \cdot [\{\pi(i+1)\} - \{\pi(i)\}] \tag{3.44}$$

$$\{\dot{m}_{c\ interp}\} = \{\dot{m}_c(i)\} + \Delta N_c \cdot [\{\dot{m}_c(i+1)\} - \{\dot{m}_c(i)\}] \tag{3.45}$$

$$\{\eta_{interp}\} = \{\eta(i)\} + \Delta N_c \cdot [\{\eta(i+1)\} - \{\eta(i)\}] \tag{3.46}$$

The quantities $\{\pi_{interp}\}$, $\{\dot{m}_c\}$ and $\{\eta_{interp}\}$ are the series of values given by the map.

Then, for the third step, it is necessary to interpolate the pressure π_{guess}. In order to do that, the pressure increment $\Delta\pi$ is calculated as

$$\Delta\pi = \frac{\pi_{guess} - \pi(j)}{\pi(j+1) - \pi(j)}$$

The index j is selected if the following condition is satisfied

$$\pi_{guess} \ > \ \pi(j+1) \ \wedge \ \pi_{guess} \ \leq \ \pi(j) \tag{3.47}$$

The index will vary from the first to the last until the condition expressed by Eq. 3.47 is satisfied. Now, it is possible to conclude the process by interpolating the given series

$$\dot{m}_c = \dot{m}_c(j) + \Delta\pi \cdot (\dot{m}_c(j+1) - \dot{m}_c(j)) \tag{3.48}$$

$$\eta = \eta(j) + \Delta\pi \cdot (\eta(j+1) - \eta(j)) \tag{3.49}$$

If the j index is not found, because the desired pressure is out of the limit, the process is stopped and, consequently, the simulation too. Another interpolation process may be adopted, for instance in the case of a fan. The input may be the corrected mass flow rate instead of the pressure ratio, then the related pressure ratio is given as the output.

3.3.5 Compressor Off-Design Analysis

During Off-design analysis, the compressor must be regulated in order to satisfy new throttle settings or different flight conditions, such as flight Mach number or altitude (Aircraft Flight level), bleed air and power extraction could change as well. As discussed in Sec. 4.5, during Off-design analysis, the compressor ratio π_c and shaft number of speed are known, as the new variables of the Newton-Raphson method iteration. Therefore, it is possible to use the compressor's map, giving as inputs the corrected number of speed and compressor ratio to obtain the corrected mass flow rate $\dot{m}_c$ and the compressor's adiabatic efficiency η_c. Then, assuming that P_{t2} and T_{t2} are known from inlet calculation (or previous compressor stage) and taking into account the case of **Calorically Perfect Gas**, it is possible to write

$$T_{t3} = T_{t2}\left[1 + \frac{1}{\eta_c}\left(\pi_c^{\frac{\gamma-1}{\gamma}} - 1\right)\right] \tag{3.50}$$

$$P_{t3} = \pi_c \cdot P_{t2} \tag{3.51}$$

The output compressor gas state is known and, to end up, specific work and power are evaluated as

$$W_c = C_p \cdot (T_{t3} - T_{t2}) \tag{3.52}$$

$$P_c = \dot{m}_2 \cdot C_p(T_{t3} - T_{t2}) \tag{3.53}$$

This process will repeat in concert with the turbine, chamber and nozzle map interpolation and calculation until the method convergence. Considering the general case of the Variable Specific Heat gas model, the procedure is different from the previous exposure, since the equations must be written in terms of enthalpy instead of temperature. So the routine *FAIR* is needed. By knowing the reduced pressure P_{rt2} and total pressure P_{t2} from the preceding station, it is possible to compute the compressor output reduced pressure in the ideal case, using the Eq. 3.27. Then, by calling *FAIR* routine and by giving the new value as input, the total ideal output compressor enthalpy is computed. Since η_c is obtained from map interpolation, it is possible to calculate the output enthalpy, replacing Eq. 3.18, knowing the ideal enthalpy h_{3i} from *FAIR*

$$h_{t3} = h_{t2} + \frac{1}{\eta_c}(h_{t3i} - h_{t2}) \tag{3.54}$$

It is possible to solve the $t3$ state completely, recalling *FAIR* and giving h_{t3} as input. The calculation of specific power and work exposed above, concludes the process.

3.4 Combustion Chamber

3.4.1 Introduction

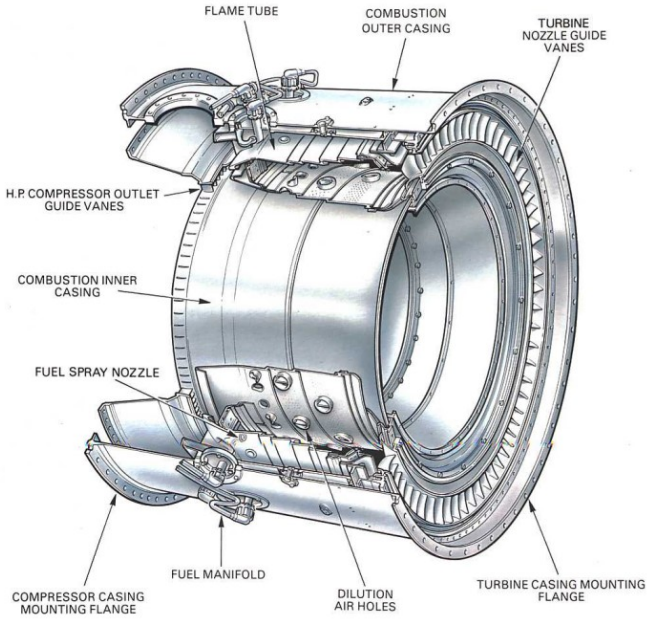

Figure 3.11: Annular combustion chamber architecture

The main chamber plays a critical role in increasing thermal energy through the exothermic combustion process, where fuel reacts with oxygen from the ingested air stream. For this thesis, a simple model based on combustion efficiency to estimate chamber performance during On-design conditions is employed. Subsequently, the Off-design, the map scaling and interpolation are discussed.

3.4.2 The Chamber Model

By knowing the P_{t3}, h_{t3}, or T_{t3}, computed at the previous station, typically representing the gas state results of the compressor stage and considering the Lower Heating Value of the fuel, it is possible to define the **combustion efficiency** as

$$\eta_b \doteq \frac{\dot{m}_4 h_{t4} - \dot{m}_3 h_{t3}}{\dot{m}_f h_{PR}} \leq 1 \tag{3.55}$$

Here, $\dot{m}_f$ is the fuel mass flow rate, $\dot{m}_3$ is the air mass flow upstream of the chamber and $\dot{m}_4$ is the sum of these rates. Typically, during On-design simulations, η_b is specified as a design parameter and is related to the engine level of technology.

From the combustion efficiency expression, it is possible to calculate the **fuel-to-air ratio** (f) as follows

$$f \doteq \frac{\dot{m}_f}{\dot{m}_3} \tag{3.56}$$

This represents the fuel fraction in relation to air, impacting performance, emissions and the constant pressure heat (C_p) variation. By using Eq. 3.56, Eq. 3.55 is rewritten as

$$f = \frac{h_{t4} - h_{t3}}{\eta_b h_{PR} - h_{t3}} \tag{3.57}$$

In many engine analyses, the **inlet temperature of the turbine (TIT)** is typically specified by the designer, represented here as T_{t4}, rather than the related enthalpy. If the gas is modeled as calorically perfect, Eq. 3.57 can be simplified as

$$f = \frac{C_{pt} T_{t4} - C_p T_{t3}}{\eta_b h_{PR} - C_p T_{t3}} \tag{3.58}$$

In this context, C_{pt} is assigned by the user according to the **Modified Specific Heat Gas Model** (see Sec 2.4). As described in the Gas Model sections, an average value might be

$$C_{pt} = 1184 \ [J/(kg \cdot K)]$$

The **Lower Heating Value** depends on the specific fuel used during combustion. Representative jet fuels yield values such as

$$h_{PR} = 43.260 \ [MJ/kg] \ (C_{12}H_{23})$$

For a more general **Variable Specific Heat** gas model, Eq. 3.57 may not be used directly. In such cases, an iterative algorithm is employed to calculate the fuel-to-air ratio of the mixture until convergence is reached, using a predefined tolerance.

Given η_b, P_{t3} and $\Delta T = T_{t4} - T_{t3}$, it is possible to scale a generic combustor map for Off-design simulation. The pressure losses are considered constant, with the parameter π_b chosen from Fig. 3.24 and defined as

$$\pi_b \doteq \frac{P_{t4}}{P_{t3}} \tag{3.59}$$

3.4.3 Stoichiometric Fuel-Air Mixture Ratio

An interesting scenario is the case of complete combustion, where all oxygen atoms are consumed by the fuel. This allows to calculate the fuel-air ratio using the stoichiometric equation

$$C_xH_y + \left(x + \frac{y}{4}\right)\left[O_2 + \frac{79}{21}N_2\right] \Rightarrow xCO_2 + \frac{y}{2}H_2O + \frac{79}{21}\left(x + \frac{y}{4}\right)N_2 \tag{3.60}$$

As it is possible to observe, the fuel is completely burned, transforming into carbon dioxide, water and nitro-oxides. The stoichiometric mass-basis fuel-air ratio is used in order to quantify the effective quantity of fuel consumed during the combustion, it is given by

$$f_{st} = \frac{36x + 3y}{103\,(4x + y)} \tag{3.61}$$

For the jet fuel described earlier (with $x = 12$ and $y = 23$), the stoichiometric fuel-to-air ratio is $f_{st} = 0.0685$. Finally, it is possible to define the **equivalence ratio** as

$$\phi \doteq \frac{f}{f_{st}} \tag{3.62}$$

This parameter determines whether the mixture is "fuel-rich" or "fuel-lean."

3.4.4 Nitro-Oxides Emission Index Estimation

The previous section exposes a model of a complete reaction of the fuel quantity with the air, in real situations the combustion is incomplete and other chemical species such as **Nitro-oxides (NOx)**, **Carbon monoxide (CO)** and **Unburned Hydrocarbon (UHC)** are produced.

Estimating the emissions of exposed species is a really hard procedure since many factors involve the species generation, such as the chamber geometry and the combustion time. However, the preliminary evaluation of the emission indexes of the novel engine must be carried out during the early phases of the project, because aviation legislation imposes restrictions on jet emission production. Matching the requirements related to this aspect is not the main purpose of this thesis work. However, to give an evaluation of the emission index, simple formulas are reported. The **emission index of NOx nitro-oxides**, according to Ref. [3] and Ref. [13] for annual combustors is given as

$$\mathrm{EI}_{NOx} = 23 \cdot \left(\frac{P_{t3}\ [kPa]}{2965}\right)^{0.4} \cdot exp\left(\frac{T_{t3} - 826\ [K]}{194\ [K]}\right) \tag{3.63}$$

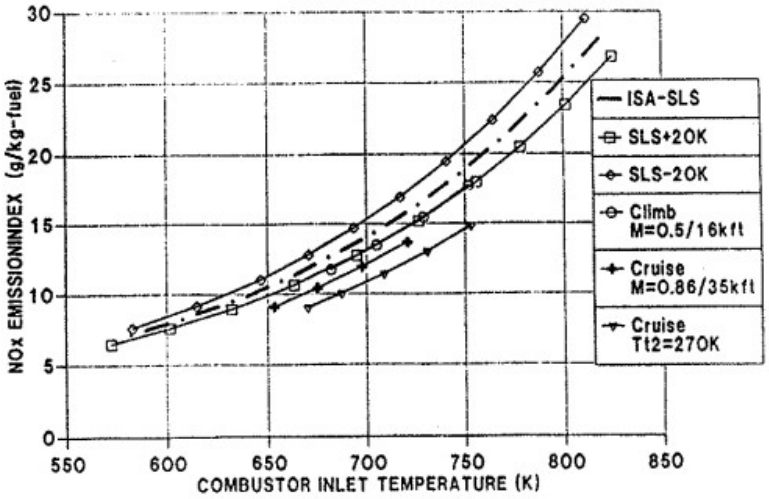

Figure 3.12: Emission Index: NOx formation

The Eq. 3.63 shows how the temperature and pressure at the inlet of the chamber affect the index, particularly if the overall pressure ratio of the engine increases, this will inevitably lead to an increase in the emission index, which challenges the engine design and configuration. As it will be discussed in the next sections, a greater value of OPR (Overall Pressure Ratio) provides a lower value of the fuel used by the engine, but concurrently the emission Index of Nitro-Oxides will rise as well. Therefore, a trade-off may be performed in order to satisfy the engine requirements in terms of thrust and fuel to one side and the emission index to the other. In order to estimate the **UHC and CO emissions**, it is possible to use the following equations

$$100 - \eta_b[\%] = 0.1 \cdot (0.232 \cdot EI_{\mathrm{CO}} + EI_{UHC}) \tag{3.64}$$

$$log(EI_{\mathrm{UHC}}) = 3.15 \cdot log(EI_{\mathrm{CO}}) - 4.3 \tag{3.65}$$

The UHC and CO formations are related essentially to the combustor efficiency η_b. From the combustor map (see Sec. 3.4.5) the efficiency remains constant for a wide range of temperature values, except for low throttle settings, leading to a constant formation of the two species.

3.4.5 Combustor Map Scaling

The maps of the combustion chamber are provided by GSP 11 Software. The generic combustor map has the temperature variation across the chamber ($\Delta T = T_{t4} - T_{t3}$)

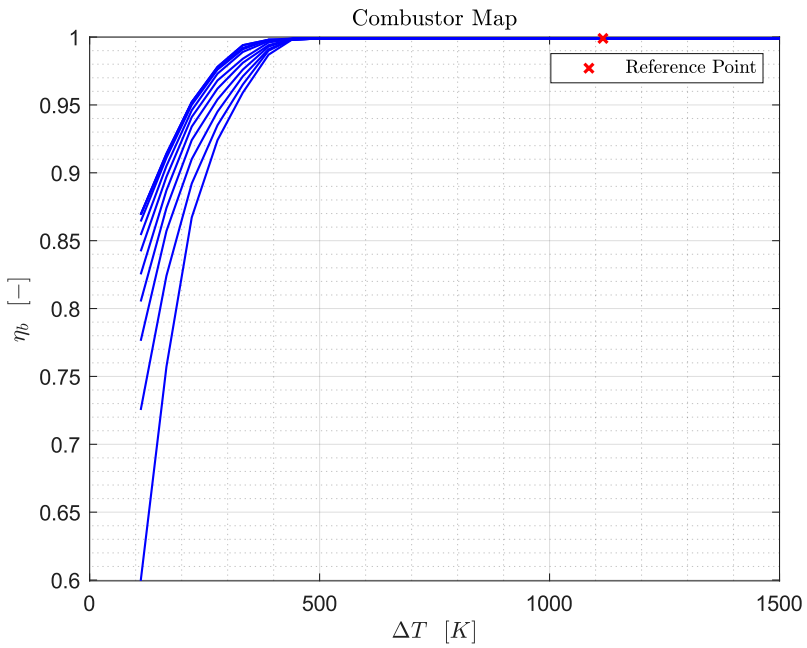

Figure 3.13: Combustor Map

on the x-axis and the curves represent efficiencies (η_b) for different P_{t3}/P_{ref} values on y-axis, as shown in Fig. 3.13.

The scaling procedure is straightforward. Knowing the reference value of the combustion efficiency ($\eta_{b,OD}$) and the one from the map ($\eta_{b,map}$), the scaling factor is given as

$$f_\eta = \frac{\eta_{b,OD}}{\eta_{b,map}} \tag{3.66}$$

Then, each map efficiency value is multiplied by f_η.

3.4.6 Off-Design Analysis

Off-design analysis of the chamber is similar to the On-design one. The primary difference leads to combustor map interpolation, which adjusts the efficiency value. Subsequent calculations for the fuel-air are replied and the chamber exit pressure is computed using Eq. 3.59. In summary, given the temperature variation ΔT_t and the relative pressure P_{t3}/P_{ref}, it is possible to evaluate the combustor efficiency η_b by linear interpolation of the scaled map.

3.5 Turbine

3.5.1 Introduction

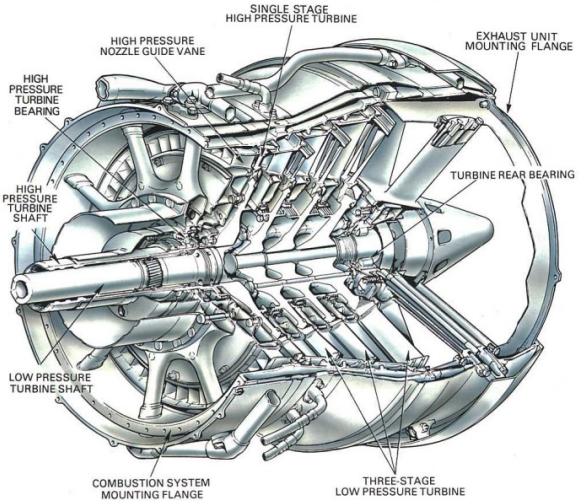

Figure 3.14: A twin turbine and shaft arrangement

The turbine's primary function is to provide power to drive the compressor and accessories by extracting energy from the hot gases released from the combustion system. As hot gases expand to lower pressure and temperature, they drive the turbine at high rotational speeds. In this section, likewise the compressor, the aim is to develop simple models for estimating turbine performance during the early stages of engine design.

3.5.2 Turbine Model

Similarly to the compressor, the **isentropic efficiency** η_t of a turbine is defined as

$$\eta_t \doteq \frac{\text{actual turbine work for a given } \pi_t}{\text{ideal turbine work for a given } \pi_t} \tag{3.67}$$

Modern turbines are cooled, so the assumption of adiabatic flow is not entirely accurate. However, for preliminary design purposes, assuming adiabatic flow provides a reasonable approximation, thus from the first law of thermodynamics

$$W_i + \cancelto{0}{Q_e} = \Delta h_t \Rightarrow -W_t = h_{t5} - h_{t4}$$

$$W_t = h_{t4} - h_{t5} \tag{3.68}$$

The **adiabatic turbine efficiency** can be expressed, using the definition as

$$\eta_t = \frac{h_{t4} - h_{t5}}{h_{t4} - h_{t5i}} \tag{3.69}$$

For a calorically perfect gas, Eq. 3.69 can be simplified

$$\eta_t = \frac{T_{t4} - T_{t5}}{T_{t4} - T_{t5i}} \tag{3.70}$$

The ratios τ_t and π_t are defined as

$$\tau_t \doteq \frac{T_{t5}}{T_{t4}} \tag{3.71}$$

$$\pi_t \doteq \frac{P_{t5}}{P_{t4}} \tag{3.72}$$

Generally, τ_t represents the ratio between the total exit turbine enthalpy and the entry enthalpy.

The **polytropic turbine efficiency** e_t is defined similarly to the isentropic compressor efficiency

$$e_t \doteq \frac{\text{actual turbine work for a differential pressure change}}{\text{ideal turbine work for a differential pressure change}} \tag{3.73}$$

Mathematically, the relationship between isentropic efficiency and polytropic efficiency is

$$\eta_t = \frac{1 - \tau_t}{1 - \tau_t^{1/e_t}} \tag{3.74}$$

The input parameter is e_t, which is related to the engine's level of technology. The pressure and enthalpy ratio can be evaluated based on the power balance at the shaft.

3.5.3 Shaft Power Balancing

The **Mechanical Efficiency of Power Shaft** is defined as:

$$\eta_m \doteq \frac{\dot{W}_c}{\dot{W}_t} \tag{3.75}$$

Using this definition it is possible to write

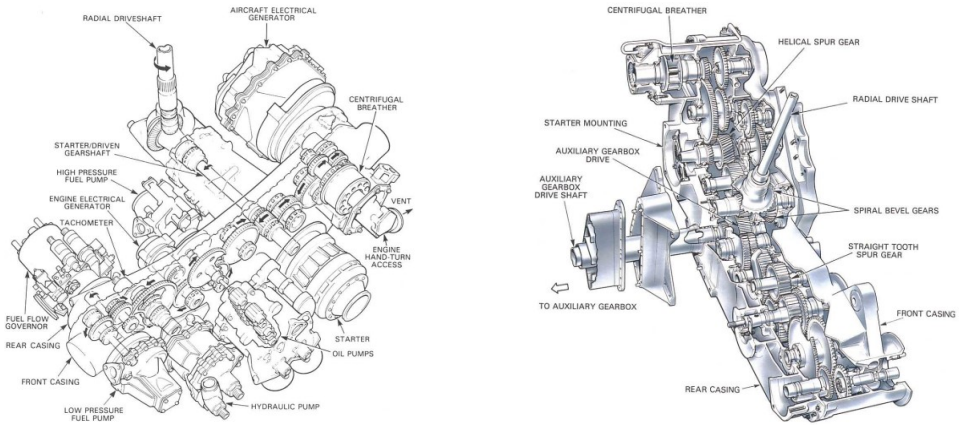

Figure 3.15: Examples of jet engine gearbox

$$\dot{W}_c = \dot{W}_t \cdot \eta_m$$

$$\dot{m}_3 \cdot (h_{t3} - h_{t2}) = \dot{m}_4 \, (h_{t4} - h_{t5}) \cdot \eta_m$$

In the balancing equation, the stagnation enthalpy at station 5 (h_{t5}, turbine outlet) is calculated, instead, the enthalpy at station 4 is determined by the throttle ratio and fuel-to-air mixture ratio. The compressor power is computed based on the Overall Pressure Ratio, as described in Sec. 3.3 and the Mechanical Shaft Efficiency is generally set to reflect the engine's level of technology, accounting for power losses due to accessories driving, fuel pumps and oil leakages, which are often close to 1.

To calculate the mass flow rates at *station 4* and *station 5*, the mass conservation in the engine flow path is employed

$$\sum \dot{m}_i \doteq 0 \tag{3.76}$$

The results depend on engine architecture, if the simple case of a single-spool turbojet with no turbine cooling, accessories, or air bleed is considered, the calculation is straightforward. The inlet mass flow rate at *station 4* is equal to the compressor inlet mass flow rate. At the turbine entry, the fuel mass flow rate is added, thus using the fuel-to-air definition, it is possible to write

$$\dot{m}_4 = \dot{m}_3 + \dot{m}_b$$

$$\dot{m}_4 = \dot{m}_3 \cdot (1 + f) = \dot{m}_0 \cdot (1 + f)$$

Applying these simplifications to the power balance equation, the turbine exit enthalpy is calculated as

$$h_{t5} = h_{t4} - \frac{\eta_m}{(1 + f)} (h_{t3} - h_{t2}) \tag{3.77}$$

For calorically perfect gas, this equation reduces

$$T_{t5} = T_{t4} - \frac{\eta_m \cdot C_{pt}}{C_p \cdot (1 + f)} (T_{t3} - T_{t2}) \tag{3.78}$$

In order to increase the accuracy of the model, the power extraction of accessories P_T at each present shaft with the related efficiency η_{mP} may be included, which will modify the balancing equation as follows

$$\dot{W}_c = \dot{W}_t \cdot \eta_m + P_T/\eta_{mP} \tag{3.79}$$

The shaft gives another important equation related to the number of speed congruence between compressors and turbines installed

$$N_c = N_t \tag{3.80}$$

3.5.4 Turbine Off-design Analysis

The turbine scaling procedure and interpolation are identical to the compressor one, exposed in Sec. 3.3.3 and Sec. 3.3.4. Thus, by giving as input the turbine pressure ratio π_t, the corrected ratio of the number of speed $\%N_t$, the corrected mass flow rate $\dot{m}_{c,t}$ and the adiabatic efficiency η_t will be interpolated (outputs).

The turbine during the regulation, has a constraint related to **the congruence of the shaft number of speed**, particularly Eq. 3.80 has to be ensured. This relation involves the turbine map interpolation because is one of the two inputs of the map. Particularly, considering the shaft in which a compressor and a turbine are installed, it is possible to write

$$N_t = N_c$$
$$\frac{N_t}{\sqrt{T_{t4}}} = \frac{N_c}{\sqrt{T_{t2}}} \cdot \sqrt{\frac{T_{t2}}{T_{t4}}}$$
$$N_{c,t} = N_{c,c} \cdot \sqrt{\frac{T_{t2}}{T_{t4}}}$$

Generally in the compressor's and turbine's map, the corrected number of speed is scaled about the reference point, so defining N_c the corrected number of speed, it is possible to derive

$$\frac{N_t}{\sqrt{T_{t4}}} = \frac{N_c}{\sqrt{T_{t2}}} \cdot \sqrt{\frac{T_{t2}}{T_{t4}}}$$

$$\frac{N_{c,t}}{N^r_{c,t}} = \frac{N_{c,c}}{N^r_{c,c}} \cdot \sqrt{\frac{T_{t2}}{T_{t4}}} \cdot \frac{N^r_{c,c}}{N^r_{c,t}}$$

$$(N_{c,t})_{\%} = (N_{c,c})_{\%} \cdot \sqrt{\frac{T_{t2}}{T_{t4}}} \cdot \frac{N^r_{c,c}}{N^r_{c,t}} \tag{3.81}$$

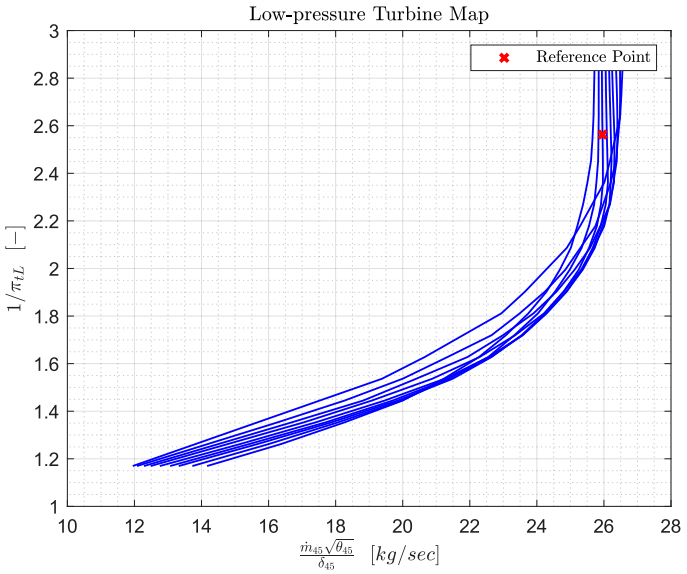

Figure 3.16: An example of Turbine Map

By knowing the efficiency and pressure ratio, it is possible to solve the gas state output of the turbine, considering the general case of the **Variable Specific Heat Model**, supposing that the upstream station of the turbine is $t4$, thus the downstream reduced pressure at turbine exit is given by

$$P_{rt5,ideal} = \pi_t \cdot P_{rt4} \tag{3.82}$$

Calling the "FAIR" routine the gas state in ideal condition at turbine exit $t5$ is solved, so it is possible to use the definition of adiabatic efficiency, to calculate the real enthalpy at turbine exit

$$h_{t5} = h_{t4} - \eta_t \cdot (h_{t4} - h_{t5i}) \tag{3.83}$$

The output pressure is calculated using the π_t definition

$$P_{t5} = \pi_t \cdot P_{t4} \tag{3.84}$$

Concluding the calculations, the power and work both in ideal and real conditions are evaluated using Eq. 3.68

$$W_{t,ideal} = h_{t4} - h_{t5i} \tag{3.85}$$
$$P_{t,ideal} = \dot{m}_4 \cdot (h_{t,4} - h_{t5i}) \tag{3.86}$$

$$W_t = h_{t4} - h_{t5} \tag{3.87}$$
$$P_t = \dot{m}_4 \cdot (h_{t,4} - h_{t5}) \tag{3.88}$$

In the case of a calorically perfect gas the Eq. 3.83 is simplified as

$$T_{t5} = T_{t4} - \eta_t \cdot (T_{t4} - T_{t5i}) \tag{3.89}$$

3.6 Turbine Air Cooling Systems

Turbine air cooling systems are an integral part of aircraft engines, particularly jet engines and are used to maintain the engine's temperature within safe operating limits. These systems help to manage the high temperatures generated during the combustion process and ensure that the engine components, particularly the turbine blades and vanes, remain within their design temperature limits. The purposes of turbine air cooling are:

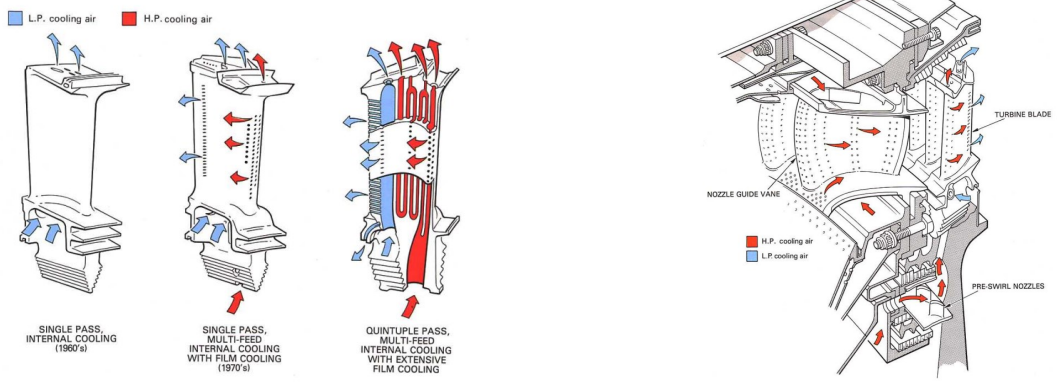

(a) Development of high-pressure turbine blade cooling

(b) Nozzle guide vane and turbine blade cooling arrangement

Figure 3.17: Turbine air cooling systems

1. **Temperature Management**: Aircraft engines operate at extremely high temperatures, especially in the turbine section where the hottest gases flow. Cooling is essential to prevent components from overheating and potentially failing.

2. **Efficiency and Performance**: Cooling allows the engine to operate more efficiently and produce more thrust. Lowering the temperature of the incoming air increases its density, leading to improved engine performance.

3. **Component Durability**: Cooling helps to extend the lifespan of critical components like turbine blades and vanes, reducing maintenance and replacement costs.

A general common cooling method is the **Compressor Bleed Air**, which involves extracting a small fraction of air from the engine's compressor (before it enters the combustion chamber) and routing it through internal passages within the engine to cool various components. This bleed air is then released into the turbine section to provide cooling.

The fraction of the total mass flow rate used for cooling in an aircraft engine varies depending on the specific engine design and operating conditions. It's typically a relatively small percentage of the total airflow (ε) in the range of 1% to 6% of the total airflow. The exact fraction may vary based on factors such as engine type, power settings and environmental conditions. The precise air distribution within the engine is carefully designed to ensure that critical components receive adequate cooling while minimising the impact on engine efficiency. A possible way

to estimate the cooling fractions is to use the Eq. 3.90 and Eq. 3.91 reported in Ref. [2]

$$\varepsilon = \frac{1.8 \cdot T_{t4,max} - 2400}{16000} \qquad \text{if} \quad T_{t4,max} \geq 1332 \tag{3.90}$$

$$\varepsilon = 0 \qquad \text{if} \quad T_{t4,max} < 1332 \tag{3.91}$$

The proposed model is derived from a power balance and mass flow rate conservation. As described above it is possible to define the compressor bleed air fraction as

$$\varepsilon \doteq \frac{\dot{m}_{cool}}{\dot{m}_c}$$

this fraction is subtracted from the compressor's outlet and added to the nozzle vanes of the coolant mixer. By applying the mass flow conservation

$$\sum \dot{m} = 0 \Rightarrow$$

$$\dot{m}_{4.1} = \dot{m}_4 + \varepsilon \cdot \dot{m}_3 \Rightarrow$$

$$\dot{m}_{4.1} = \dot{m}_3 \cdot [(1-\varepsilon)(1+f) + \varepsilon]$$

The stagnation enthalpy at the outlet of the coolant mixer is given by the power balance equation:

$$\dot{m}_{4.1} h_{t4.1} = \dot{m}_4 h_{t4} + \varepsilon \cdot \dot{m}_3 h_{t3}$$

No pressure losses are taken into account in this model. The engines proposed in this thesis feature two turbines and thus, the relevant equations are applied for each turbine to determine their respective states.

3.7 Mixer

3.7.1 Introduction

The turbofan engine essentially has two main configurations: mixed flows and separated flows. Mixing the hot and cold streams from the bypass (or duct) with the hot stream from the core offers several advantages. Firstly, it can increase thrust, provided that the total pressure in the core and bypass streams is similar; in this way, the mixing process does not cause a significant pressure drop. Secondly,

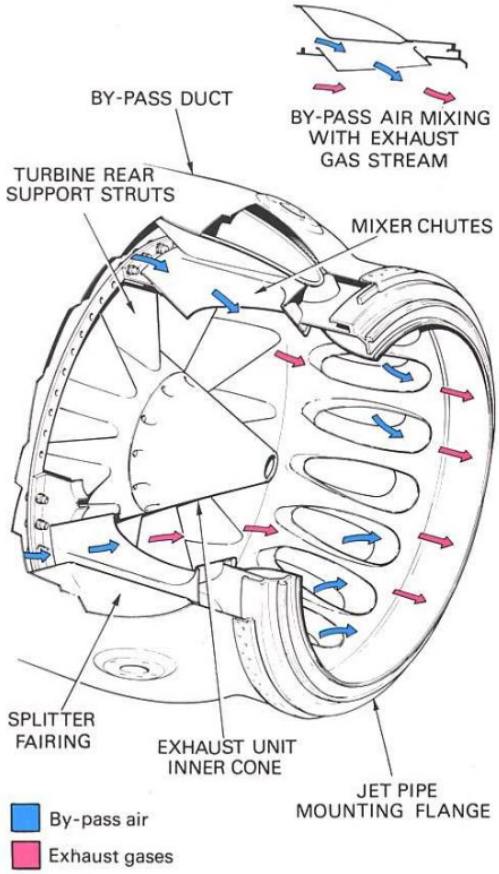

Figure 3.18: Mixer Architecture

mixing can result in reduced noise during takeoff, which is one of the primary objectives of the **MORE & LESS** European project, as stated in Ref. [10]. Engine noise varies to the eighth power of jet velocity, making mixing highly recommended for supersonic applications. Lastly, mixing is necessary for the use of afterburners or reheater devices. Additionally, a reduction in exhaust temperature corresponds to a reduced infrared signature for stealth applications, although these aspects are not considered in this thesis work. The main disadvantage of using mixers is the added weight to the system. Therefore, engine designers must carefully consider all aspects related to this technique in order to achieve optimal performance.

3.7.2 Mixer Model

The proposed model is derived from the textbook titled "Aircraft Engine Design," authored by J.D. Mattingly [2]. This model enables the calculation of the exit state of the engine mixer under ideal conditions (neglecting wall friction). It is

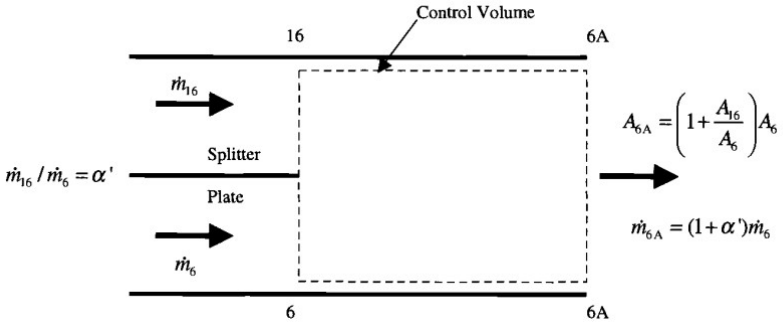

Figure 3.19: Constant-area Mixer Model

based on a set of equations corresponding to the principles of Mass Conservation, Energy Conservation and Momentum Conservation while assuming constant area mixer and Kutta condition. The "station" 16 is the fan or duct outlet, "station" 6 is the inlet of the core stream and the $6A$ is the outlet of the mixer. In this discussion, the gas properties and mass flow rates at stations 16 and 6 are assumed to be known. Furthermore, the process between station 13 (fan outlet) and the 16 is assumed to be isentropic without duct losses.

From Mass Conservation, it is possible to write

$$\dot{m}_{6A} = \dot{m}_6 + \dot{m}_{16} \tag{3.92}$$

A useful parameter is the **mixer by-pass ratio** α', defined as

$$\alpha' \doteq \frac{\dot{m}_{16}}{\dot{m}_6} \tag{3.93}$$

The second equation is *energy balance*, applied at the control volume

$$\dot{m}_{6A} h_{t6A} = \dot{m}_6 h_{t6} + \dot{m}_{16} h_{t16} \tag{3.94}$$

from which it is possible to derive the exit total enthalpy and the related ratio

$$h_{t6A} = \left(\frac{1 + \alpha' \cdot h_{t16}/h_{t6}}{1 + \alpha'} \right) \cdot h_{t6} \tag{3.95}$$

$$\tau_M \doteq \frac{h_{t6A}}{h_{t6}} = \left(\frac{1 + \alpha' \cdot h_{t16}/h_{t6}}{1 + \alpha'} \right) \tag{3.96}$$

In order to calculate the pressure ratio across the mixer, the definition of the **Mass Flow Rate Parameter** is employed

$$\mathrm{MFP} \doteq \frac{\dot{m} \cdot \sqrt{T_t}}{P_t \cdot A} \tag{3.97}$$

Solving Eq. 3.97 for P_t the ratio P_{t6A}/P_{t6} yields

$$\pi_{M,ideal} \doteq \frac{P_{6A}}{P_{t6}} = (1+\alpha') \cdot \sqrt{\tau_M} \cdot \frac{A_6}{A_{6A}} \cdot \frac{\mathrm{MFP}(M_6, T_{t6}, f_6)}{\mathrm{MFP}(M_{6A}, T_{t6A}, f_{6A})} \tag{3.98}$$

The evaluation of area at the mixer outlet is given by the first condition, of constant area: it is assumed that the outlet area of the mixer is equal to the sum of inlet ones

$$A_{6A} = A_6 + A_{16}$$

In addition, the fuel-to-air ratio at the 6A station is given by

$$f_{6A} = \frac{f_6}{1+\alpha'}$$

Generally, during the On-design M_6 is specified by the user in Eq. 3.98. The M_{6A} is calculated from the momentum equation, involving the M_6 and M_{16}. The area ratio is also calculated from the Mach numbers of the mixer's inlets

$$\frac{A_{16}}{A_6} = \alpha' \cdot \sqrt{\frac{T_{t16}}{T_{t6}}} \cdot \frac{P_{t6}}{P_{t16}} \cdot \frac{\mathrm{MFP}(M_6, T_{t6}, f_6)}{\mathrm{MFP}(M_{16}, T_{t16}, f_{16})} \tag{3.99}$$

The Kutta condition at the splitter plate $P_6 = P_{16}$ is taken into account yielding

$$\left(\frac{P_t}{P}\right)_{16} = \left(\frac{P_t}{P}\right)_6 \cdot \frac{P_{t16}}{P_{t6}}$$

If the half-ideal gas model is applied, the *RGCOMPR* routine must be employed to determine the gas state at station 16, from the total pressure ratio P_{t16}/P_{t6} and the Mach number M_6. The calculations are considerably streamlined, resulting in reduced computational costs when dealing with a calorically perfect gas model (Modified Specific Heat). This is achievable since the isentropic formula can be applied directly.

$$\left(\frac{P_t}{P}\right)_{16} = \frac{P_{t16}}{P_{t6}} \cdot \left(\frac{P_t}{P}\right)_6 \Rightarrow$$

$$\left(1 + \frac{\gamma - 1}{2} \cdot M_{16}^2\right)^{\frac{\gamma}{\gamma-1}} = \frac{P_{t16}}{P_{t6}} \cdot \left(1 + \frac{\gamma' - 1}{2} \cdot M_6^2\right)^{\frac{\gamma'}{\gamma'-1}} \Rightarrow$$

$$M_{16} = \sqrt{\frac{2}{\gamma - 1}\left[\frac{P_{t16}}{P_{t6}} \cdot \left(\left(1 + \frac{\gamma' - 1}{2} \cdot M_6^2\right)^{\frac{\gamma'}{\gamma'-1}}\right)^{\frac{\gamma-1}{\gamma}} - 1\right]} \tag{3.100}$$

The Eq. 3.100 illustrates the necessity of adjusting both M_6 and the ratio P_{t16}/P_{t6} to ensure that M_{16} remains real. This adjustment is essential as it has a physical implication: the inlet Mach number at the mixer from the core and the total pressure ratio must undergo variation in such a way as to prevent reverse flow from occurring either from the core to the duct or vice versa.

To solve Eq. 3.98, it becomes necessary to evaluate M_{6A}, and this can be achieved by applying the momentum equation. Expressing the momentum equation in terms of the impulse function (I) is appropriate for the constant-area mixer model.

$$I_{6A} = I_6 + I_{16} \tag{3.101}$$

where

$$I = P \cdot A \cdot \left(1 + \gamma M^2\right) \tag{3.102}$$

Thus

$$P_{6A}A_{6A}\left(1 + \gamma_{6A}M_{6A}^2\right) = P_6A_6\left(1 + \gamma_6M_6^2\right) + P_{16}A_{16}\left(1 + \gamma_{16}M_{16}^2\right)$$

Using the Kutta condition $P_6 = P_{16}$,

$$P_{6A}A_{6A}\left(1 + \gamma_{6A}M_{6A}^2\right) = P_6A_6\left[\left(1 + \gamma_6M_6^2\right) + \frac{A_{16}}{A_6}\left(1 + \gamma_{16}M_{16}^2\right)\right]$$

Now it is possible to use the mass flow rate definition and the perfect gas equation

$$PA = P \cdot \frac{\dot{m}}{\rho V} = \dot{m}\frac{RT}{M\sqrt{\gamma RT}} = \frac{\dot{m}}{M}\sqrt{\frac{RT}{\gamma}}$$

$$\sqrt{\frac{R_{6A}T_{6A}}{\gamma_{6A}}}\frac{1+\gamma_{6A}M_{6A}^2}{M_{6A}} = \sqrt{\frac{R_6T_6}{\gamma_6}}\frac{(1+\gamma_6M_6^2)+A_{16}/A_6\cdot(1+\gamma_{16}M_{16}^2)}{M_6(1+\alpha')} \tag{3.103}$$

The right-hand side of Eq. 3.103 remains constant and is derived from earlier computations. This equation is inherently nonlinear, with the variable of interest being, naturally, M_{6A}. The determined value of M_{6A} is subsequently employed in the calculation of $\pi_{M,ideal}$.

The constant-area mixer model evaluates the pressure variation solely attributable to the thermodynamic mixing of the flows. However, in order to take into account the wall friction effects, the author Ref. [2] proposes a straightforward relationship for estimating friction losses.

$$\pi_M = \pi_{M,ideal} \cdot \pi_{M,max} \tag{3.104}$$

In the context of this discussion, $\pi_{M,max}$ represents an estimation of losses due to friction and it is generally assumed to be around 0.97.

It is crucial to emphasize, as demonstrated in Eq. 3.100, that it is essential to finely adjust the total pressure ratio P_{t16}/P_{t6} to prevent reverse flows. Specifically, this ratio must be ensured near to 1.

$$\frac{P_{t16}}{P_{t6}} \approx 1 \tag{3.105}$$

That means

$$\frac{P_{t16}}{P_{t6}} = \frac{\pi_f}{\pi_{cL}\pi_{cH}\pi_b\pi_{tH}\pi_{tL}} \approx 1 \tag{3.106}$$

A potential strategy for tuning the engine involves selecting π_f during the parametric performance analysis (On-Design) to satisfy Eq. 3.106. During simulation, this ratio is constrained within a range of 0.95 to 1.10. Typically, the entry core Mach number M_6 is set within the range of 0.400 to 0.600.

In conclusion, the equations presented here can be employed for On-design simulations. By specifying $\pi_{M,max}$ and M_6, it is possible to solve the thermodynamics and determine the mixer areas. In the case of Off-design simulations, the model remains applicable, but the equations need to be reformulated equivalently. It is important to note that during Off-design, all mixer upstream quantities are held constant during a Newtonian-Raphson iteration, with the only unknown parameters being the mass flow rates.

$$\mathrm{MFP}(M_6, T_{t6}, f_6) = \frac{\dot{m}_6 \cdot \sqrt{T_{t6}}}{A_6 \cdot P_{t6}}$$

$$\mathrm{MFP}(M_{16}, T_{t16}, f_{16}) = \frac{\dot{m}_{16} \cdot \sqrt{T_{t16}}}{A_{16} \cdot P_{t16}}$$

By using *RGCOMPR* it is possible to evaluate the two Mach numbers, only the subsonic solutions will considered as well. The subroutine allows to calculate the ratio

$$\left(\frac{P_t}{P}\right)_6 = f(T_{t6}, M_6, P_{t6}, \mathrm{MFP}_6)$$

$$\left(\frac{P_t}{P}\right)_{16} = f(T_{t16}, M_6, P_{t16}, \mathrm{MFP}_{16})$$

From which it is possible to evaluate the static pressure

$$P_6 = \frac{P_{t6}}{(P_t/P)_6}$$

$$P_{16} = \frac{P_{t16}}{(P_t/P)_{16}}$$

It is of utmost importance to ensure that these two values are equal. To achieve this, the mixer introduces an "error equation" as part of the Off-design algorithm evaluation of the engine (see Sec. 4)

$$\varepsilon = P_6 - P_{16} \tag{3.107}$$

Readers will note that the static pressure error is contingent upon numerous parameters of the upstream flows, including $P_{t6},\ P_{t16},\ T_{t6},\ T_{t16},\ \alpha'$, among others. Consequently, the Off-design algorithm is tasked with finding a solution for the entire engine's parameters in order to satisfy Eq. 3.107 as well.

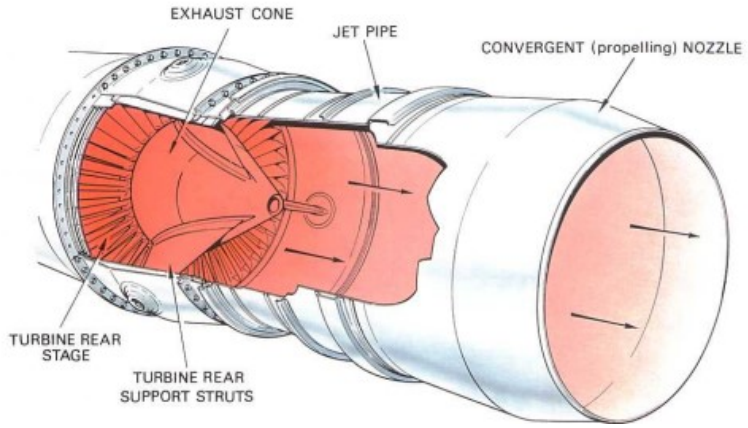

Figure 3.20: Basic Exhaust System Architecture

3.8 Exhaust Nozzle

3.8.1 Introduction

The exhaust nozzle plays a crucial role in increasing the velocity of exhaust gases before discharge. Considering the uninstalled thrust equation ([2])

$$F = \dot{m}_9 V_9 + A_9 \cdot (P_9 - P_0) - \dot{m}_0 V_0 \tag{3.108}$$

It can be demonstrated that the maximum thrust in Eq. 3.108 is achieved when the exit pressure of the nozzle equals the external pressure ($P_9 = P_0$).

The functions of a nozzle can be summarized as follows:

- Accelerating the flow to high velocity with minimal total pressure loss.
- Matching exit and atmospheric pressure as closely as desired.
- Permitting afterburner operations, which allow variation of the nozzle throat area.
- Allowing for cooling if necessary.
- Mixing core and bypass streams if required.
- Allowing thrust reversing if desired.
- Suppressing jet noise, radar reflection and infrared radiation (IFR) if required.
- Allowing thrust vector control if necessary.

Generally, the Nozzles for aeronautical applications present two basic configurations: the **simple convergent** and the **convergent-divergent (C-D)**.

3.8.2 Simple Convergent Nozzle

The simple convergent nozzle is employed when the pressure ratio between the upstream total pressure of the nozzle (P_{t9}) and the static external pressure (P_0) is less than 4.

$$\frac{P_{t9}}{P_0} < 4 \tag{3.109}$$

This configuration is ideal for subsonic applications due to its simplicity, as it lacks of moving parts. The first assumption of the nozzle model is that the flow is one-dimensional and adiabatic, meaning there is no thrust loss due to the non-axial exit of exhaust gases. In other words, the **Angularity Coefficient** is equal to 1.

$$C_A \doteq \frac{1}{\dot{m}} \cdot \int \cos\alpha_j \, d\dot{m} = 1 \tag{3.110}$$

The second assumption relates to the duct total pressure losses (π_n), which are considered constant and equal to a predefined value of 0.98.

$$\pi_n \doteq \frac{P_{t9}}{P_{t8}} = 0.98 \tag{3.111}$$

The third assumption concerns the preliminary sizing of the nozzle, specifically the exit Mach number (M_9), which is set to satisfy the condition $P_9 = P_0$. The exit nozzle area is calculated using the mass flow rate parameter definition.

$$A_9 = \frac{\dot{m}_9 \cdot \sqrt{T_{t9}}}{P_{t9} \cdot \mathrm{MFP}(M_9, T_{t9}, f_9)} \tag{3.112}$$

To evaluate nozzle performance, two cases must be distinguished: On-design analysis, where the exit Mach number is arbitrarily set to 1 to achieve choked flow and Off-design analysis, where the exit nozzle conditions depend on upstream nozzle flow and external pressure. In Off-design, the calculations are the same, but the critical pressure ratio is computed and compared to

$$\frac{P_{t9}}{P_0} \leq \left(\frac{P_t}{P}\right)_{M=1} \tag{3.113}$$

If condition Eq. 3.113 is met, the flow is unchoked and the nozzle static exit pressure equals the external pressure ($P_9 = P_0$). The Mach number (M_9) is calculated using compressible flow routines. If the flow is choked, then

$$\frac{P_{t9}}{P_0} \geq \left(\frac{P_t}{P}\right)_{M=1} \tag{3.114}$$

The exit Mach number is set to one and the ratio

$$\frac{P_{t9}}{P_9} = \left(\frac{P_t}{P}\right)_{M=1} \tag{3.115}$$

allows to calculate the exit static pressure, which, of course, is not equal to the external pressure

$$P_9 = \frac{P_{t9}}{(P_t/P)_{M=1}} \tag{3.116}$$

The ratio $(P_t/P)_{M=1}$ can be evaluated using compressible routines (RGCOMPR) for the real gas model (VSH) or using isentropic relations for the modified gas model

$$\left(\frac{P_t}{P}\right)_{M=1} = \left(1 + \frac{\gamma' - 1}{2} \cdot M^2\right)^{\frac{\gamma'}{\gamma'-1}} = \left(\frac{\gamma' + 1}{2}\right)^{\frac{\gamma'}{\gamma'-1}} \tag{3.117}$$

To prevent flow separation resulting from the interaction of the nozzle boundary layer and strong oblique shock waves, it is important to limit over-expansion in the nozzle. In extreme over-expansion conditions, flow separation can occur. A simple estimate for the maximum allowable ratio of the pressure preceding the shock wave (P_s) to the external pressure is suggested by Summerfield Ref. [2]

$$\frac{P_s}{P_0} \approx 0.37 \tag{3.118}$$

To conclude, it is possible to evaluate the exit gas state in terms of T_9 and V_9.

Concluding the nozzle model, the corrected mass flow rate is evaluated using the definition

$$\dot{m}_{c8} = \frac{\dot{m}_8 \cdot \sqrt{T_{t8}/T_{ref}}}{P_{t8}/P_{ref}} \tag{3.119}$$

The Eq. 3.119 is used only during On-design simulation, while during Off-design, the correct mass flow rate is calculated using the nozzle map (see Sec. 3.8.4).

3.8.3 Convergent-Divergent Nozzle

A more complex configuration is the **Convergent-Divergent (C-D)** nozzle, which is generally used in supersonic applications where the pressure ratio described in

Eq. 3.109 is significantly high. This type of nozzle is characterized by moving parts, which can change the throat and exit areas affecting the engine thrust.

In the model developed, all engine areas remain constant, except for the throat area (A_8) and the exit area of the nozzle (A_9). They may also be set constants or variables. The exit engine area A_9 can be changed to automatically achieve $P_9 = P_0$. In some cases, the throat area will be manually adjusted from its reference value to avoid surging in certain operating conditions. These conditions appear especially when the throttle ratio is near the minimum and the flight Mach number and altitude are low as well. The first and second assumptions made for the simple convergent nozzle are still valid.

Firstly, the exit Mach number (M_9) is determined from $P_{t9}/P_{9=0}$ by using *RGCOMPR* for the real gas model or isentropic relations for the calorically perfect gas. By knowing M_9, it is possible to calculate the Mass Flow Parameter (MFP_9) and the temperature ratio (T_{t9}/T_9). The area ratio is then calculated using Eq. 3.112, taking into account the condition $P_9 = P_0$. By the temperature ratio T_{t9}/T_9, it is possible to calculate the static temperature (T_9) and subsequently, the exit velocity using the "FAIR" routine.

For On-design analysis, it is beneficial to have the throat choked, particularly if M_8 is set to 1. If the Mach number (M_9) is greater than one (choke conditions), M_8 is set equal to M_9 ($M_8 = M_9$). The throat area is then computed using the Mass Flow Parameter definition

$$A_8 = \frac{\dot{m}_8 \cdot \sqrt{T_{t8}}}{P_{t8} \cdot \text{MFP}(M_8, T_{t8}, f_8)} \tag{3.120}$$

The entire procedure remains the same for both On-design and Off-design calculations. The only difference is in the interpolation of the corrected mass flow rate ($\dot{m}_{c8}$).

3.8.4 Nozzle Map Generation and Interpolation

As mentioned earlier, the corrected mass flow rate is calculated through interpolation using the nozzle map, which is approximated to a conic function. To generate this curve, the critical pressure ratio of the nozzle and the critical mass flow rate are required as the primary inputs. Assuming that $\dot{m}_{c8,M=1}$ and $(P_t/P)_{M=1}$ are known, the corrected mass flow rate is given by

$$\frac{P_t}{P}(n) = 1.0 + \frac{n-1}{N-1} \cdot \left[\left(\frac{P_t}{P}\right)_{M=1} - 1\right] \quad \forall\ n = 1 \div N-1$$

$$\dot{m}_{c8}(n) = \dot{m}_{c8,M=1} \cdot \sqrt{1 - \frac{\left[\frac{n-1}{N-1} \cdot \left[\left(\frac{P_t}{P}\right)_{M=1} - 1\right] - \left[\left(\frac{P_t}{P}\right)_{M=1} - 1\right]\right]^2}{\left[\left(\frac{P_t}{P}\right)_{M=1} - 1\right]^2}} \quad \forall\ n = 1 \div N-1$$

The last point is calculated as follows

$$\frac{P_t}{P}(N) = 10 \cdot \frac{P_t}{P}(N-1)$$

$$\dot{m}_{c8}(N) = \dot{m}_{c8}(N-1)$$

The nozzle map is essentially a combination of two series in which the index n varies from 1 to a predefined value N.

Once the nozzle map is generated, it is possible to calculate the corrected mass flow rate at the desired pressure ratio using simple linear interpolation.

3.9 Thrust and Specific fuel consumption

From the thermodynamics cycle solution, it is possible to evaluate the engine performance, in terms of thrust, thrust-specific fuel consumption and the fuel mass flow rate. The thrust generated by the propulsion system must be compared with the aerodynamic forces and thrust weight of the reference aircraft, avoiding the over-sizing or under-sizing of the system. Completed both On-design and Off-design analysis, it is possible to calculate the **Uninstalled Thrust** as (Ref. [2]).

$$F = \dot{m}_9 V_9 - \dot{m}_0 V_0 + A_9(P_9 - P_0) \tag{3.121}$$

During mission operations, the amount of thrust that is generated by an engine is known as **Installed Thrust**. It is important to note that this value is lower than the uninstalled one due to the external drag created by the nacelle or "engine self-drag". As stated in Ref. [2], estimating engine drag losses can be achieved by examining inlet and nozzle drag

$$T = F \cdot (1 - \phi_{inlet} - \phi_{outlet}) \tag{3.122}$$

During the flight, the coefficients ϕ_{inlet} and ϕ_{outlet} of the engine can change depending on the engine throttle settings and the geometries of the inlet and the

nozzle. Although a preliminary estimation of these coefficients is possible for this thesis work. According to current literature, the installation losses account for approximately 5% of the uninstalled thrust.

The **Uninstalled Specific Thrust Fuel Consumption (SFC)** and **Installed Specific Thrust Fuel Consumption (TSFC)** can be calculated using their respective definitions.

$$\mathrm{SFC} \doteq \frac{\dot{m}_b}{F} \tag{3.123}$$

$$\mathrm{TSFC} \doteq \frac{\dot{m}_b}{T} \tag{3.124}$$

Simulations can help optimise these two important parameters. In particular, for the MORE&LESS European project, it is crucial to minimise the Thrust Specific Fuel Consumption by reducing the amount of fuel required for each flight. Therefore, during the conceptual design of supersonic aircraft, various aspects such as aerodynamics, weight, power requirements of the systems and the mission profile must be considered along with the propulsion system. A preliminary estimate for a low-bypass-ratio, mixed flow turbofan (the case of our interest) is provided by Ref. [6], which links the TSFC to the flight Mach number and altitude.

$$\mathrm{TSFC} = (1.0 + 0.35 \cdot M_0)\sqrt{\frac{T_0}{T_{ref}}} \tag{3.125}$$

Observing the Eq. 3.125, the flight Mach Number inevitably increases the fuel consumption. In other words, a greater propellant quantity must be burned to produce the same thrust. Either way, it is not possible to change this parameter since it is fixed or imposed by the mission's high-level requirements. To mitigate this effect, the flight altitude must be increased as much as possible since it implies a decrease in the external temperature.

A final consideration concerns the engine type and the role of current technology. By observing Fig. 3.21, the **Turbofan With Mixed Exhausts engine** performs less fuel consumption in the supersonic regime than the turbojet, providing the required amount of thrust as well. The current literacy and references, used for this thesis confirm this result.

3.10 Estimating the air mass flow rate

The size of the inlet diameter is crucial for ensuring sufficient air mass flow rate for engine operations and minimum frontal area for aerodynamics. Throughout this thesis, the inlet area A_1 is determined by the aircraft layout analysis and aerodynamics. Assuming that the flight Mach number at the engine intake is equal

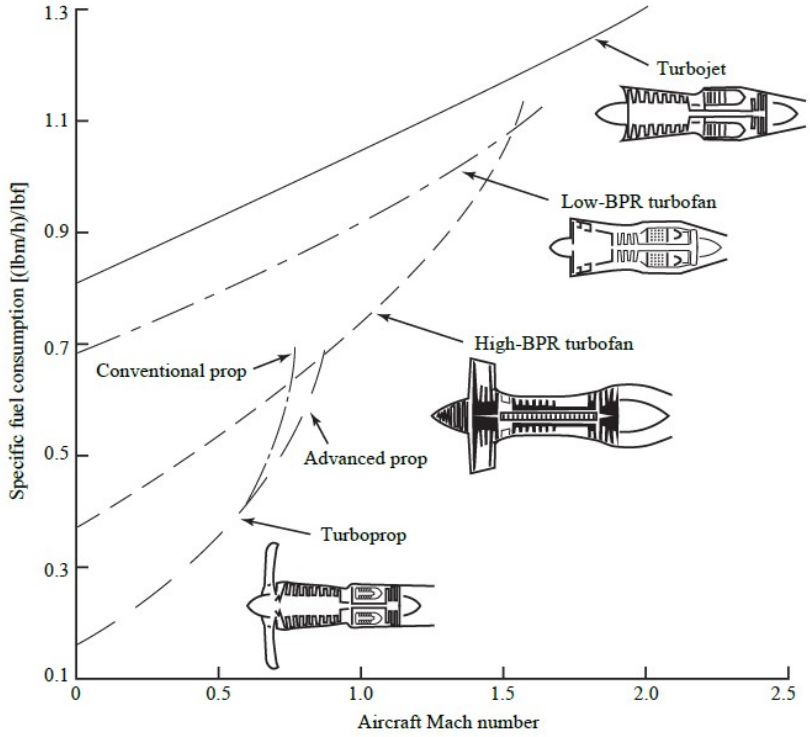

Figure 3.21: Thrust-fuel consumption characteristics of typical aircraft engines. (Pratt & Whitney)

to the flight one ($M_1 = M_0$), and an isentropic flow from station 0 to station 1, therefore using the mass conservation law ($\dot{m}_1 = \dot{m}_0$), it is possible to conclude that $A_1 = A_0$. Adding a safety factor of +5%, the air mass flow rate can be derived from the Mass flow rate parameter definition.

$$\dot{m}_0 = 1.05 \cdot \frac{P_{t0} \cdot A_1 \cdot \text{MFP}(M_0, T_{t0}, 0)}{\sqrt{T_{t0}}} \tag{3.126}$$

Another way to estimate the air mass flow rate is to use the standard values of specific thrust at sea level for low-bypass turbofan engines without afterburners. Referring to Figure 4 in the inlet section, an average value of approximately 7 $N/(kg \cdot sec)$ (69 lbf/(lbm/sec)) can be estimated. Based on the required thrust at sea level $T_{SL,req}$ given by mission requirements, it is possible to calculate the air mass flow rate at sea level while stationary.

$$\dot{m}_{0,SL} = \frac{T_{SL,req}}{T/\dot{m}_{0,SL}} \tag{3.127}$$

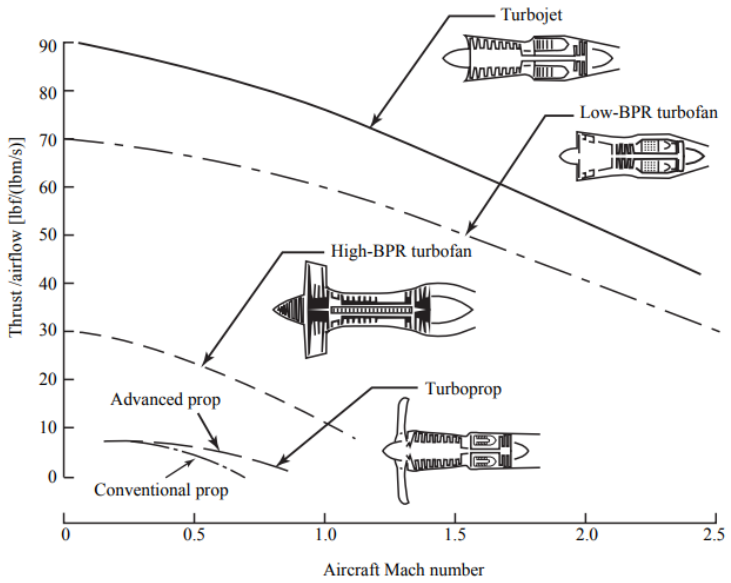

Figure 3.22: Thrust characteristics of typical aircraft engines. (Pratt & Whitney)

Engine type	Compressor pressure ratio (π_c)	Fan pressure ratio (π_f)	Bypass ratio (α)	T_{t7}, °R	T_{t4}, °R	$F/\dot{m}_0$, lbf/lbm/s	S, l/h
Turbojet	10–20	——	——	——	2000	54–58	1.0–1.1
no A/B					3000	93–96	1.3–1.4
Turbojet	10–20	——	——	3600	2000	94–101	2.0–2.2
with A/B					3000	115–119	1.7–1.8
Turbofan	20–30	2–4	0.2–1	——	2000	23–47	0.85–1.0
low α					3000	53–84	0.96–1.5
no A/B							
Turbofan	8–30	2–4	0.2–1	3600	2000	75–98	2.1–2.7
low α	10–30				3000	102–116	1.7–2.0
with A/B							
Turbofan	30–40	1.4–1.6	5–7.5	——	2000	5.5–12	0.76–0.97
high α		1.4–4	5–10		3000	13–27	0.67–1.03
no A/B							

Figure 3.23: Typical $F/\dot{m}_0$ and TSFC (S) values

The reported data in the figure are referred to *Sea Level Conditions*, so the value in reference condition is given scaling as

$$\dot{m}_0 = \dot{m}_{0,SL}\sqrt{\frac{T_{t0,SL}}{T_{t0}}}\frac{P_{t0}}{P_{t0,SL}} \tag{3.128}$$

In conclusion, it is possible to compare the two estimated values for the reference

aircraft of these study works, the equations agree with the results obtained by Ref. [14] for the case of the low-boom supersonic jet.

3.11 Theta break and throttle ratio

According to Ref. [2] and Ref. [6] a crucial parameter to choose is the **throttle ratio** defined as

$$\mathrm{TR} \doteq \frac{T_{t4,max}}{T_{t4,SLS}} \tag{3.129}$$

A typical value chosen by the industry for TR is 1.07 and it is used for this thesis work as well. The importance of the throttle ratio can be noted by considering the following equation

$$T_{t4,lim} = \theta_{t0} \cdot \frac{T_{t4,max}}{\mathrm{TR}} = \frac{T_0}{T_{ref}} \left(1 + \frac{\gamma - 1}{2} \cdot M_0^2\right) \cdot \frac{T_{t4,max}}{\mathrm{TR}} \tag{3.130}$$

As can be observed, the **maximum available temperature inlet turbine** $T_{t4,lim}$, is limited by the altitude and flight Mach number. The final throttle τ, used to tune the power and thrust setting of the entire engine is defined as

$$\tau \doteq \frac{T_{t4}}{T_{t4,lim}} \leq 1 \tag{3.131}$$

The inlet temperature turbine will vary according to the engine envelope established by Eq. 3.130 and Eq. The idle thrust is conventionally established as (Ref. [9])

$$S_{\mathrm{idl}} = 0.05 \cdot S_{\mathrm{ref}} \tag{3.132}$$

Where S_{ref} in Eq. 3.132 is the reference Uninstalled thrust. Since there is not a linear relationship between the thrust and inlet temperature turbine, a check is imposed during calculations which will stop the simulations.

3.12 Engine Level of Technology

In this chapter, the models of the main engine components are exposed, in all cases a lot of parameters are still unknown during the conceptual design of the aircraft or of the propulsion system, such as the adiabatic efficiency of the compressor e_c.

If the purpose of the model is to replicate an existing engine, then the parameters have to be tuned to the corresponding ones. In this thesis work, the main goal is to generate a database involving the performances of the propulsion system

for novel supersonic aircraft. Since its components, which will be used for the reference engine have not yet been produced today, the related parameters must be assumed. In Ref. [6] it is exposed a table (Fig. 3.24) showing the average value of the specific parameter in relation to the time and technology (**Engine Level of Technology**) and application. For our purpose, it is reasonable to assume that the future components will have the highest **level of technology IV**.

			Level of technology[b]			
Component	Figure of merit	Type[a]	1	2	3	4
Diffuser	$\pi_{d\,\max}$	A	0.90	0.95	0.98	0.995
		B	0.88	0.93	0.96	0.98
		C	0.85	0.90	0.94	0.96
Compressor	e_c		0.80	0.84	0.88	0.90
Fan	e_f		0.78	0.82	0.86	0.89
Burner	π_b		0.90	0.92	0.94	0.95
	η_b		0.88	0.94	0.99	0.999
Turbine	e_t	Uncooled	0.80	0.85	0.89	0.90
		Cooled		0.83	0.87	0.89
Afterburner	π_{AB}		0.90	0.92	0.94	0.95
	η_{AB}		0.85	0.91	0.96	0.99
Nozzle		D	0.95	0.97	0.98	0.995
	π_n	E	0.93	0.96	0.97	0.98
		F	0.90	0.93	0.95	0.97
Mechanical shaft	η_m	Shaft only	0.95	0.97	0.99	0.995
		With power takeoff	0.90	0.92	0.95	0.97
Maximum T_{t4}		(K)	1110	1390	1780	2000
		(R)	2000	2500	3200	3600
Maximum T_{t7}		(K)	1390	1670	2000	2220
		(R)	2500	3000	3600	4000

[a]A = subsonic aircraft with engines in nacelles
B = subsonic aircraft with engine(s) in airframe
C = supersonic aircraft with engine(s) in airframe
D = fixed-area convergent nozzle
E = variable-area convergent nozzle
F = variable-area convergent-divergent nozzle

[b]Notes: Stealth may reduce $\pi_{d\max}$, π_{AB}, and π_n. The levels of technology can be thought of as representing the technical capability for 20-yr increments in time beginning in 1945. Thus level 3 of technology presents typical component design values for the time period 1985–2005.

Figure 3.24: Engine Level of technology

Chapter 4

Aircraft Engine Systems Modeling

4.1 Introduction

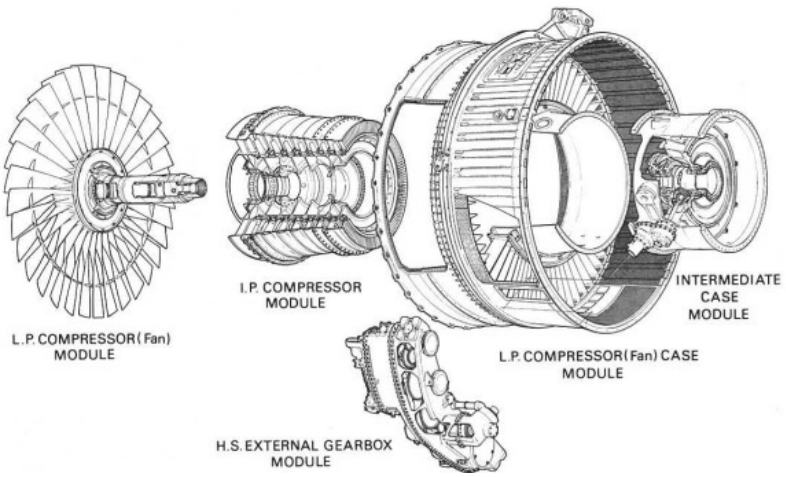

Figure 4.1: Typical jet engine architecture

The twin-spool mixed-flow turbofan engine is a sophisticated propulsion system used in aviation, specifically for military applications. It represents an evolution of the traditional turbofan design, offering enhanced performance and efficiency. This technology has played a crucial role in modern aircraft design, balancing power output and fuel efficiency. The concept of the twin-spool mixed-flow turbofan engine traces its origins back to the mid-20th century when engineers sought to

improve the efficiency and power of aircraft engines. This type of engine offers various advantages, including enhanced thrust levels, efficiency and reduced jet noise. However, several factors of its design related to the engine's complexity, mixer weight and pressure balancing must be considered.

This engine has been chosen for novel supersonic civil aircraft, as can be observed in Ref. [15] and in the "Overture Program Advances" ([1]), which will be equipped with the new engine called "*Symphony*" ([2]). This section will expose how to model the entire engine, considering this as a system of components. Particularly, the modeling of the block diagram approach is adopted.

4.2 Station Numbering

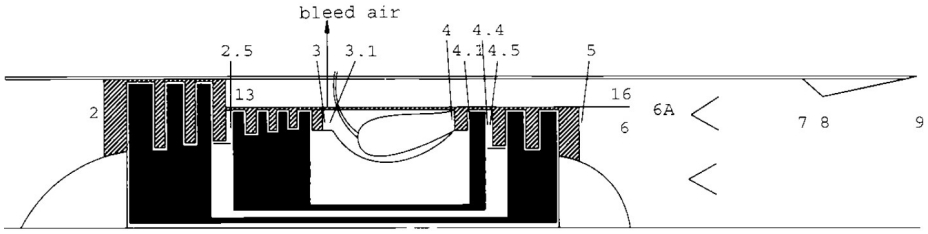

Figure 4.2: Reference Stations for Mixed-Flow Turbofan Engine.

The engine has two spools: a low-pressure spool, where a fan, a low-pressure compressor and a low-pressure turbine are installed; a high-pressure spool, where a high-pressure compressor and a high-pressure turbine are mounted, as it is possible to see in Fig. 4.2 and Fig. 4.3. The turbines are both cooled with bleed air fractions extracted from the high-pressure compressor outlet, the two flow streams, the hot from the core and the cold from the fan are mixed. The exhaust nozzle is a convergent-divergent with a variable exit area. Finally, a bleed air fraction is extracted from the high-pressure compressor. The Tab. 4.1 and Tab. 4.2 show the components of the engine with their subscript and the number of inlet stations and outlets.

The pressure and the enthalpy ratio of each component are listed in the following equations.

For the free stream, the flow is considered adiabatic and isentropic, so

[1] `https://boomsupersonic.com/`

[2] `https://boomsupersonic.com/symphony`

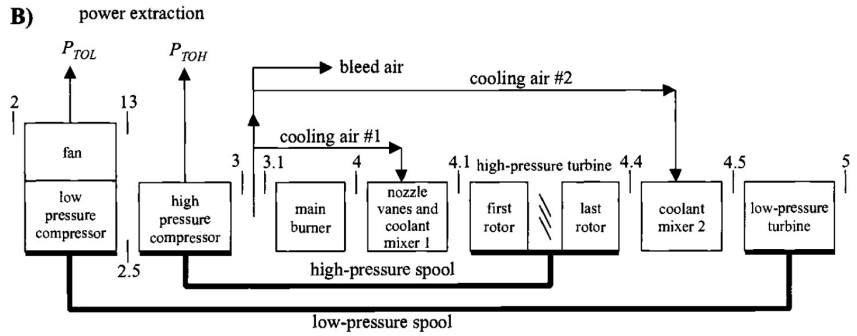

Figure 4.3: Reference Stations for Bleed and Turbine Cooling Airflows.

Subscript	Component	Station
b	Burner	$3.1 \rightarrow 4$
c	Compressor	$2 \rightarrow 3$
cH	High-pressure Compressor	$2.5 \rightarrow 3$
cL	low-pressure Compressor	$2 \rightarrow 2.5$
d	inlet	$0 \rightarrow 2$
f	fan	$2 \rightarrow 13$
-	fan duct	$13 \rightarrow 16$
m1	Coolant Mixer 1	$4 \rightarrow 4.1$
m2	Coolant Mixer 2	$4.4 \rightarrow 4.5$
M	Mixer	$6 \rightarrow 6.A$
n	Exhaust Nozzle	$7 \rightarrow 9$
t	Turbine	$4 \rightarrow 5$
tH	High-pressure turbine	$4 \rightarrow 4.5$
tL	low-pressure turbine	$4.5 \rightarrow 5$

Table 4.1: Turbofan Mixed flows: Components, stations and subscripts

$$\tau_r \doteq \frac{h_{t0}}{h_0} \qquad \pi_r \doteq \frac{P_{t0}}{P_0} = \frac{P_{tr0}}{P_{r0}} \tag{4.1}$$

For the inlet

$$\pi_d = \frac{P_{t2}}{P_{t0}} \qquad \tau_d = \frac{h_{t2}}{h_{t0}} = 1 \tag{4.2}$$

For the fan

$$\pi_f = \frac{P_{t13}}{P_{t2}} \qquad \tau_f = \frac{h_{t13}}{h_{t2}} \tag{4.3}$$

Station	Location
0	Far upstream or freestream
1	Inlet or diffuser entry
2	Inlet or diffuser exit, fan (low compressor and duct) entry
13	Fan exit
2.5	Low-pressure compressor exit
	High-pressure compressor entry
3	High-pressure compressor exit
3.1	Burner entry
4	Burner exit
	Nozzle vanes entry
	Modeled coolant mixer 1 entry
	High-pressure turbine entry
4.1	Nozzle vanes exit
	Coolant mixer 1 exit
4.4	High-pressure turbine exit
	Modeled coolant mixer entry
4.5	Coolant mixer 2 exit
	Low-pressure turbine entry
5	Low-pressure turbine exit
6	Core stream mixer entry
16	Fan bypass stream mixer entry
6A	Mixer entry
7	Exhaust nozzle entry
8	Exhaust nozzle throat
9	Exhaust nozzle exit

Table 4.2: Station and Location of Turbofan Mixed Flows

For the low-pressure compressor

$$\pi_{cL} = \frac{P_{t2.5}}{P_{t2}} \qquad \tau_{cL} = \frac{h_{t2.5}}{h_{t2}} \tag{4.4}$$

For the high-pressure compressor

$$\pi_{cH} = \frac{P_{t3}}{P_{t2.5}} \qquad \tau_{cH} = \frac{h_{t3}}{h_{t2.5}} \tag{4.5}$$

The overall pressure ratio and related temperature ratio are calculated as

$$\pi_c = \frac{P_{t3}}{P_{t2}} \qquad \tau_c = \frac{h_{t3}}{h_{t2}} \tag{4.6}$$

For the burner

$$\pi_b = \frac{P_{t4}}{P_{t3}} \qquad \tau_b = \frac{h_{t4}}{h_{t3}} \tag{4.7}$$

For the coolant mixer 1

$$\pi_{m1} = \frac{P_{t4.1}}{P_{t4}} = 1 \qquad \tau_{m1} = \frac{h_{t4.1}}{h_{t4}} \tag{4.8}$$

For the High-pressure turbine

$$\pi_{tH} = \frac{P_{t4.4}}{P_{t4}} \qquad \tau_{tH} = \frac{h_{t4.4}}{h_{t4}} \tag{4.9}$$

For the coolant mixer 2

$$\pi_{m2} = \frac{P_{t4.5}}{P_{t4.4}} = 1 \qquad \tau_{m2} = \frac{h_{t4.5}}{h_{t4.4}} \tag{4.10}$$

For the low-pressure turbine

$$\pi_{tL} = \frac{P_{t5}}{P_{t4.5}} \qquad \tau_{tL} = \frac{h_{t5}}{h_{t4.5}} \tag{4.11}$$

For the mixer

$$\pi_M = \frac{P_{t6A}}{P_{t6}} \qquad \tau_M = \frac{h_{t6A}}{h_{t6}} \tag{4.12}$$

For the exhaust nozzle

$$\pi_n = \frac{P_{t9}}{P_{t8}} \qquad \tau_n = \frac{h_{t9}}{h_{t8}} \tag{4.13}$$

For the mass flow rate, it is convenient to introduce dimensionless parameters. The most useful of these is the **bypass ratio** defined as

$$\alpha \doteq \frac{\text{bypass flow}}{\text{core flow}} = \frac{\dot{m}_F}{\dot{m}_c} \tag{4.14}$$

A leakage of air mass flow rate from the compressor (in this case high-pressure) is introduced as a fraction of the core flow

$$\beta \doteq \frac{\text{bleed flow}}{\text{core flow}} = \frac{\dot{m}_{bl}}{\dot{m}_c} \tag{4.15}$$

The cooling fractions are given by

$$\varepsilon_1 \doteq \frac{\dot{m}_{cool1}}{\dot{m}_C} \tag{4.16}$$

$$\varepsilon_2 \doteq \frac{\dot{m}_{cool2}}{\dot{m}_C} \tag{4.17}$$

Other important parameters are related to the fuel-to-air ratios across the stations since these will be one of the primary inputs of the *FAIR* function (see Sec. 2.3.4). In this case, the fuel-to-air ratio in the burner is defined as

$$f \doteq \frac{\text{burner fuel flow}}{\text{burner inlet air flow}} = \frac{\dot{m}_b}{\dot{m}_{3.1}} \tag{4.18}$$

The mixer bypass ratio (Sec. 3.7.2) is given by

$$\alpha' = \frac{\text{fan air entering mixer}}{\text{turbine gas entering mixer}} = \frac{\dot{m}_{16}}{\dot{m}_6} \tag{4.19}$$

The fuel-to-air ratio at station 4.1 is given considering

$$f_{4.1} = \frac{f}{1 + f + \varepsilon_1/(1 - \beta - \varepsilon_1 - \varepsilon_2)} \tag{4.20}$$

The fuel-to-air ratio at station 4.5 is given considering

$$f_{4.5} = \frac{f}{1 + f + (\varepsilon_1 + \varepsilon_2)/(1 - \beta - \varepsilon_1 - \varepsilon_2)} \tag{4.21}$$

The mixer fuel-to-air ratio is given by

$$f_{6A} = \frac{f_{4.5}(1 - \beta)}{1 + \alpha - \beta} \tag{4.22}$$

Through the fan duct (stations 13- 16), it has assumed an isentropic expansion, therefore $P_{t13} = P_{t16}$, $h_{t13} = h_{t16}$ and it has the same from 3 to 3.1 as well, leading to $P_{t3.1} = P_{t3}$, $h_{t3} = h_{t3.1}$. The station numbers are assigned following Ref. [2], as shown in the scheme reported in Fig. 4.2 and Fig. 4.3,

Finally, considering the scheme reported in Fig. 4.3 and the exposed parameters, it is possible to relate the core mass flow rate to one of each station

$$\dot{m}_0 = \dot{m}_C + \dot{m}_F = (1 + \alpha)\dot{m}_C \tag{4.23}$$

$$\dot{m}_3 = \dot{m}_C \tag{4.24}$$

$$\dot{m}_{3.1} = \dot{m}_c(1 - \beta - \varepsilon_1 - \varepsilon_2) \tag{4.25}$$

$$\dot{m}_4 = \dot{m}_C(1 - \beta - \varepsilon_1 - \varepsilon_2) \tag{4.26}$$

$$\dot{m}_{4.1} = \dot{m}_{4.4} = \dot{m}_C \left[(1 - \beta - \varepsilon_1 - \varepsilon_2)(1 + f) + \varepsilon_1\right] \tag{4.27}$$

$$\dot{m}_{4.5} = \dot{m}_5 = \dot{m}_C \left[(1 - \beta - \varepsilon_1 - \varepsilon_2)(1 + f) + \varepsilon_1 + \varepsilon_2\right] \tag{4.28}$$

4.3 Model Assumptions - Matrix Iteration Method

The following assumptions are employed:

- The flow is, on average, steady.
- The flow is one-dimensional at the entry of each component and at each axial station.
- The working fluid is modeled as a "half-ideal gas" using Variable Specific Heat.
- The inlet is modeled according to MIL-E-5008B.
- The low-pressure turbine drives the fan and low-pressure compressor and provides mechanical power for accessories (P_{TOL}).
- The high-pressure turbine drives the high-pressure compressor and provides mechanical power for accessories (P_{TOH}).
- The flow in the bypass duct is isentropic.
- The turbines are cooled.
- The mixer is modeled with a "Constant Area Mixer" model.

For off-design simulations, additional assumptions are required:

- The flow areas are constant at stations 4, 4.5, 6, 16 and 6A.
- The exit area of the nozzle (A_9) is adjustable to maintain the exit pressure ratio of the exhaust equal to the external one ($P_9 = P_0$) or to a selected ratio P_9/P_0.
- The area of station 8 remains constant to its reference value.
- The map scaling procedure is adopted.
- The Off-design non-linear system is solved using the Newton-Raphson algorithm.

4.4 Engine Off-design - Matrix Iteration Method: Balancing Equations

The **Matrix Iteration Method** also known as **Components Matching Method** is used for off-design simulations, which employs the balancing equation of power and (corrected) mass flow rate. In the case of dual-spool mixed flows, **the vector state** chosen follows Ref. [16], although the present method is expected to align with Refs. [17], [9] and [18].

$$\vec{\mathbf{X}} = \{\pi_{cL}, \pi_{cH}, \pi_{tL}, \pi_{tH}, (\%N_{cL}), (\%N_{cH})\}^T \tag{4.29}$$

Then, it is necessary to formulate the **Function Vector** requiring at least six balancing equations, as discussed above.

The first equation is derived from **low-pressure spool power balance** (see Sec. 3.5.3), considering that the low-pressure turbine drives the fan (duct and core). For hypothesis [5], mechanical power extraction is considered, in the equation, yielding

$$\dot{m}_{2.5}(h_{t2.5} - h_{t2}) + \alpha\ \dot{m}_{13}(h_{t13} - h_{t2}) + P_{TOL}/\eta_{mPL} = \dot{m}_{4.5}(h_{t4.5} - h_{t5})\eta_{mL} \tag{4.30}$$

The second equation involves **power balance at the high-pressure spool**, also accounting for mechanical power extraction (hypothesis [6])

$$\dot{m}_{2.5}(h_{t3} - h_{t2.5}) + P_{TOH}/\eta_{mPH} = \dot{m}_{4.1}(h_{t4.1} - h_{t4.4})\eta_{mH} \tag{4.31}$$

The third equation pertains to the constant-area mixer model (see Sec. 3.7.2), ensuring the **Kutta condition**

$$P_6 = P_{16} \tag{4.32}$$

The other four equations relate to the conservation of the corrected mass flow rate through components. Specifically, the fourth equation deals with the **congruence of the corrected mass flow rate between the high-pressure compressor and the high-pressure turbine**

$$\dot{m}_{c4.1} = \dot{m}_{c2.5}\left[(1 - \beta - \varepsilon_1 - \varepsilon_2)(1 + f) + \varepsilon_1\right]\frac{P_{t2.5}}{P_{t4.1}}\sqrt{\frac{T_{t4.1}}{T_{t2.5}}} \tag{4.33}$$

The fifth equation involves the conservation of the **corrected mass flow rate between the high-pressure compressor and the low-pressure turbine**

$$\dot{m}_{c4.5} = \dot{m}_{c2}\frac{\left[(1 - \beta - \varepsilon_1 - \varepsilon_2)(1 + f) + \varepsilon_1 + \varepsilon_2\right]}{1 + \alpha}\frac{P_{t2}}{P_{t4.5}}\sqrt{\frac{T_{t4.5}}{T_{t2}}} \tag{4.34}$$

The sixth equation pertains to nozzle-engine matching and addresses the congruence of **the corrected mass flow between the mass flow rate at the inlet of the nozzle and the low-pressure compressor**

$$\dot{m}_{c8} = \dot{m}_{c2} \frac{[(1-\beta-\varepsilon_1-\varepsilon_2)(1+f)+\varepsilon_1+\varepsilon_2]}{1+\alpha} \frac{P_{t2}}{P_{t8}} \sqrt{\frac{T_{t8}}{T_{t2}}} \tag{4.35}$$

During off-design calculations, the fan is modeled as a compressor, using a different map interpolation. As expected, the fan's corrected speed ratio is identical to that of the low-pressure compressor.

$$(\%N_{cL})_{\text{fan}} = (\%N_{cL})_{\text{LPC}} = (\%N_{cL}) \tag{4.36}$$

To interpolate the data from the map, the fan pressure ratio π_f is required. However, including this variable in the vector would introduce inconsistency in the problem formulation. The low-pressure compressor and fan must exhibit equal corrected mass flow rates, satisfying

$$(\dot{m}_{c2})_{\text{fan}} = (\dot{m}_{c2})_{\text{LPC}} = \dot{m}_{c2} \tag{4.37}$$

By definition, the two interpolated corrected mass flow rates must be equal and, consequently, the fan pressure ratio is constrained by the low-pressure compressor operating point. This procedure entails calculating the low-pressure compressor first (as a reminder of the calculation in Sec. 3.3.5) and then employing the fan with the mentioned modification. Of course, the reverse procedure is also applicable. The bypass ratio appears in the presented equations and it is calculated using the corrected mass flow of the fan $\dot{m}_{c2}$ and $\dot{m}_{c3}$ of the high-pressure compressor, following the definition of corrected mass flow rate.

The function vector is formulated by rewriting the equations from Eq. 4.30 to Eq. 4.35 as follows

$$\vec{\mathbf{F}}(\vec{\mathbf{X}}) = \left\{ \begin{array}{c} P_{cL} + P_{cf} + P_{TOL}/\eta_{mPL} - P_{tL}\eta_{mL} \\ P_{cH} + P_{TOH}/\eta_{mPH} - P_{tH}\eta_{mH} \\ P_6 - P_{16} \\ \dot{m}_{c4.1} - \dot{m}_{c2.5}\,[...]\,P_{t2.5}/P_{t4.1}\sqrt{T_{t4.1}/T_{t2.5}} \\ \dot{m}_{c4.5} - \dot{m}_{c2}[...]/(1+\alpha)P_{t2}/P_{t4.5}\sqrt{T_{t4.5}/T_{t2}} \\ \dot{m}_{c8} - \dot{m}_{c2}[...]/(1+\alpha)P_{t2}/P_{t8}\sqrt{T_{t8}/T_{t2}} \end{array} \right\} = \vec{\mathbf{0}} \tag{4.38}$$

Each equation represents a function of the vector state, resulting in a **nonlinear system**.

$$\vec{\mathbf{F}}(\vec{\mathbf{X}}) = \begin{Bmatrix} f_1(\{\pi_{cL}, \pi_{cH}, \pi_{tL}, \pi_{tH}, (\%N_{cL}), (\%N_{cH})\}^T) \\ f_2(\{\pi_{cL}, \pi_{cH}, \pi_{tL}, \pi_{tH}, (\%N_{cL}), (\%N_{cH})\}^T) \\ f_3(\{\pi_{cL}, \pi_{cH}, \pi_{tL}, \pi_{tH}, (\%N_{cL}), (\%N_{cH})\}^T) \\ f_4(\{\pi_{cL}, \pi_{cH}, \pi_{tL}, \pi_{tH}, (\%N_{cL}), (\%N_{cH})\}^T) \\ f_5(\{\pi_{cL}, \pi_{cH}, \pi_{tL}, \pi_{tH}, (\%N_{cL}), (\%N_{cH})\}^T) \\ f_6(\{\pi_{cL}, \pi_{cH}, \pi_{tL}, \pi_{tH}, (\%N_{cL}), (\%N_{cH})\}^T) \end{Bmatrix} \tag{4.39}$$

To solve this nonlinear system of equations, the Newton-Raphson method is implemented in conjunction with the component models presented in chapter 3. During the Off-design phase, the state vector essentially represents the **list of dependent variables** of the engine. In order to obtain a solution, the **independent variables** must be specified. These include:

- The flight Mach Number M_0
- The external pressure P_0 and temperature T_0
- The burner exit temperature T_{t4}

By using the International Standard Atmosphere (ISA) model (Sec. 3.1 and Appendix A.1), it is possible to relate the external pressure and temperature to the flight altitude. Furthermore, the mechanical power extraction and bleed air may vary during the flight. Hence, P_{TOL}, P_{TOH} and β are also independent.

Table 4.3: Engine Dependent and Independent Variables

Variable	Nomenclature	Designation Group
Flight Mach Number	M_0	Flight Conditions
Flight Altitude	h or Alt	Flight Conditions
Main burner exit temperature	T_{t4}	Throttle Settings
Mechanical power extractions	P_{TOL} and P_{TOH}	Engine System Interface
Air leakage	β	Engine System Interface

The parameters listed in Tab. 4.3 are provided by the user to simulate specific flight conditions and throttle settings. Deviations of the independent parameters from the reference point introduce **imbalances in the equations**. Consequently, the state vector must be computed to satisfy each parameter. In other words, the operating conditions of the compressor and turbine must be regulated to achieve a new engine operating condition (if applicable) while meeting mixer and nozzle constraints. To compute this new state vector, the **Newton-Raphson Method** is employed.

4.5 Engine Off-design - The Newton-Raphson Method

In the preceding section, the problem formulation was presented. The primary objective is to find a solution for the state vector that satisfies all equilibrium equations. To achieve this, the **Newton-Raphson Method** is employed in the case of a multidimensional vector. As per Refs. [9], [17] and [16], the mathematical formulation of the Off-design engine regulation involves finding the state vector such that

$$\vec{F}(\vec{X}) = \vec{F}(\vec{X}_0) + \left[\frac{\partial F}{\partial X}\right] \cdot \left(\vec{X} - \vec{X}_0\right) = \vec{0} \tag{4.40}$$

In Eq. 4.40, the function vector $\vec{F}$ is equal as formulated in Eq. 4.38 and 4.39, $\vec{X}_0$, is the state vector in the previous iteration, of course, if the first is considered, it will be equal to the reference one, and $\vec{F}_0$ is the function vector computed in $\vec{X}_0$. The **Jacobian Matrix** is calculated as

$$\left[\frac{\partial F}{\partial X}\right] = \begin{Bmatrix} \frac{\partial f_1}{\partial \pi_{cL}} & \frac{\partial f_1}{\partial \pi_{cH}} & \frac{\partial f_1}{\partial \pi_{tL}} & \frac{\partial f_1}{\partial \pi_{tH}} & \frac{\partial f_1}{\partial (\%N_{cL})} & \frac{\partial f_1}{\partial (\%N_{cH})} \\ \frac{\partial f_2}{\partial \pi_{cL}} & \frac{\partial f_2}{\partial \pi_{cH}} & \frac{\partial f_2}{\partial \pi_{tL}} & \frac{\partial f_2}{\partial \pi_{tH}} & \frac{\partial f_2}{\partial (\%N_{cL})} & \frac{\partial f_2}{\partial (\%N_{cH})} \\ \frac{\partial f_3}{\partial \pi_{cL}} & \frac{\partial f_3}{\partial \pi_{cH}} & \frac{\partial f_3}{\partial \pi_{tL}} & \frac{\partial f_3}{\partial \pi_{tH}} & \frac{\partial f_3}{\partial (\%N_{cL})} & \frac{\partial f_3}{\partial (\%N_{cH})} \\ \frac{\partial f_4}{\partial \pi_{cL}} & \frac{\partial f_4}{\partial \pi_{cH}} & \frac{\partial f_4}{\partial \pi_{tL}} & \frac{\partial f_4}{\partial \pi_{tH}} & \frac{\partial f_4}{\partial (\%N_{cL})} & \frac{\partial f_4}{\partial (\%N_{cH})} \\ \frac{\partial f_5}{\partial \pi_{cL}} & \frac{\partial f_5}{\partial \pi_{cH}} & \frac{\partial f_5}{\partial \pi_{tL}} & \frac{\partial f_5}{\partial \pi_{tH}} & \frac{\partial f_5}{\partial (\%N_{cL})} & \frac{\partial f_5}{\partial (\%N_{cH})} \\ \frac{\partial f_6}{\partial \pi_{cL}} & \frac{\partial f_6}{\partial \pi_{cH}} & \frac{\partial f_6}{\partial \pi_{tL}} & \frac{\partial f_6}{\partial \pi_{tH}} & \frac{\partial f_6}{\partial (\%N_{cL})} & \frac{\partial f_6}{\partial (\%N_{cH})} \end{Bmatrix} \tag{4.41}$$

In practice, the Jacobian is computed numerically by considering a small increment ε, therefore it is possible to use the following expression for the computation

$$\frac{\partial F_{i,j}}{\partial X_j} = \frac{F_{i,j} - F_{0,i,j}}{X_j - X_{0,i,j}} = \frac{F_{i,j} - F_{0,i,j}}{\varepsilon X_{0,j}} \tag{4.42}$$

As per Ref. [9], the Eq. 4.40 can be formulated as a linear system of equations

$$[A]\vec{X} = \vec{b} \tag{4.43}$$

In Eq. 4.43, the matrix $[A]$ is equivalent to the Jacobian and the known vector $\vec{b}$ is given by

$$\vec{b} = \left[\frac{\partial F}{\partial X}\right] \cdot \vec{X}_0 - \vec{F}_0 \tag{4.44}$$

The solution of the system is obtained by multiplying the inverse of the Jacobian with the known vector. This operation is carried out using the lower-upper (LU) decomposition, employing the MATLAB function "lu" (see lu documentation in Ref. [19]). The state vector is iterative and requires a convergence criterion, which is determined by a residual defined as

$$\text{res} \doteq \frac{\|\vec{R}\| - \|\vec{R}_0\|}{\|\vec{R}_0\|} \tag{4.45}$$

Where:

$$\vec{R} = \left[\frac{\pi_{cL}}{\pi_{cL,r}}, \frac{\pi_{cH}}{\pi_{cH,r}}, \frac{\pi_{tL}}{\pi_{tL,r}}, \frac{\pi_{tH}}{\pi_{tH,r}}, \frac{(\%N_{cL})}{(\%N^r_{cL})}, \frac{(\%N_{cH})}{(\%N^r_{cH})}\right]^T \tag{4.46}$$

$$\vec{R}_0 = \left[\frac{\pi_{cL,0}}{\pi_{cL,r}}, \frac{\pi_{cH,0}}{\pi_{cH,r}}, \frac{\pi_{tL,0}}{\pi_{tL,r}}, \frac{\pi_{tH,0}}{\pi_{tH,r}}, \frac{(\%N_{cL,0})}{(\%N^r_{cL})}, \frac{(\%N_{cH,0})}{(\%N^r_{cH})}\right]^T \tag{4.47}$$

In Eq. 4.46 and Eq. 4.47, all parameters with "r" subscript refer to reference conditions (On-design). The entire procedure is implemented using the **MATLAB** environment, as previously described. The chosen values for the residual and increment are

$$\varepsilon = 10^{-12} \tag{4.48}$$

$$\text{res} = 10^{-13} \tag{4.49}$$

It is important to note that choosing a very small increment and residual is essential to achieve an accurate solution. However, reducing the increment below 10^{-14} leads to numerical instabilities due to the *machine precision* of the MATLAB environment. Additionally, an excessively small tolerance increases simulation time. Therefore, the specified parameters offer a balance between accuracy and computational efficiency.

4.6 Engine Off-design - Serial Nested Loops Procedure

Another possible procedure to solve the Off-design engine cycle of the dual-spool turbofan with mixed exhausts is exposed in Ref. [2] and Ref. [6] elaborated by professor J.D. Mattingly and professor G.C. Oates. This procedure calculates the engine's Off-design performances, solving the cycle, without the use of the components' map and introducing a simplification in the component efficiencies. The hypothesis of the model are

- The flow is, on average, steady.
- The flow is one-dimensional at the entry of each component and at each axial station.
- The working fluid is modeled as a "half-ideal gas" using Variable Specific Heat.
- The inlet is modeled according to MIL-E-5008B.
- The low-pressure turbine drives the fan and low-pressure compressor and provides mechanical power for accessories (P_{TOL}).
- The high-pressure turbine drives the high-pressure compressor and provides mechanical power for accessories (P_{TOH}).
- The flow in the bypass duct is isentropic.
- The turbines are cooled.
- The mixer is modeled with a "Constant Area Mixer" model.
- The flow areas are constant at stations 4, 4.5, 6, 16 and 6A.
- The exit area of the nozzle (A_9) is adjustable to maintain the exit pressure ratio of the exhaust equal to the external one ($P_9 = P_0$) or to a selected value P_9/P_0.
- The area of station 8 changes to maintain constant pressure at the nozzle entrance.
- The flow is choked at the high-pressure turbine entrance nozzle (choking area 4), at the low-pressure entrance nozzle (choking area 4.5) and at the exhaust nozzle (station 8). At the low throttle settings, the nozzle throat may be unchoked so this particular case is carried out too.

- The components efficiencies (η_f, η_{cL}, η_{cH}, η_b, η_{tL}, η_{tH}, η_b, η_{mL}, η_{mH}, η_{mPL}, η_{mPH}) also the component pressure ratios (π_b, $\pi_{M,max}$, π_n) remain constants, each parameter assumes the value obtained from On-design Analysis.
- Bleed air and cooling air fractions and power extractions are all constants.

High-pressure turbine and low-pressure turbine are reasonably considered chocked in their entrance stator airfoils since both are originally designed to work under such circumstances. Generally, it is possible to assume that in a great range of operative conditions, the exposed hypothesis related to the turbines is valid, except for the descending and landing phases, in which the throttle ratio is as low as the altitude and flight Mach number. This limits the use of the described procedure, as exposed in Appendix D. of Ref. [2].

The analysis begins from the high-pressure turbine thermodynamics state, following the low-pressure one. Specifically, from the Mass flow rate parameter definition, it is possible to write

$$\frac{\dot{m}_4}{\dot{m}_{4.5}} \frac{P_{t4.5}/P_{t4}}{\sqrt{T_{t4.5}/T_{t4}}} = \frac{\mathrm{MFP}(M_{4'}, T_{t4}, f)}{\mathrm{MFP}(M_{4.5'}, T_{t4.5}, f_{4.5})} \tag{4.50}$$

Considering Eq. 4.26 and Eq. 4.28 for the mass flow rates and since π_{m2}, $\pi_{tH} = P_{t4.4}/P_{t4}$, then

$$\frac{\pi_{tH}}{\sqrt{T_{t4.5}/T_{t4}}} = \left[1 + \frac{(\varepsilon_1 + \varepsilon_2)}{(1 - \beta - \varepsilon_1 - \varepsilon_2)(1 + f)}\right] \frac{A_4}{A_{4.5}} \frac{\mathrm{MFP}(M'_4,\ T_{t4},\ f)}{\mathrm{MFP}(M'_{4.5},\ T_{t4.5},\ f_{4.5})} \tag{4.51}$$

the Mach Numbers at stations 4 (M_4) and 4.5 ($M_{4.5}$) are equal to 1 for the hypothesis, the cooling air ε_1, ε_2 and bleed β fractions are also constants and the fuel-to-air f ratio changes with really small rates, thus

$$\frac{\pi_{tH}}{\sqrt{T_{t4.5}/T_{t4}}} \propto \frac{\mathrm{MFP}(1,\ T_{t4},\ f)}{\mathrm{MFP}(1,\ T_{t4.5},\ f_{4.5})} \tag{4.52}$$

The Eq. 4.61 implies that for a value of T_{t4} and f, the turbine enthalpy ratio π_{tH} and stagnation temperature at the turbine outlet $T_{t4.5}$ are fixed and it is possible to obtain them by using an iterative procedure. Assuming the enthalpy at station 4 (h_{t4}) and fuel-to-air ratio (f) which are both given by throttle settings, it is possible to calculate the fuel-to-air at station 4.5 by Eq. 4.21. Then the following steps are performed

1. Assuming the exit turbine temperature equal to reference conditions for the first iteration

$$T_{t4.5}^{(n)} = T_{t4.5,r} \tag{4.53}$$

2. The total enthalpy at station 4.1 is given using

$$h_{t4.1} = h_{t4}\frac{h_{t4.1}}{h_{t4}} = h_{t4}\tau_{m1} \tag{4.54}$$

where τ_{m1} is given by

$$\tau_{m1} = \frac{(1-\beta-\varepsilon_1-\varepsilon_2)(1+f)+\varepsilon_1\tau_r\tau_{cL}\tau_{cH}/\tau_\lambda}{(1-\beta-\varepsilon_1-\varepsilon_2)(1+f)+\varepsilon_1} \tag{4.55}$$

3. Using the definition, it is possible to evaluate the reduced pressure in ideal conditions at station 4.4

$$P_{rt4.4i} = \pi_{tH}P_{rt4.1} \tag{4.56}$$

4. The high-pressure turbine adiabatic efficiency is constant and known per Hypothesis, so it is possible to evaluate

$$\tau_{tH} = 1-\eta_{tH}(1-\tau_{tHi}) \tag{4.57}$$

5. It is possible to evaluate the enthalpy ratio at the coolant Mixer 2 as

$$\tau_{m2} = \frac{(1-\beta-\varepsilon_1-\varepsilon_2)(1+f)+\varepsilon_1+\varepsilon_2\left[\tau_r\tau_{cH}\tau_{cL}/(\tau_\lambda\tau_{m1}\tau_{tH})\right]}{(1-\beta-\varepsilon_1-\varepsilon_2)(1+f)+\varepsilon_1+\varepsilon_2} \tag{4.58}$$

6. Given h_{t4}, τ_{m1}, τ_{tH}, τ_{m2} and $f_{4.5}$ the total enthalpy at station 4.5 is calculated as

$$h_{t4.5} = h_{t4}\frac{h_{t4.1}}{h_{t4}}\frac{h_{t4.4}}{h_{t4.1}}\frac{h_{t4.5}}{h_{t4.4}} = h_{t4}\tau_{m1}\tau_{tH}\tau_{m2} \tag{4.59}$$

7. Using the FAIR routine, it is possible to evaluate the temperature at station 4.5 for n-iteration $T_{t4.5}$ then this is compared with the supposed one. If the absolute error is greater than 0.01 then

$$T_{t4.5}^{(n)} = T_{t4.5} \tag{4.60}$$

The steps are repeated from 2 to 7 and the iterations are performed until convergence.

A really similar consideration could be done for the low-pressure turbine, but in this case, the conditions to satisfy is

$$\frac{\pi_{tL}}{\sqrt{T_{t5}/T_{t4.5}}} = \frac{A_{4.5}}{A_6}\frac{\mathrm{MFP}(M'_{4.5},\ T_{t4.5},\ f_{4.5})}{\mathrm{MFP}(M'_6,\ T_{t5},\ f_{4.5})} \tag{4.61}$$

The two described iterative procedures for the turbine solutions are implemented in two MATLAB functions, called "TURBC" and "TURB".

By knowing all turbine parameters and states, it is possible to complete the entire Off-design procedure as follows: the low-pressure turbine imposes a constrain in the fan enthalpy calculation, by the low-pressure spool power balance equation (Sec. 3.5.3). Therefore, it is possible to calculate the fan exit total enthalpy h_{t13} and the related ratio τ_f as

$$\tau_f = 1 + \frac{(1-\tau_{tL})\eta_{mPL}\left[\frac{\dot{m}_4}{\dot{m}_c}\frac{\tau_\lambda \tau_{tH}}{\tau_r} + (\varepsilon_1\tau_{tH} + \varepsilon_2)\tau_{cL}\tau_{cH}\right] - \frac{(1+\alpha)}{\tau_r\eta_{mPL}}\frac{P_{TOL}}{\dot{m}_0 h_0}}{(\tau_{cL}-1)/(\tau_f - 1) + \alpha} \tag{4.62}$$

It is reasonable that the enthalpy ratio across the fan is proportional to the low-compressor one

$$\frac{h_{t13} - h_{t2}}{h_{t2.5} - h_{t2}} = \frac{\tau_f - 1}{\tau_{cL} - 1} = \frac{\tau_{f,r} - 1}{\tau_{cL,r} - 1} \tag{4.63}$$

The enthalpy ratio of the low-pressure compressor can be determined as

$$\tau_{cL} = 1 + (\tau_f - 1)[(\tau_{cL,r} - 1)/(\tau_{f,r} - 1)] \tag{4.64}$$

Thus, it is possible to calculate the total enthalpy and pressure as follows

$$h_{t13i} = h_{t2}[1 + \eta_f(\tau_f - 1)] \tag{4.65}$$

Given h_{t13i}, the reduced pressure P_{rt13i} is calculated using the FAIR routine

$$\pi_f = \frac{P_{rt13i}}{P_{rt2}} \tag{4.66}$$

Similarly, it is possible to obtain the total exit enthalpy for the low-pressure compressor

$$h_{t2.5i} = h_{t2}[1 + \eta_{cL}(\tau_{cL} - 1)] \tag{4.67}$$

$$\pi_{cL} = \frac{P_{rt2.5i}}{P_{rt2}} \tag{4.68}$$

The same calculations may be done for high-pressure compressor

$$\tau_{cH} = \frac{1 + (1-\tau_{tH})\eta_{mH}\left[(1-\beta-\epsilon_1-\epsilon_2)(1+f)\left(\frac{\tau_\lambda}{\tau_r\tau_{cLL}}\right) - \left[\frac{(1+\alpha)}{\tau_r\tau_{cL}\eta_{mPH}}\right]\frac{P_{TOL}}{\dot{m}_0 h_0}\right]}{1 - \epsilon_1(1-\tau_{tH})\eta_{mH}} \tag{4.69}$$

$$h_{t3i} = h_{t2.5}[1 + \eta_{cH}(\tau_{cH} - 1)] \tag{4.70}$$

$$\pi_{cH} = \frac{P_{rt3i}}{P_{rt2.5}} \tag{4.71}$$

The mixer model is the same as the one reported in Sec. 3.7.2, but in this case the Kutta condition is imposed directly for the Off-design calculations. The Mach at station 16 is calculated from compressors and turbines settings

$$\frac{P_{t16}}{P_{t6}} = \frac{\pi_f}{\pi_{cL}\pi_{cH}\pi_b\pi_{tH}\pi_{tL}} \tag{4.72}$$

The Mach at station 16 is imposed in order to have $P_{t16} > P_{t6}$ (flow in the proper direction) and subsonic ($M_{16} < 1$). The bypass ratio at the mixer entrance is calculated by definition

$$\alpha' = \frac{\pi_f}{\pi_{cL}\pi_{cH}\pi_b\pi_{tH}\pi_{tL}} \frac{A_{16}}{A_6} \frac{\mathrm{MFP}_{16}}{\mathrm{MFP}_6} \sqrt{\frac{T_{t6}}{T_{t16}}} \tag{4.73}$$

From Eq. 4.73 it is possible to calculate the bypass ratio from the definition

$$\alpha = \alpha' \left[(1 - \beta - \varepsilon_1 - \varepsilon_2)(1 + f) + \epsilon_1 + \epsilon_2\right] \tag{4.74}$$

The Mach number at station 6 is calculated from the mass flow rate parameter and mass conservation

$$\mathrm{MFP}_6 = \frac{P_{t8}}{P_{t6}} \frac{A_8}{A_6} \frac{\mathrm{MFP}_8}{(1 + \alpha)} \sqrt{\frac{T_{t6}}{T_{t6A}}} \tag{4.75}$$

To conclude, it is possible to calculate the inlet mass flow rate parameter and the Mach number at station 9, from the definition of the bypass ratio

$$\dot{m}_0 = (1 + \alpha)\dot{m}_c = (1 + \alpha)\frac{P_{t4} A_4 \mathrm{MFP}_4}{\sqrt{T_{t4}}} = \tag{4.76}$$

$$= \frac{(1 + \alpha) P_0 \pi_r \pi_f \pi_{cL} \pi_{cH} \pi_b}{(1 - \beta - \varepsilon_1 - \varepsilon_2)(1 + f)} \frac{A_4}{\sqrt{T_{t4}}} \mathrm{MFP}_4 \tag{4.77}$$

The Mach number is calculated from the nozzle model (see Sec. 3.8.3), considering a convergent-divergent nozzle.

The system of equations is also nonlinear: to solve it, an ad-hoc algorithm must be set. The dependent variables to be calculated for all iterations are f, α', M_6, M_8 and $\dot{m}_0$. The total number of equations is 24: each one is related to a specific variable. The algorithm is divided into four blocks, each one has an error check and

the flow of calculations is reported in Ref. [2]. This simple algorithm has been used for the first iteration of database development, due to its versatility and simplicity of implementation. The related results are therefore shown in Sec. 5.6.2.

4.7 Engine weight estimation

During the conceptual design and system sizing, a crucial aspect is related to the system weight for all aerospace applications, the propulsion system is also involved. It is impossible to exactly calculate the mass of the engine in these early phases, therefore simple formulas for estimation may be used in order to give a preliminary "idea" of the future weight.

According to Ref.[20] the most accurate formula is developed by E. Torenbeek and is reported in Eq. 4.78. This relation is used in a similar work of this thesis Ref. [15].

$$m_{eng} = 12.24 \cdot F_{N,\text{ref}} \cdot \left(1 - \frac{1}{\sqrt{1 + 0.75 \cdot \alpha}}\right) + \dot{m}_0 \cdot \frac{10 \cdot \alpha^{0.25}}{1 + \alpha} \tag{4.78}$$

The engine mass result m_{eng} is given in kilograms kg. The main input of the formula is the $F_{N,\text{ref}}$, which is the thrust produced by the engine in reference condition given in kN. Besides this, the air mass flow rate $\dot{m}_0$ and the bypass ratio α must be given as inputs as well.

4.8 Propulsive database generation

The main goal of this thesis work is to generate the propulsive databases for the reference case study. At this point of the discussion, it is easy to explain how to develop a propulsive database. After the On-design calculations, many Off-design iterations might be run by varying the throttle, the flight Mach number and the altitude (Independent Variables). Of course, in real operative conditions, other parameters may change during the flight, such as the power request by other systems and the bleed air of the aircraft. However, it is reasonable to consider these two parameters in the worst-case scenario and constants, since they have no significant impact on engine performance.

To conclude, it is possible to summarise the database generation in the following steps

1. **Propulsion system requirements analysis**: the requirements are always the starting point of the entire procedure. Without them, it is impossible to size an engine that is configured for the aircraft. These are derived from the previous analyses of the aircraft and from the initial sizing of its systems.

Figure 4.4: ASTOS Software logo

2. **Selecting the engine type and the overall architecture**: having a clear idea of which engine type is more appropriate for the reference study and considering different configurations such as turbofan mixed, turbofan separated, turbojet with a single spool or dual spools. This step is probably really hard to develop because engine simulations require a lot of parameters as input that are unknown. In the early phase of the project, in this case, a good suggestion is to carefully analyse the propulsion systems of other aircraft belonging to the same category of reference one. At the end of this step, the overall architecture of the engine is known and it is possible to represent it using a block diagram.

3. **On-design/reference point selection**: by knowing the architecture, it is possible to set up a thermodynamic model of the engine in order to size it, matching all requirements expressed above and the figure of merit that could be reached using trial and error techniques.

4. **Off-design simulations**: the off-design or the "regulation" of the engine evaluates the performance of the engine in different conditions, using one or both two exposed algorithms. An example is the take-off thrust which the engine must provide. According to all references of this study, the procedure is iterative, in which if the Off-design results do not satisfy the constraint, the only way is to change the On-design or Off-design reference point.

5. **Engine database building**: at this point, the conceptual design of the entire propulsion system is completed and it is possible to run different Off-design simulations, changing the flight conditions and the throttle settings to cover all flight mission phases. The database will be used by the optimization software

that will perform other tasks related to the aircraft systems development.

The flowchart reported in Fig. 4.5 explains the previously described points, underlying the iterative procedure of the entire process.

For this work, the last point is developed by **ASTOS**, a software that performs mission optimization for different aerospace applications. Its final goal is to evaluate the CO_2 **Metric Value** of the supersonic aircraft during a hypothetical mission profile.

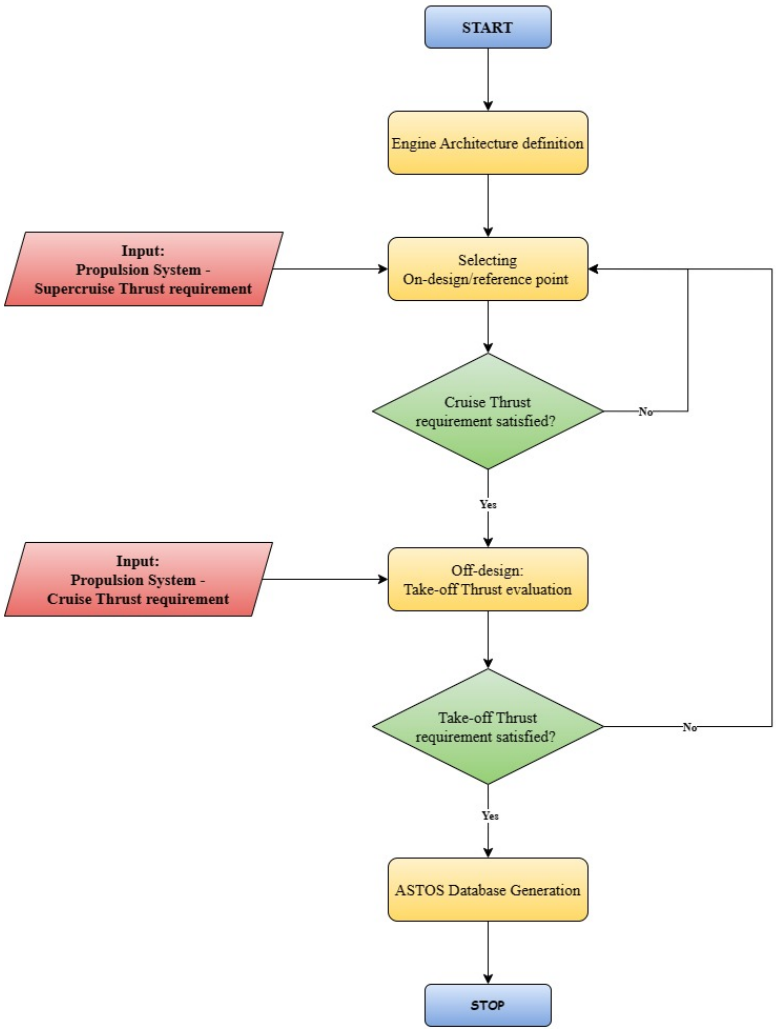

Figure 4.5: Work-flow of Engine Sizing Procedure and Database generation

4.9 CO_2 Metric Value calculations

One of the main goals of **MORE&LESS** project is to estimate the quantity of carbon dioxide (CO_2) produced during a hypothetical mission of a novel supersonic aircraft. The project team implements the CO_2 **emission standard** defined by **ICAO ANNEX 16 Volume III**. The existing requirements for subsonic aircraft were adapted, as necessary, to reflect the specifics of SST airplanes, while maintaining compatibility in terms of metrics and procedures as far as possible.

The CO_2 **Metric Value** essentially represents a fuel-efficiency analysis, and it is defined as

$$CO_2MV = \frac{\left(\frac{1}{SAR}\right)_{avg}}{(RGF)^{0.24}} \tag{4.79}$$

The parameter exposed in Eq. 4.79 are defined as follows

- Specific Air Range (SAR) in cruise flight.
- Reference Geometric Factor (RGF) a measure of cabin size.

The RGF is strictly related to the geometry of the aircraft. Instead, the specific Air Range is defined as in Eq. 4.80 and it depends on the mission range and the propulsion system's "efficiency": this aspect underlines the importance of this system during the design development.

$$\text{SAR} = \frac{d\ [km]}{m_b\ [kg]} \tag{4.80}$$

Chapter 5

Engine Proposal for a Low-boom Business Jet

5.1 Introduction

This section applies the exposed models and procedures to size a propulsion system for a **low-boom supersonic business jet**. As discussed in the previous chapter, the first step is to perform the On-design analysis to obtain the reference point. In addition, the sea-level thrust is evaluated using Off-design and, finally, by matching all propulsion system requirements, it is possible to develop the **ASTOS** database, running several Off-design simulations. A MATLAB script is created for this thesis work by using different libraries (see Sec. 6.2).

5.2 The Reference Aircraft

The case of study is a low-boom Supersonic Business jet flying at high speed for civilian missions, belonging to the **CAV**[1]. The aircraft's high-level requirements are listed in Tab. 5.1

The main issues of the case study project are summarized in the following points:

- **Sonic Boom** - The adopted configuration is a slender fuselage with a long spike and a minimum cross area, the main purpose is to minimise as much as possible the effect of the sonic boom at the ground.
- **Propellant** - The fuel used is the **FT-SPK/A** 100% composed, which belongs to the SAF (Sustainable Category Fuel).

[1]category, air-breathing cruise and acceleration vehicle aircraft

Aircraft Requirements	
Sonic Boom	$\Delta p_{\text{MAX,cruise}} < 1.5$ psf
Propellant	Biofuel
Supercruise Mach Number	1.5
Range	Up to 6500 km
Payload	8-12 passengers

Table 5.1: Low-boom Supersonic business jet: High-level requirements

- **Mach Number** - The supercruise Mach number is a convenient trade-off between current planes and future supersonic CAVs since the aircraft must perform a supersonic regime with a low bypass turbofan without the use of an afterburner.
- **Range** - The range is up to 6500 km which allows the aircraft to perform medium and long-range in supercruise.
- **Payload** - 8 to 12 passengers is the typical payload value for the business jet category.

The final configuration of the aircraft is shown in Fig. 5.1. The mission profile is performed using ASTOS software. By analysing its results, it is possible to derive the **Propulsive System Requirements**, in terms of thrust, Mach number and altitude, which will be the inputs of the engine sizing procedure. Finally, from the propulsive database, the CO_2 Metric Value is calculated according to the model of ICAO Annex 16 Volume III, described in Sec. 4.9.

5.3 Propulsion System: High-level requirements and Sizing procedure

The propulsion system requirements are primarily derived from the ASTOS mission profile, aerodynamics and configuration layout. The model developed for this thesis does not consider the utilization of **BIOFUEL** or **SAF** blends. This choice is influenced by the fact that the current **Chemical Equilibrium** software (Ref. [5]) is designed to evaluate the chemical reactions of conventional aviation fuels, such as **Jet-A1**, **JP-5** and **JP-10**. Additionally, for the engine design, a preliminary simplification is applied, assuming the fuel to have a chemical structure of $C_{12}H_{23}$ (as described in Sec. 3.4.3).

Recent research, as highlighted in Ref. [21], indicates that the use of SAF can potentially reduce thrust fuel consumption by 1% to 3% compared to Jet-A.

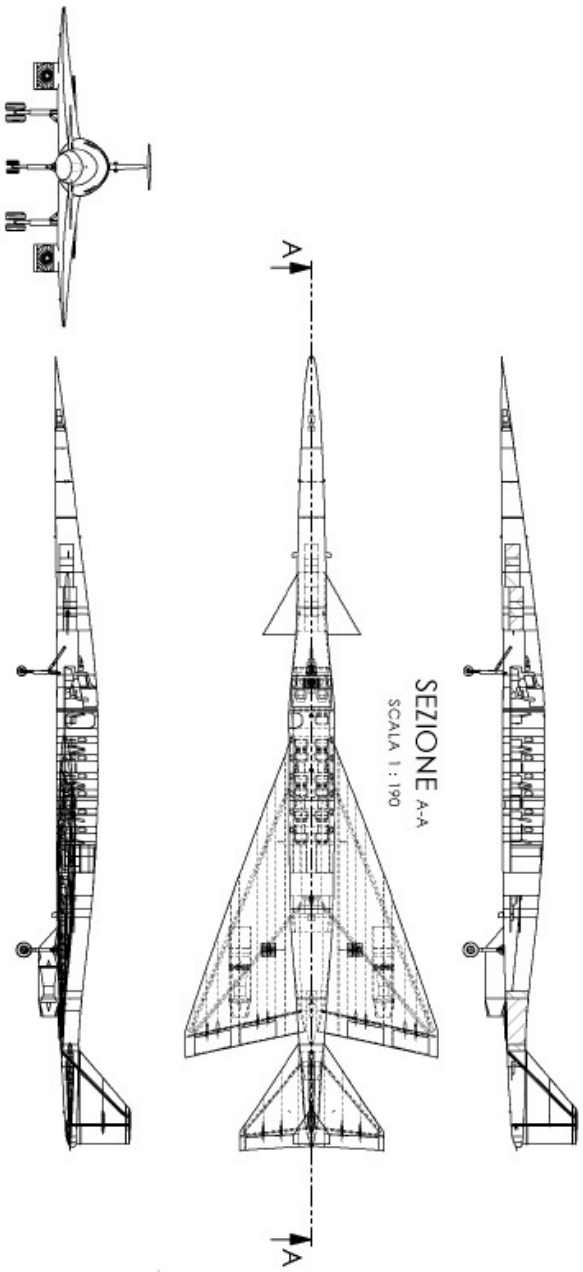

Figure 5.1: Case of study layout: Low-boom supersonic business jet

Moreover, Ref. [22] demonstrates that the emission index of biofuel is comparable to that of Jet-A. In conclusion, the assumptions made in this thesis regarding fuel choice are justifiable for an initial system sizing analysis.

The ASTOS results are reported in Fig. 5.2 and in Tab. 5.2 referred to one

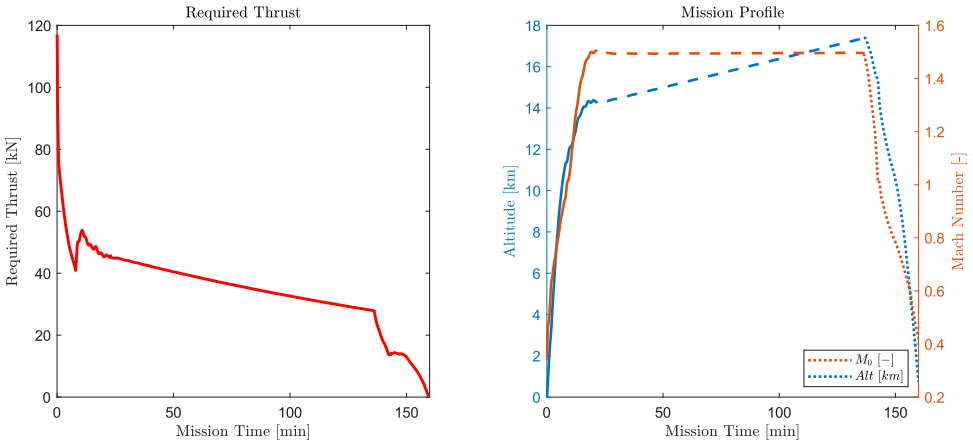

Figure 5.2: ASTOS results: Mission profile

engine. The **supercruise altitude**, as it is possible to see in Fig. 5.2, is not constant but it increases during most parts of this mission phase: therefore an average value must be considered. The **required thrust** is evaluated with a **safety margin of** 10% which includes the **installed losses** (5%) and a possibly greater aircraft thrust demand (5%).

Propulsion System Requirements		
Number of engine	2	[-]
Supercruise Altitude	15.4	[km]
Flight Mach number	1.5	[-]
Inlet Diameter	1.10	[m]
Supercruise Thrust (x1)	$\geq$ 45.0	[kN]
Take-off Thrust (x1)	$\geq$ 128.0	[kN]
Total Power extraction (x1)	240	[kW]
bleed air	0	[kg/sec]

Table 5.2: Low-boom Supersonic business jet: propulsion system requirements

Considering the **Turbofan Mixed flows** with the **highest level of technology** (Sec. 3.12), it is possible to perform the On-design during the supercruise to begin a preliminary size of the system. The thrust and specific fuel consumption are evaluated for different reference engines, changing the Overall Pressure Ratio π_c from 10 to 30 and the bypass ratio α from 0.300 to 0.700 (highest value possible). The Fan Pressure Ratio π_f is automatically tuned to guarantee the total pressure balance at the mixer entry, as illustrated in (Sec. 3.7.2). The Fig. 5.3 shows the results of the parameters' variation. As it is possible to observe, the increase in the

bypass ratio induces a decrease in the thrust and, simultaneously, a decrease in TSFC.

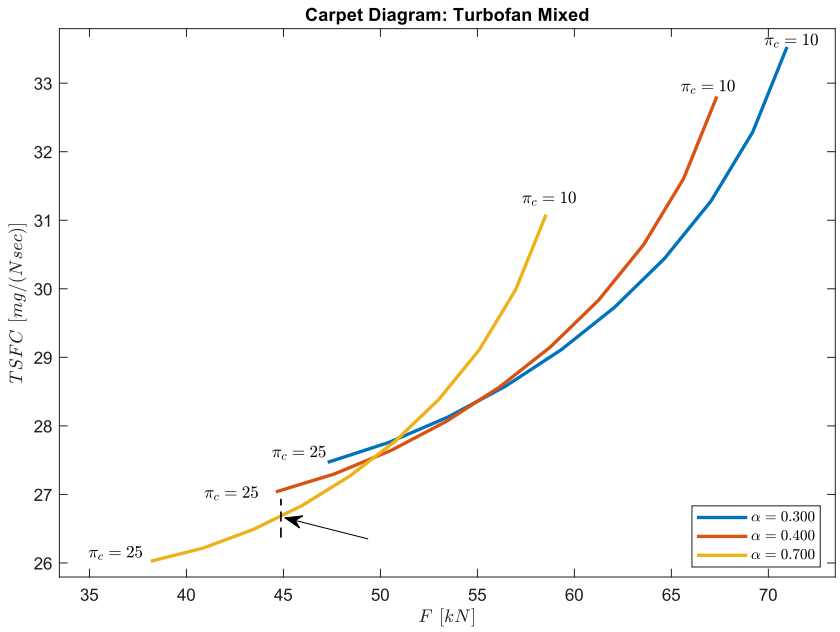

Figure 5.3: Engine parametric performance analysis: BPR and OPR selection

5.4 On-design results

The supercruise thrust is fixed by requirement, approximately around 45 kN, so it is possible to increase the bypass ratio to minimise the thrust fuel consumption. However, the chosen parameters are not the final ones, since a mission-critical point must be evaluated: the take-off, that corresponds to the first peak of the graph shown in Fig. 5.2 (Required thrust). The procedure is iterative: On-design performance establishes the bypass, overall pressure ratio and Fan-pressure ratio and the Off-design regulation confirms if the engine can provide sufficient thrust during the take-off. The results of this iterative process are shown in Tab. 5.2.

5.5 Off-design results

In this section, the results of the two Off-design methods: the **Serial Nested Loop** and **Matrix Iteration** are exposed and the results of the take-off phase will

Engine On-design results			
Parameter	Symbol	Value	Unit
Overall Pressure Ratio (OPR)	π_c	30	$[-]$
LP compressor Pressure ratio	π_{cL}	5	$[-]$
Hp compressor Pressure ratio	π_{cH}	6	$[-]$
Fan Pressure Ratio (FPR)	π_f	4.5	$[-]$
Bypass ratio (BPR)	α	0.700	$[-]$
(Max) Temperature Inlet Turbine	$T_{t4,max}$	1900	$[K]$
Air mass flow rate	$\dot{m}_0$	97.0	$[kg/sec]$
Core Mixer Mach Number	M_6	0.500	$[-]$
Cooling fractions	$\varepsilon_{1,2}$	6.38	$[\%]$
Level of Technology	LT	IV	$[-]$
Installed supercruise Thrust	T_{cruise}	58	$[kN]$
Installed Thrust-fuel consumption	$TSFC$	28.7	$[mg/(N \cdot sec)]$
Estimated Engine Mass (x1)	m_{eng}	1471	$[kg]$
Nitro Oxides Emission Index	EI_{NOx}	27.47	$[gr/kg]$

Table 5.3: Propulsion system: On-design results

be discussed as well. The first condition simulated is the supercruise, followed by the take-off.

The last part of the section deals with database development, which consists of multiple Off-design iterations by varying the three independent parameters.

5.5.1 Matrix Iteration method - Throttle variation at reference Mach number and Altitude results

The Matrix Iteration method uses the Newton-Raphson algorithm in concert with the models of the components installed in the engine to solve the Off-design problem. Here, the operating lines of the compressors, turbines and nozzle are evaluated by maintaining constant the altitude and the flight Mach number at their reference values. The throttle τ is varied from 0.600 to 1 to avoid the surge of the fan.

Fan behavior

The first component analysed is the fan, and the low-pressure compressor, the operating lines are shown in Fig. 5.4.

As expected, the two operating curves reach the surge line for low power settings. This condition is really dangerous for the engine and aircraft and it has to be avoided.

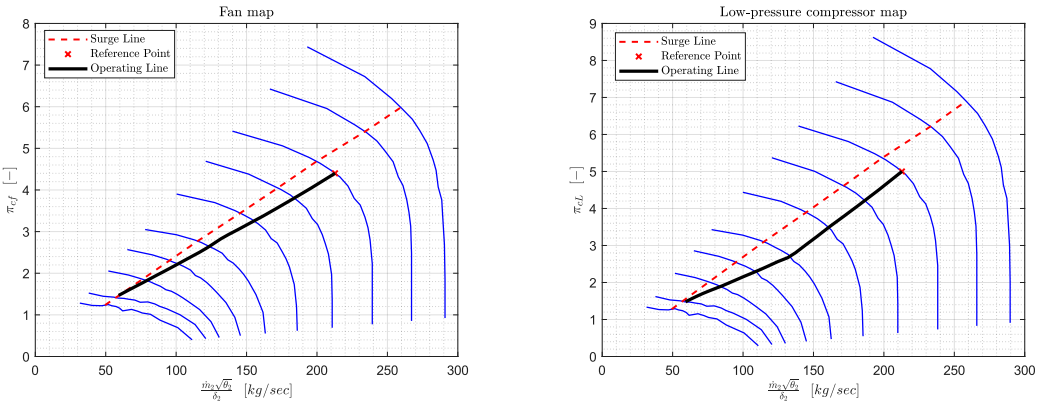

(a) Fan map **(b)** Low-pressure compressor map

Figure 5.4: Reference condition: Fan and Low-pressure compressor operating lines

High-pressure Compressor behavior

The airflow stream passes through the low-pressure compressor to the high-pressure one. Of course, the values of corrected mass flow rates are quite smaller than the fan one, caused by the flow split between the fan duct and core. The behavior of the compressor is similar to the low-pressure one but with a greater surge margin, as shown in Fig. 5.5.

Combustor behavior

The efficiency of the combustor η_b decreases during the simulation as illustrated in Fig. 5.6. This is caused by the decrease of the difference between the stagnation temperature at the inlet of the chamber T_{t3} and the outlet T_{t4}. Furthermore, the pressure loss π_b through the chamber is considered constant in this model, as described in Sec. 3.4.2, therefore the value is equal to the reference one for all power settings and flight conditions.

Turbines behavior

The behaviors of the turbines are shown in Fig. 5.7. For a large part of the simulation, both the turbines are choked: the correct mass flow rates do not change significantly from the reference value as enhanced by the author J.D. Mattingly Ref. [2]. He concludes in his works that this condition is still valid up to 1300 K.

Another important aspect related to the high-pressure turbine's curves is that for the first part of the simulation, it has a trend in which there is a compression

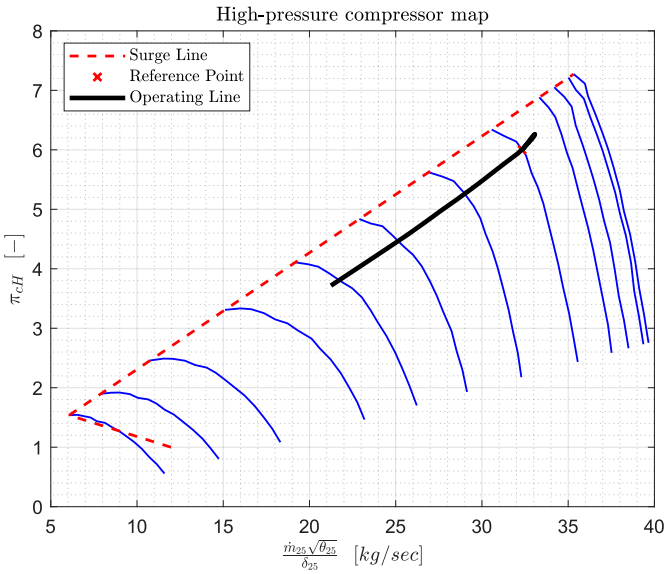

Figure 5.5: Reference condition: High-pressure compressor operating line

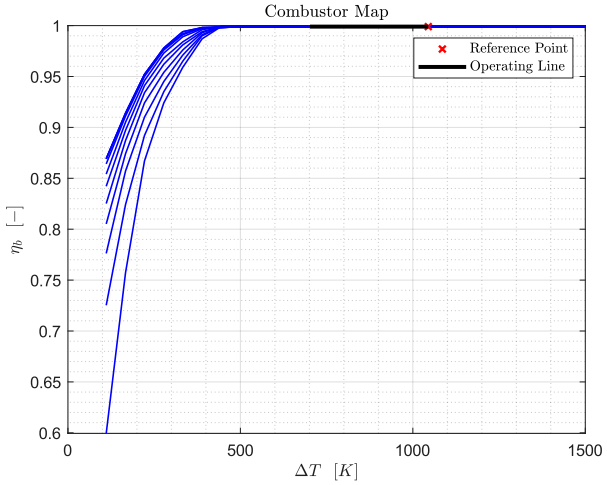

Figure 5.6: Reference condition: Efficiency Variation of the Combustion Chamber

$(d(\pi_{tL}) < 0)$, then an expansion $(d(\pi_{tL}) > 0)$. The same behavior may be observed in the high-pressure compressor Fig. 5.5.

Mixer behavior

A very interesting result is related to the mixer: the Kutta condition induces the total pressure balance at the mixer inlets. Therefore, the algorithm will tune all

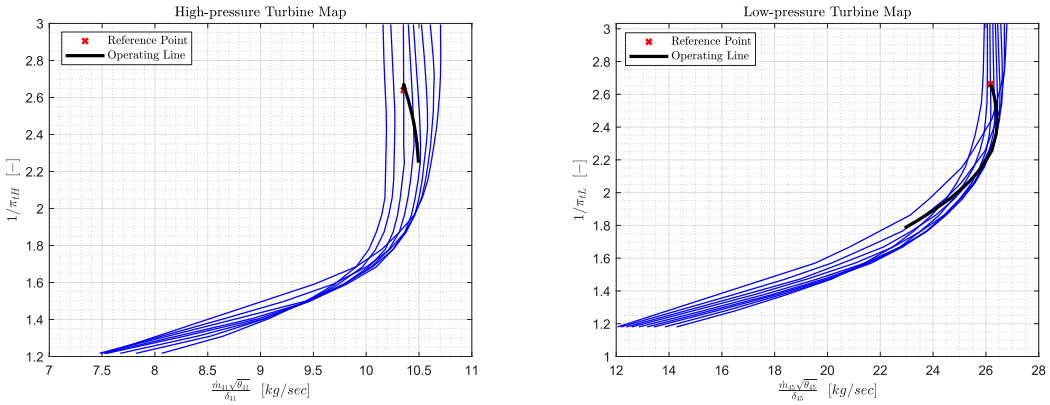

(a) High-pressure Turbine map **(b)** Low-pressure Turbine map

Figure 5.7: Reference condition: Turbines operating lines

engine parameters to satisfy it.

The total temperature ratio T_{t16} varies according to the previous exposed condition. Finally, the Mach number at the exit of the mixer is a function of the inlet ones justifying the value reduction. The results are shown in Fig. 5.8.

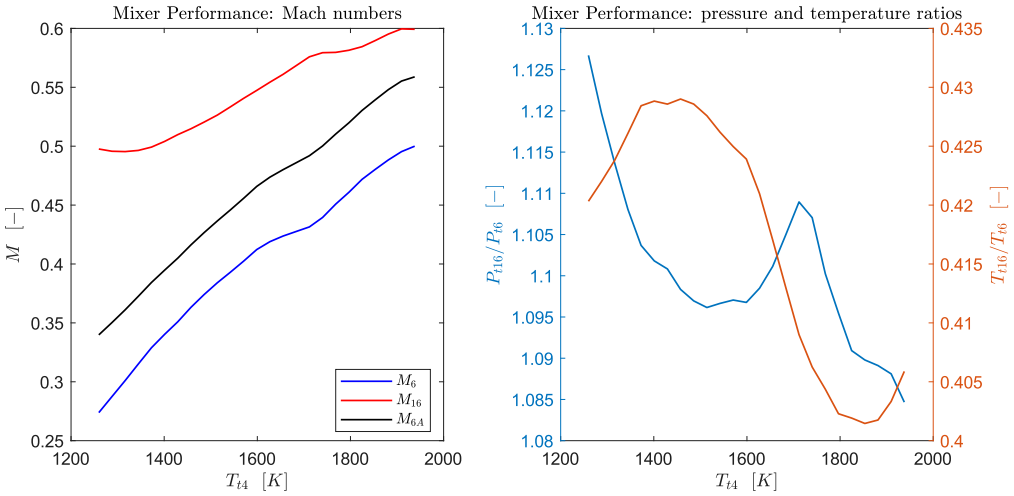

Figure 5.8: Reference condition: Mixer results

Nozzle behavior

The last component of the flow path is the nozzle. In Fig. 5.9 on the left it is possible to observe the nozzle expansion variation in the related map. The nozzle

expansion ratio decreases because the total exit pressure P_{t9} decreases as well; instead, the exit static pressure P_9 remains constant. The nozzle is a convergent-divergent with a variable exit area, therefore the algorithm simulates the nozzle petals' movements in order to maximise the gross thrust, as shown on the left of Fig. 5.9. Particularly, by using this procedure, the condition of "adapted nozzle" or $P_9 = P_0$ is always respected.

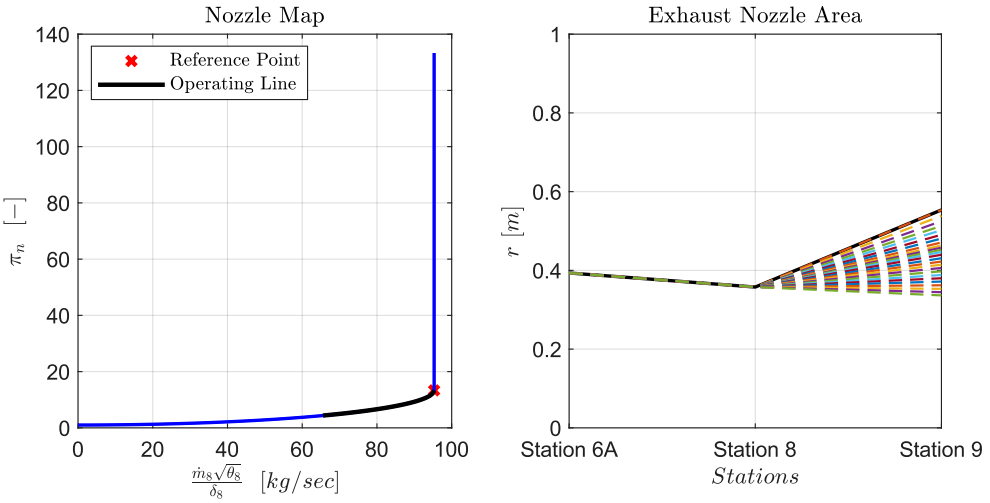

Figure 5.9: Reference condition: Nozzle operating line and exhaust area variation

Installed Thrust and Specific-thrust fuel consumption

The thrust and specific-thrust fuel consumption are calculated by using the solution of the thermodynamics cycle as shown in Fig. 5.10. The thrust decreases up to around 5 kN. However, this condition is very difficult to realise in real operative conditions. Lastly, the thrust fuel consumption increases in perfect agreement with its definition.

Simulation residuals

The simulation residuals are reported in a logarithm with base 10. The residuals are below the selected tolerance of $toll = 10^{-13}$ (see Sec. 4.4).

5.5.2 Matrix Iteration Method - Take-off performances

The take-off thrust is characterized by a very large value of engine thrust demand. To simulate this particular condition, the flight Mach number must be set to $M_0 = 0.334$, (the value is derived by ASTOS), the altitude must be equal to zero

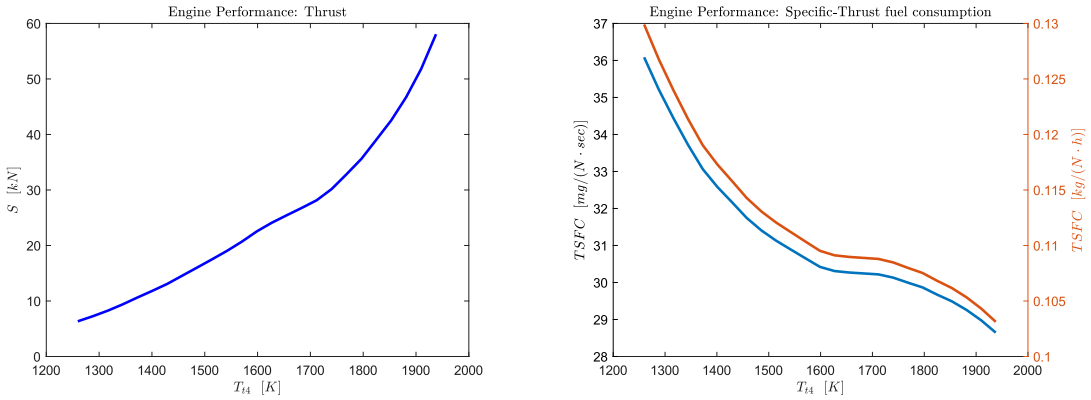

(a) Thrust curve **(b)** TSFC curve

Figure 5.10: Reference condition: Thrust and TSFC

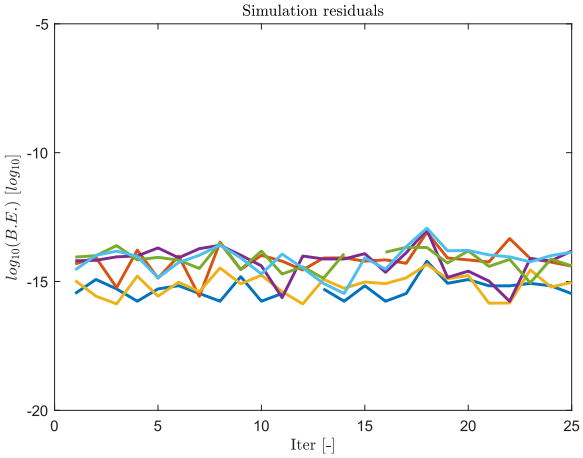

Figure 5.11: Reference condition: Simulation residuals of the balancing equations

and the throttle varies from 0.850 to 1. By running the simulations, it is possible to observe in Fig. 5.12 that the operating line is above the surge one: such condition is unacceptable since it compromises the safety of the engine causing the engine to shutdown during the take-off.

To avoid this dangerous situation, the throat area nozzle must be varied from the reference value, as shown in Fig. 5.13 (Ref. [2]). Particularly, the sixth equation of the non-linear system, described in Chapter 4, must be modified as follows

$$f_6 = \dot{m}_{c8} \cdot \frac{A_8}{A_{8,r}} - \dot{m}_{c2} \frac{[(1-\beta-\varepsilon_1-\varepsilon_2)(1+f)+\varepsilon_1+\varepsilon_2]}{1+\alpha} \frac{P_{t2}}{P_{t8}} \sqrt{\frac{T_{t8}}{T_{t2}}} \tag{5.1}$$

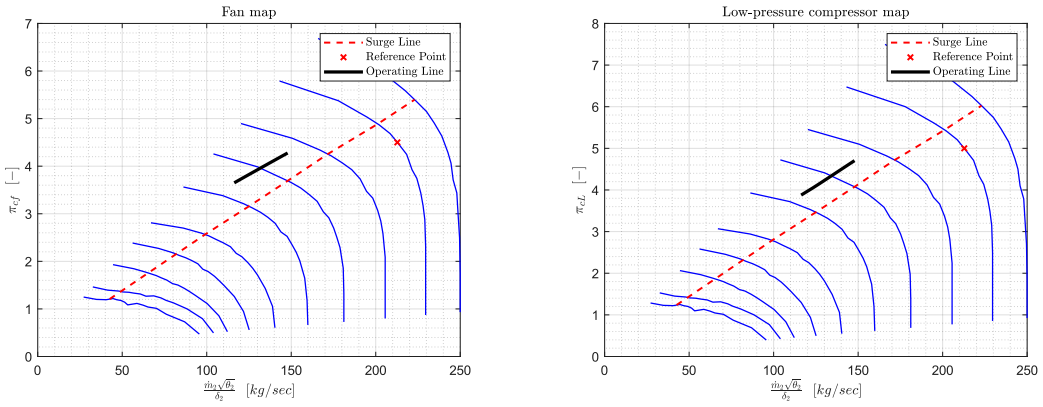

(a) Fan map **(b)** Low-pressure compressor map

Figure 5.12: Take-off: Fan and Low-pressure compressor surging

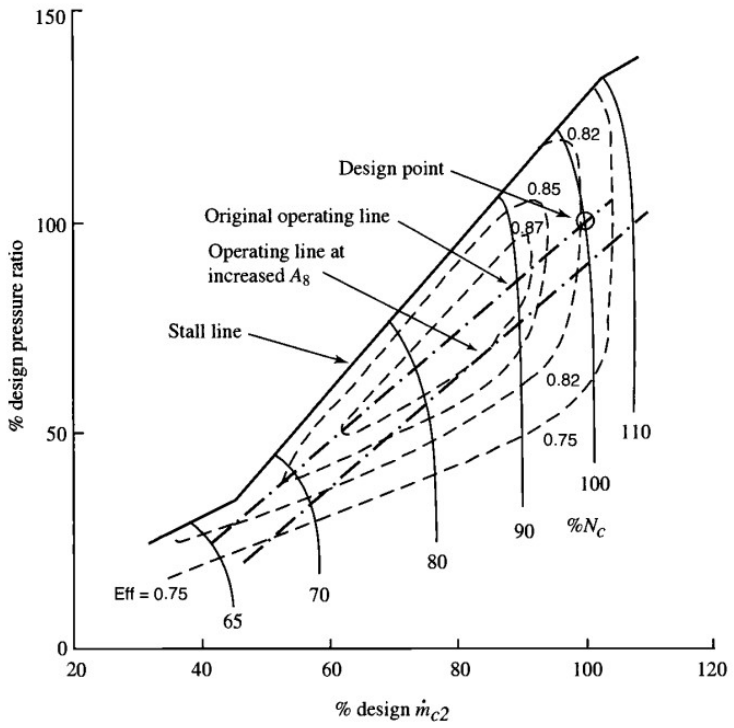

Figure 5.13: The impact of the nozzle throat area variation on fan operating line

The increment for the throat area ($A_8/A_{8,r}$) is found manually through several trial and error tests. The final chosen value is around +40% from the reference one, solving the fan and low-compressor surging condition as shown in Fig 5.14.

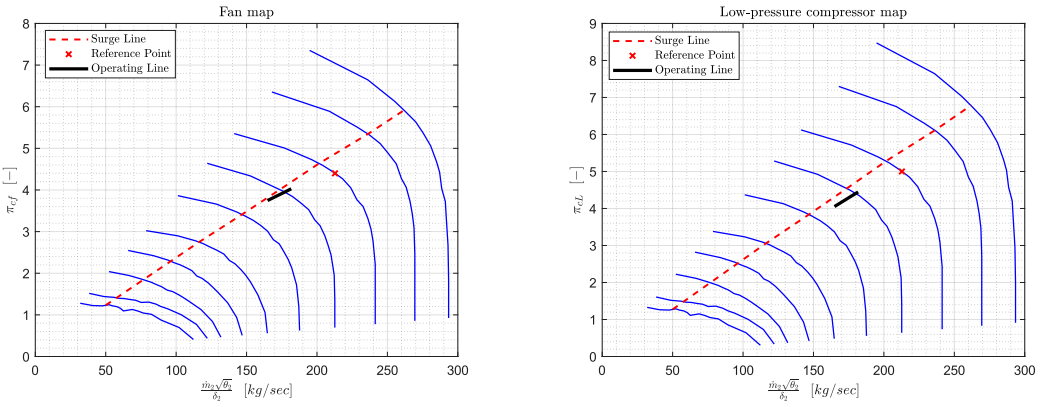

(a) fan map **(b)** Low-pressure compressor map

Figure 5.14: Take-off: Fan and Low-pressure compressor operating lines

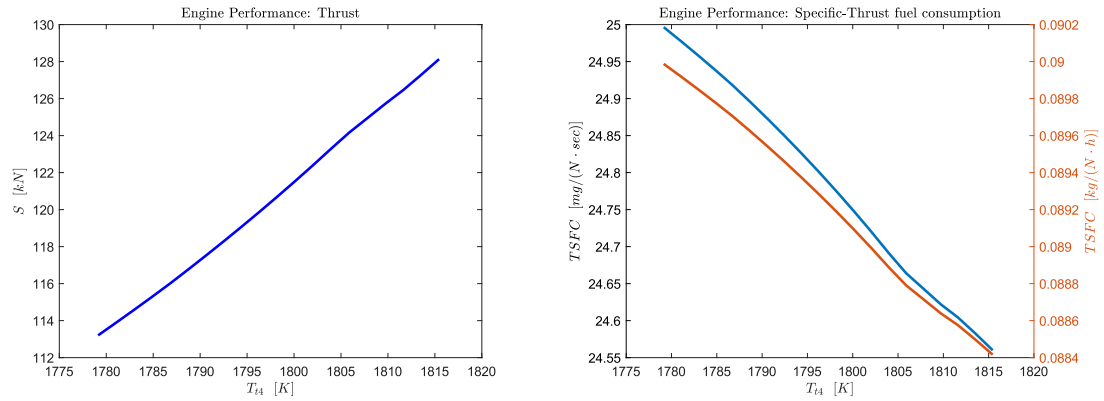

(a) Thrust **(b)** TSFC

Figure 5.15: Take-off: Thrust and TSFC

The thrust and TSFC graphs are shown in Fig. 5.15. As it is possible to see, the computed thrust perfectly matches the required one during the take-off

$$T_{\text{take-off}} \approx 128.1\ kN > T_{req} = 128.0\ kN \tag{5.2}$$

5.5.3 Matrix Iteration Method - Low power setting: Descending and Landing phases

A really interesting operative phase is the descending, followed by the landing. The required low level of thrust, flight Mach number and altitude characterise the

engine power set-up. As described above, the great challenge for the user is to choose the appropriate nozzle throat area value to avoid the surge. In this case, it is not enough to increase the nozzle throat A_8, the nozzle exit area A_9 must be decreased too. Particularly, to vary the area A_9 it is possible to change the ratio P_9/P_0 to a value minor of 1, for this case 0.700 is chosen.

The simulation results are shown from Fig. 5.16 to Fig. 5.18, considering an altitude equal to zero and a flight Mach number of $M_0 = 0.200$.

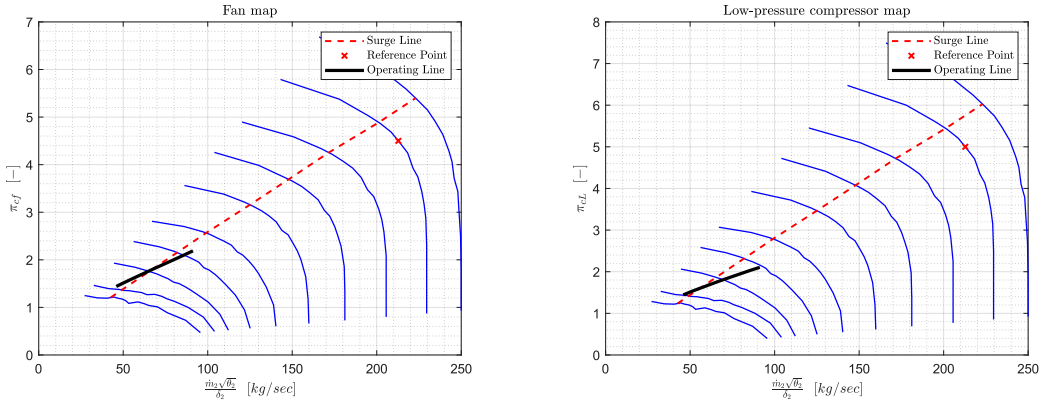

(a) Fan map **(b)** Low-pressure compressor map

Figure 5.16: Low power setting: Fan and Low-pressure compressor operating lines

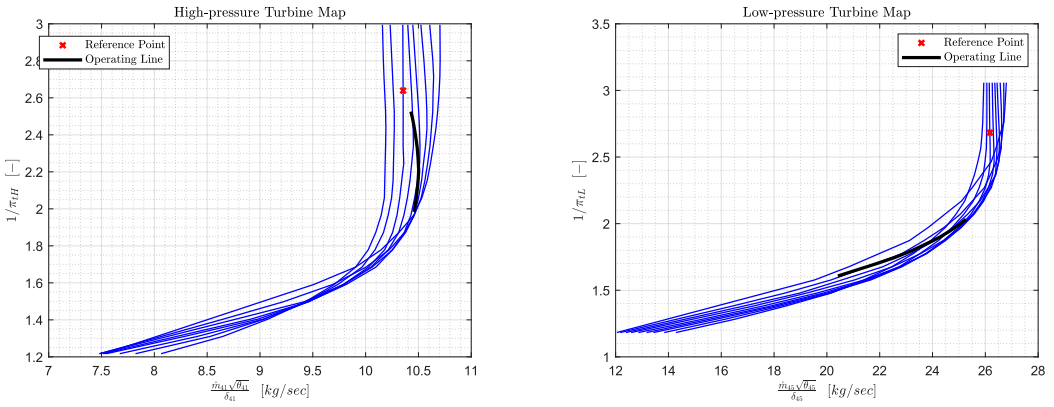

(a) High-pressure turbine map **(b)** Low-pressure turbine map

Figure 5.17: Low power setting: High-pressure and Low-pressure turbines operating lines

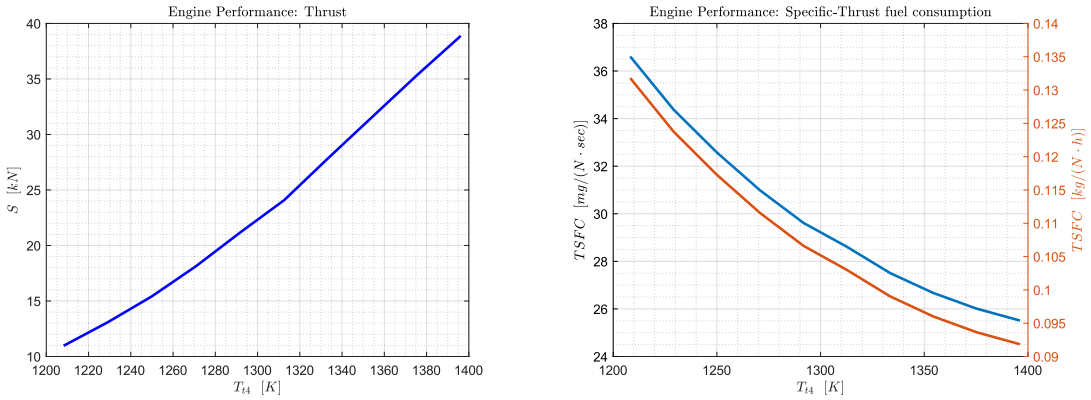

(a) Thrust **(b)** TSFC

Figure 5.18: Low power setting: Thrust and TSFC

5.6 Database Generation - Throttle Variation at different Mach numbers and Altitudes

The propulsive database generation requires the performance's computation at different altitudes and flight Mach numbers aiming to cover the entire mission profile or its greatest part. The procedure is very hard to automatise, since different flight conditions require an appropriate selection of the throttle τ in concert with the nozzle throat area variation. In most cases, selecting the throttle close to 1 protects the engine and avoids the related simulation divergence. However, selecting the maximum value for τ leads to the maximum thrust generation, therefore a minimum value must be set manually, by checking if the low-pressure components are working with a sufficient surge margin.

A first iteration is performed using the Serial Nested Loop developed by author J.D. Mattingly, as described in the following section. Then, the most accurate Matrix Iteration is also used for a second more accurate database.

5.6.1 Serial Nested Loop (Mattingly Model) - First database generation results

The first iteration developed for the database generation, was performed by using the Mattingly model exposed in Sec. 4.6 and by setting the Modified Specific Heat for the gas. As shown in Fig. 5.19, the engine model is very accurate for the take-off, ascending and supercruise, but the simulation diverges for descending and landing phases. These inconsistencies in the results are caused by these assumptions: during the descending and landing phases, the throttle setting is low, therefore the

turbines are not still chocked, as assumed. This condition can be clearly seen in Fig. 5.17 and in Fig. 5.7. In both cases the low-pressure turbine's curve is not always "vertical", making the assumptions to fall.

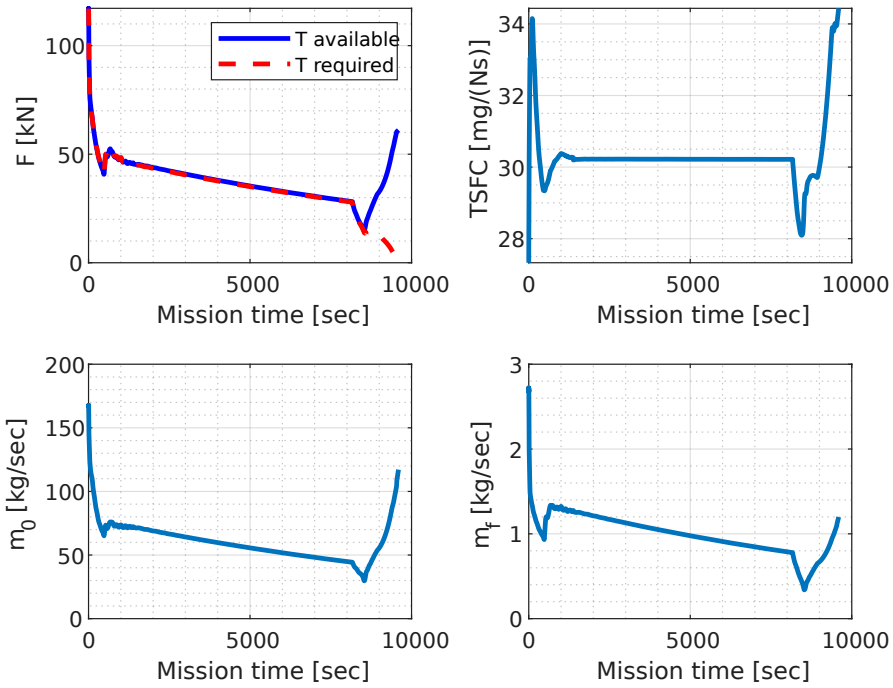

Figure 5.19: Engine database: first iteration

5.6.2 Matrix Iteration - database generation results

As described above, for the first iteration of database development multiple Off-design simulations are performed by varying the three independent variables. For simplicity, the reported results of this section are related to 2 values of altitude and 3 Mach numbers.

The results are shown in Fig. 5.20, the flight altitude is maintained constant at 11 km, while the Mach number varies from 0.95 to 1.50. The nozzle throat area is equal to its reference value and the throttle starts from 0.780 to 1, covering a wide range of thrust. Another equivalent iteration is performed by setting the altitude at 14 km (Fig. 5.21).

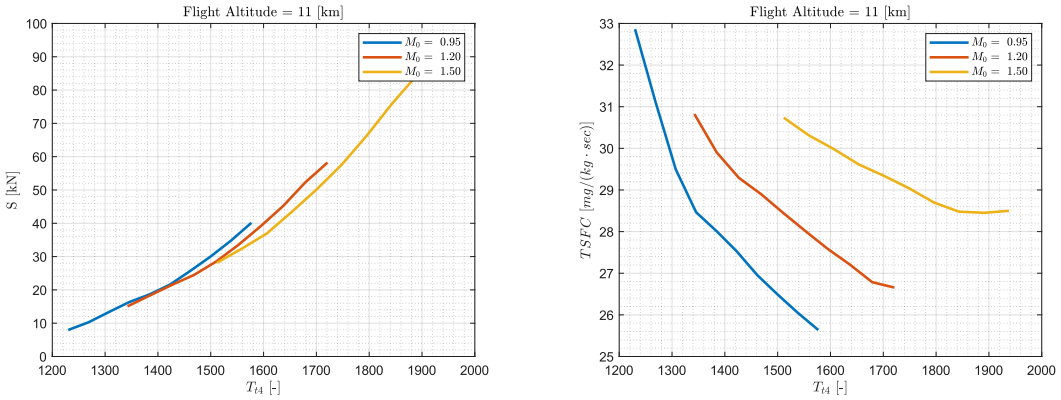

(a) Fan behavior **(b)** low-pressure compressor

Figure 5.20: Throttle variation at different Mach number and Altitude of 11 km

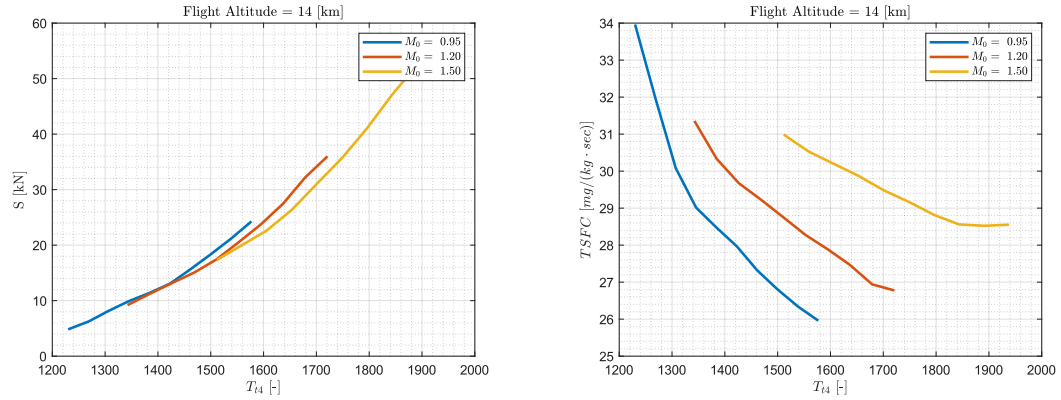

(a) Fan behavior **(b)** low-pressure compressor

Figure 5.21: Throttle variation at different Mach number and Altitude of 14 km

5.7 CO_2 Metric Value results

Following the development of the propulsive database of the case of study, it is possible to perform different ASTOS simulations to calculate the CO_2 metric value defined as in Eq. 4.80. The results in supercruise conditions are shown in Tab. 5.4 and for the entire mission in Tab. 5.5, considering an $RGF = 50.2$. **The estimated propellant** used for the entire mission is around $m_b = 18343\ kg$. The two related CO_2 **metric values are** 1.683 kg/km **and** 2.047 kg/km.

A really interesting comparison between the considered case of study and other aircraft belonging to the same category is reported in Fig. 5.22. The figure

Time [min]	Altitude [km]	Mach [-]	Mass Flow Rate [kg/s]	SAR [km/kg]
1147.42	14.26	1.4999	2.6044	0.170
8211.19	17.39	1.4783	1.3893	0.314
4230.59	15.56	1.4941	2.0733	0.213

Table 5.4: SAR Calculations for during the supercruise

Time [min]	Altitude [km]	Mach [-]	Mass Flow Rate [kg/s]	SAR [km/kg]
1138.51	14.26	1.4997	2.6108	0.169
4319.70	15.60	1.4941	2.0609	0.214
2626.63	14.82	1.4941	2.3293	0.189

Table 5.5: SAR Calculations for during the supercruise

represents the CO_2 Metric Values, expressed in kilograms per kilometer, for different SSTs, including the case of study of this thesis work in function of the Maximum take-off mass. The continuous lines represent the limits of the subsonic case, according to the ICAO reference. The calculation of the metric value is performed by considering three points of the cruise phase mission, in which the aircraft has a high gross mass, mid gross mass and low gross mass.

It is possible to observe that the calculated value of CO_2 is really close to the NASA SST, which confirms the accuracy of the results, including the developed propulsive database. Another consideration is related to the final sustainability of SSTs' future systems. As it is possible to observe in the graph, all the business jets present a greater emission of carbon dioxide than the subsonic ones belonging to the same aircraft category. Of course, the supersonic flight requires a greater thrust demand which implies an increase in the total fuel consumed and, therefore, this will inevitably raise the CO_2 emission. However, this study is conducted by considering a formula that is valid for the subsonic regime, thus the research must provide a greater fidelity model for the emission estimation specifically related to SSTs or confirm the accuracy of the proposed one.

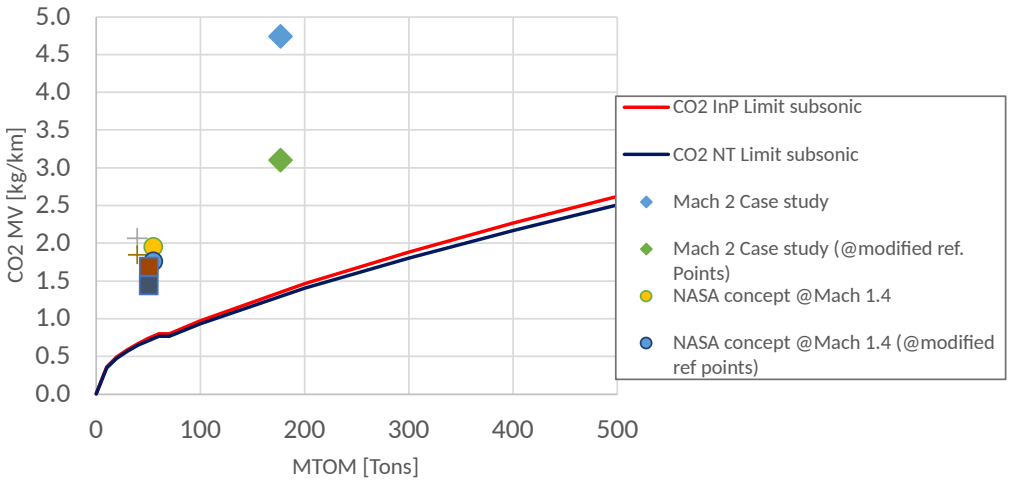

Figure 5.22: CO_2 Metric Values for different applications and subsonic limits

Chapter 6

Model Validation and Software Architecture

6.1 Model Validation

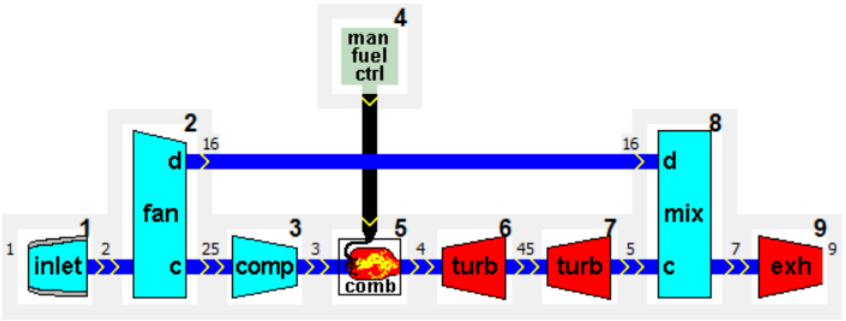

Figure 6.1: GSP 11: Turbofan Mixed flows model

A really important aspect of model development is validation. The experimental validation of an engine can be conducted for an existing one by tuning the parameters in order to replicate it, in the only case of reference point. For the Off-design, lots of variables and the components' maps are generally unknown, therefore the only way is to use commercial software and compare the results.

In this thesis work, this second way is adopted, using the open source **GSP 11**

(Ref. [4]). The case of interest is the turbofan mixed flows. GSP 11 offers several models in which all parameters are set and ready for the simulation. Thus, the MATLAB code is tuned in order to simulate the proposed GSP 11 Turbofan with Mixed exhausts. Then, the results are compared. The main input parameters are reported in Tab. 6.2

The On-design results are reported in Tab. 6.1, and, as it is possible to observe, the maximum relative error is around the 1%, in perfect agreement with the model assumption and code settings. The error probably is induced by the difference in the gas model: the "FAIR" routine, which uses a generic fuel $C_{12}H_{23}$. Instead, GSP 11 uses an accurate model for the specific fuel (The Jet-A1, in this instance).

Physical Quantity	GSP 11	MATLAB code	absolute error	relative error
Thrust $[kN]$	11.48	11.54	$60(N)$	0.52%
TSFC $[kg/(N \cdot h)]$	0.0538	0.0541	$2.71\ 10^{-4}$	0.51%
fuel flow rate $[kg/sec]$	0.0172	0.0174	0.002	1.01%
Mixer exit Area $[m^2]$	0.200	0.198	0.002	1.00%

Table 6.1: On-design GSP 11 and MATLAB code comparison

The Off-design validation is performed by replicating the same parameters and settings of GSP 11, including the components' maps as well. The simulation is performed by considering the altitude and flight Mach number set to their reference values and by varying the inlet temperature turbine from the reference 1123 K to 1290 K. The minimum inlet temperature turbine is selected in order to avoid the surge condition since a lower value causes the simulation divergence. Therefore, the same minimum throttle is set in GSP 11. The results are shown in Fig. 6.2, and as expected the MATLAB thrust perfectly agrees with the GSP 11 for all temperature settings. Instead, the TSFC seems to be affected by an error that increases for the lower values of temperature.

Considering the definition of **TSFC** as

$$\text{TSFC} = \frac{\dot{m}_b}{T}$$

It is clear that the error may be induced by the "fraction" of the two parameters, therefore it is interesting to see the behavior of the fuel mass flow rate as well. Looking at the graph shown in Fig. 6.3, it is possible to confirm that the error is influenced by the fraction since the fuel mass flow rate curve generated by the MATLAB code is really close to the GSP 11 one.

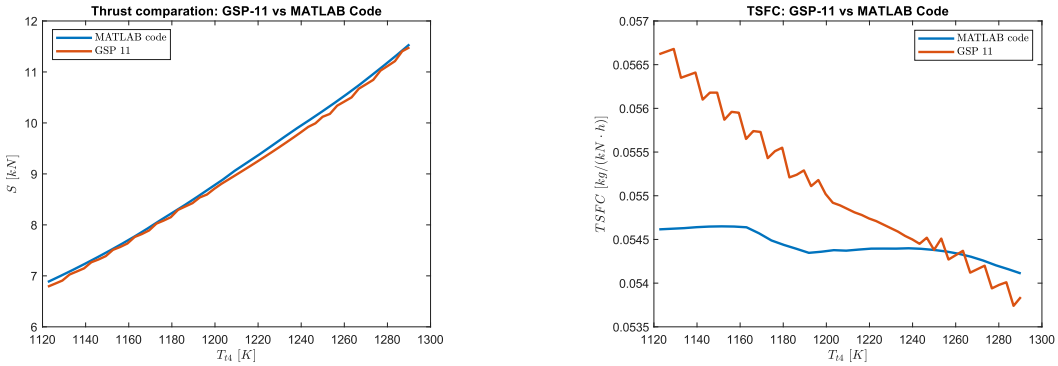

(a) Thrust **(b)** TSFC

Figure 6.2: GSP 11 and MATLAB code results comparison

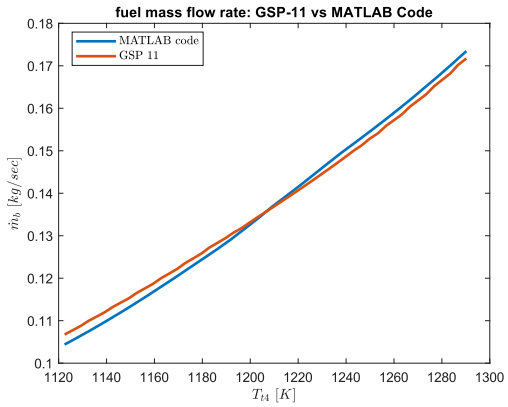

Figure 6.3: GSP 11 and MATLAB code: fuel mass flow rate results comparison

6.2 The Software Architecture

The models described in the previous sections are implemented in the MATLAB environment in order to perform On-design, Off-design simulations, and, finally database generation. The resulting software architecture is quite complex, involving different MATLAB scripts and subroutines grouped in function libraries. The main structure consists of a MATLAB Script that performs both On-design and Off-design of a specific engine[1], a library concerning the selected gas model, a library for the map scaling and interpolation a library related to the thermodynamic cycles (Fig. 6.4). Each of these contains multiple functions as shown in Fig.

[1]As described in the introduction, different models of engine architecture are developed

Parameter	Value	Unit
Flight Conditions		
M_0	0.0	-
$\dot{m}_0$	35.24	kg/sec
Alt	0.0	m
Fan and Core		
e_f	0.786	-
π_f	1.605	-
α	2.620	-
e_{cL}	0.800	-
π_{cL}	1.560	-
High Compressor		
e_{cH}	0.780	-
π_{cH}	6.712	-
Combustion chamber		
η_b	0.995	-
T_{t4}	1290.2	K
High pressure turbine		
e_{tH}	0.890	-
η_{mH}	0.990	-
Low pressure turbine		
e_{tL}	0.880	-
η_{mL}	0.990	-
Mixer		
$\pi_{M,max}$	1.0	-
M_6	0.289	-
Simple Convergent Nozzle (Fixed Area)		
π_n	1.00	-
M_9	0.779	-
A_9	0.135	m^2

Table 6.2: GSP 11 Turbofan Mixed flows: main engine parameters

6.4. Regarding the "Maps Manager Library" not all functions are reported in the flowchart because, for each engine's component model, there are essentially three routines: the reading of the map, the scaling procedure and the interpolation one. For the nozzle, the map is generated as described in Sec. 3.8.4 so there is no reading function. The maps used for this thesis work are the same as the GSP 11 software and it is possible to consult the complete list in the Appendix C.

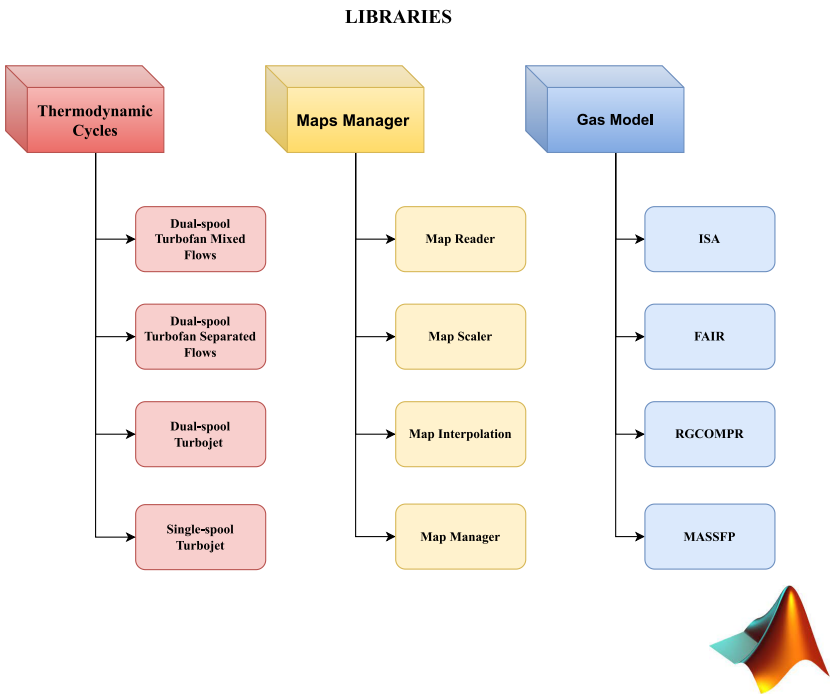

Figure 6.4: Code Libraries

The single script performs the simulation by varying the throttle, keeping constant the altitude flight Mach number, therefore to generate a propulsive database the code "architecture" must be expanded. This task is realised by changing the independent variables in multiple iterations. Specifically, to perform this operation, it is possible to define three "levels"

- **LEVEL I**: Altitude variation.
- **LEVEL II**: Mach number variation.
- **LEVEL III**: throttle variation.

At each level corresponds an independent variable variation or, in other words, a "for" command execution, as shown in the "pseudo-code" at the end of this section. For the database generation, it is not needed to execute the On-design since it is possible to import the generated reference point, from the previous session.

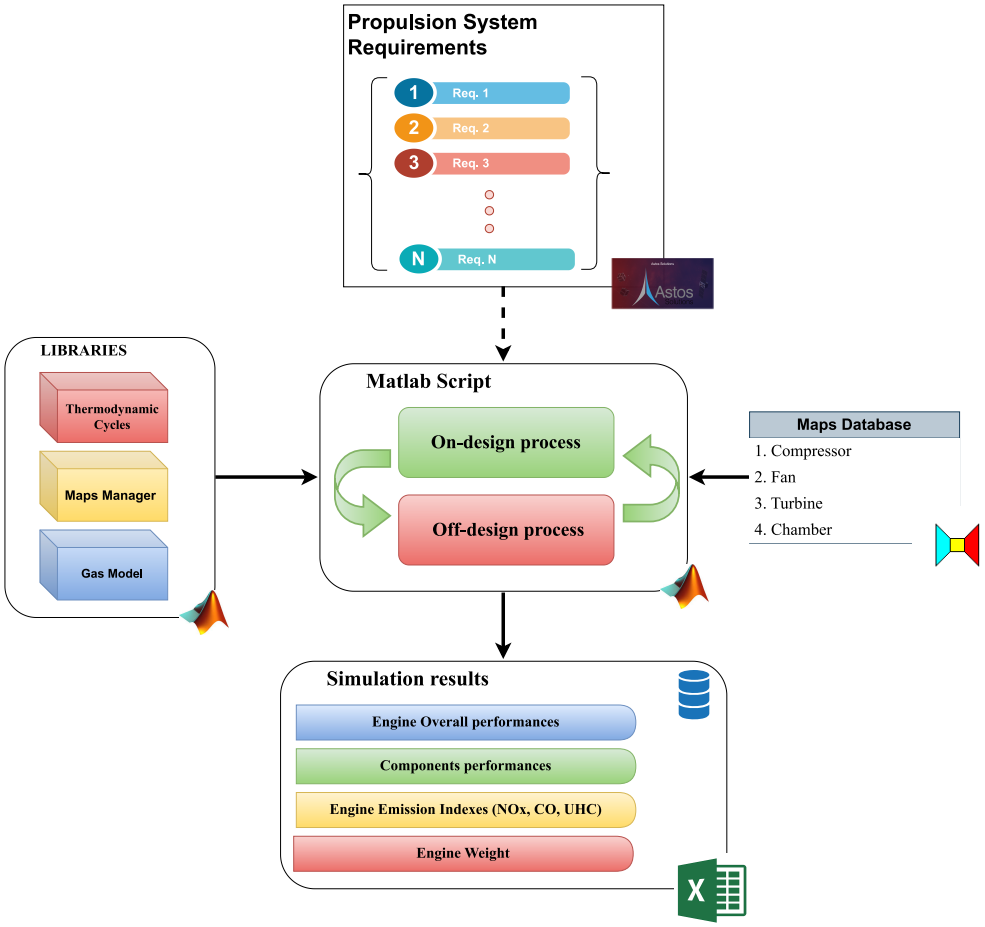

Figure 6.5: The Software Architecture

6.3 Simulation execution stop

As explained in the model discussion, some conditions may cause the stop of the simulation. These conditions probably are caused by the non-existing data when the function tries to interpolate the component maps or when the FAIR routine fails. In both cases, the program has not found a solution for the non-linear system. The software helps the user to define these situations by giving a constant feedback display in the command prompt of MATLAB as shown in Fig 6.6. The display output shows the residuals in the logarithm scale, calculated at the current Newton-Raphson iteration.

```
1  % ENGINE DATABASE GENERATION – PSEUDO CODE
2
```

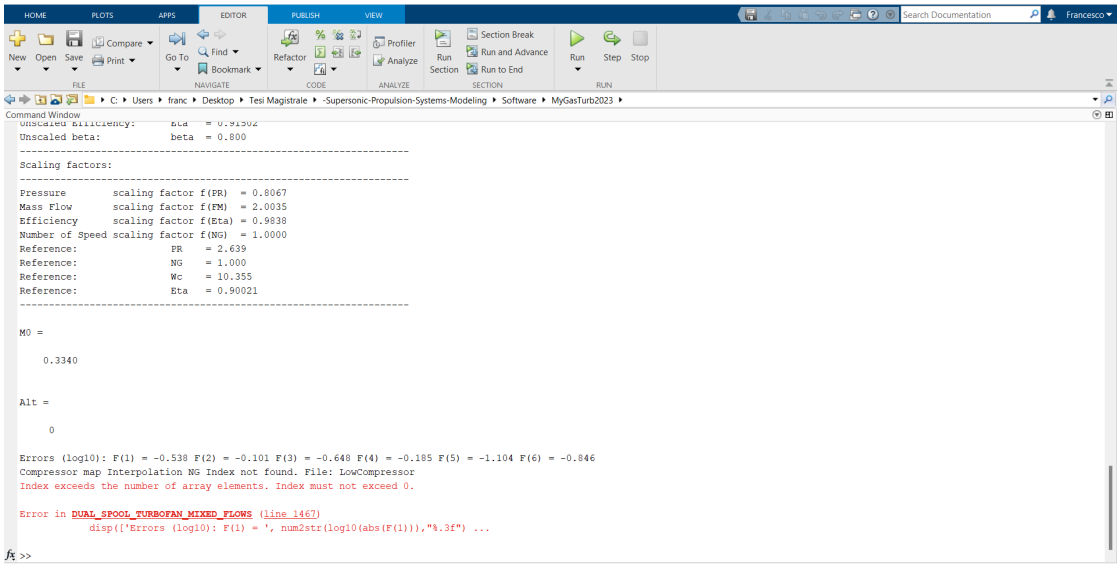

Figure 6.6: Example of simulation error

```
% Importing the reference point...
load("reference.mat");

% Defining the vector of the flight Mach numbers...
M0_vec        = [0.1, 0.2, 0.3, 0.4];                    % [-]


% Defining the vector of the altitudes...
Alt_vec       = [0, 500, 1000];                          % [m]

% Defing the vector of the throttles...
throttle_vec = [0.80, 0.85, 0.90, 0.95, 1.00];           % [-]

% Database building execution...

% LEVEL I: Changing the altitude...
for k=1:length(Alt_vec)

    % LEVEL II: Changing the Mach number...
    for j = 1:length(M0_vec)

        % LEVEL III: Changing the throttle ratio...
        for i = 1:length(throttle_vec)

            % Solving the Off-design...
            Engine_Off_design.m;

```

```
30                  % Saving data...
31                  save_dat.m;
32                end
33            end
34        end
```

Chapter 7

Conclusions and Future Works

The thesis work discusses an approach to size a novel engine for a supersonic aircraft and the development of a propulsive database, in order to estimate the carbon dioxide emission during the conceptual phase of SST. The process replicates and improves a part of the **Engine Design Process**:

- the results of the mission, of the configuration, and of the initial sizing of the aircraft's systems are reported in the form of a list of requirements;
- the most appropriate engine architecture is chosen;
- the thermodynamics cycle of the engine is developed both in On-design and Off-design;
- the reference point is selected by using the engine model in order to satisfy all engine requirements;
- the propulsive database, at this point, is generated by performing several of the Off-design simulations varying the three main independent variables;
- Finally, it is possible to evaluate the CO_2 metric value by using the formula reported in ICAO Annex 16 Volume III;

The main engine's components are modeled, and the entire engine performance is evaluated using two different approaches: the Serial Nested Loop and the Matrix Iteration. The process is applied to a novel low-boom supersonic business, with a flight Mach number of 1.5 and a supercruise altitude around of 15 km. All main engine parameters are chosen to satisfy all requirements, in terms of cruise thrust,

take-off thrust, and air mass flow rate. Simplified formulas are used to calculate the emission indexes and the engine weight.

The first database is developed using the Serial Nested Loop, elaborated by Professor J.D. Mattingly. The obtained results show that the assumptions of turbines chocked are not valid for low-power settings, leading to a great model inaccuracy during the descending phase and landing. The Matrix Iteration method is used to generate the second database solving all limitations of the Serial Nested Loops method. It is important to underline the high constraint of the map use: it must be assumed a map of an existing engine for a future one. Moreover, the method is quite complex, because different routines have to be set in order to run a single simulation. The first method is easier than the Matrix Iteration, due to its assumptions, requiring fewer functions and iterations to solve the Off-design, as described above.

Another limitation of the entire model is the simplification of the fuel: it has to be assumed that the Biofuels used for this case of study have the same chemical structure of a typical jet engine $C_{12}H_{23}$.

The work of this thesis could be extended and improved in the future, particularly in our suggestion the following points may be developed:

- The approach is suitable to other propulsion systems of other MORE&LESS case of studies, with different flight Mach numbers.
- The Chemical Equilibrium could be used in order to obtain a model of the Specific Heat Coefficient variation with the temperature and fuel-to-air ratio, taking care of the chemical structure of the fuel.
- Using optimization algorithm to solve automatically the sizing process of the engine.
- Developing the models for innovative engines, such as the variable cycle engine.
- Using the C, C++, or Fortran coding, in order to speed up the iterations, saving simulation time.
- Developing a user graphical interface for the user.

Appendix A

International Standard Atmosphere

The International Standard Atmosphere correlates the temperature and the pressure variations with the flight altitude level, here, the general model is reported.

Below 11,000 meters, the ambient temperature is given by:

$$T_0 = 288.15\,\mathrm{K} - 6.5 \times \frac{\text{altitude [m]}}{1000\,\mathrm{m}} \tag{A.1}$$

The pressure ratio is given by:

$$P_0 = 101325\,\mathrm{Pa}\left(1 - 0.0225577 \times \frac{\text{altitude [m]}}{1000\,\mathrm{m}}\right)^{5.25588} \tag{A.2}$$

Between 11,000 meters and 25,000 meters, the static temperature remains constant, and the pressure is calculated using Eq. (A.3):

$$T_0 = 216.65\,\mathrm{K} \tag{A.3}$$

$$P_0 = 22632\,\mathrm{Pa} \cdot e^{\frac{11000\,\mathrm{m} - \text{altitude [m]}}{6341.62\,\mathrm{m}}} \tag{A.4}$$

Above 25,000 meters, the temperature increases again according to Eq. (A.5):

$$T_0 = 216.65\,\mathrm{K} + 3 \times \frac{\text{altitude [m]} - 25{,}000\,\mathrm{m}}{1000\,\mathrm{m}} \tag{A.5}$$

Appendix B

The Complete List of available Maps

In this section, the complete list of maps used for this thesis work is reported. The maps are copied from GSP 11 free software, which allows the evaluation of the performance of a novel engine. The maps regard the compressor, turbines, and chamber.

The complete list of the compressor's maps is reported in Tab. B.1

File Name	Short Description
ABFANfanc.map	(afterburning turbofan fan core side map)
ABFANfand.map	(afterburning turbofan fan duct side map)
ABFANhpc.map	(afterburning turbofan HP compressor map)
compmap.map	(default compressor map)
SMALLFC.map	(small turbofan fan core side map)
SMALLFD.map	(small turbofan fan duct side map)
SMALLBST.map	(small turbofan booster map)
SMALLHPC.map	(small turbofan HP compressor map)
BIGFC.map	(small turbofan fan core side map)
BIGFD.map	(small turbofan fan duct side map)
BIGBST.map	(small turbofan booster map)
BIGHPC.map	(small turbofan HP compressor map)

Table B.1: list of compressor's maps

The complete list of the turbine's maps is reported in Tab. B.2

File Name	Short Description
ABFANHPT.map	(afterburning turbofan HP turbine map)
ABFANLPT.map	(afterburning turbofan LP turbine map)
turbimap.map	(default turbine map)
SMALLLPT.map	(small turbofan LP turbine map)
BIGLPT.map	(small turbofan LP turbine map)

Table B.2: list of turbine's maps

The complete list of the combustor's maps is reported in Tab. B.3

File Name	Short Description
combumap.map	(default combustor map)

Table B.3: list of chamber's maps

Appendix C

The single spool turbojet

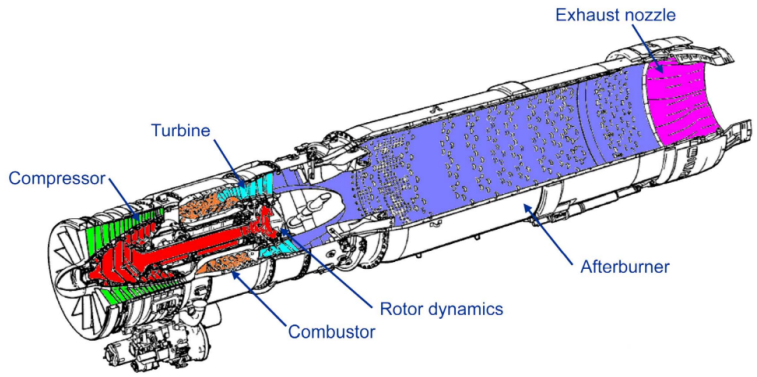

Figure C.1: The J-85 engine

In this section, the no afterburning single spool balancing equations, the related state vector, and the Jacobian matrix are reported, the procedure to find the solution of the non-linear system of equations is the same as the Turbofan Mixed flows described in Sec. 4.5. For simplicity, the bleed and cooling fractions are neglected.

Referring to the engine scheme reported in Fig. C.2, the first equation is related to the shaft power balancing

$$\dot{m}_2(h_{t3} - h_{t2}) + P_{TO}/\eta_{mP} = \dot{m}_4(h_{t4} - h_{t5}) \cdot \eta_m \tag{C.1}$$

The second equation refers to the mass flow rate balance between the compressor and the turbine

$$\dot{m}_{c2} = \frac{\dot{m}_{c4}}{1+f} \cdot \frac{P_{t4}}{P_{t2}} \cdot \frac{T_{t4}}{T_{t2}} \tag{C.2}$$

The last equation refers to the mass flow rate balance between the nozzle and turbine

$$\dot{m}_{c4} = \dot{m}_{c8} \frac{P_{t5}}{P_{t4}} \sqrt{\frac{T_{t4}}{T_{t5}}} \tag{C.3}$$

The final system is

$$\vec{\mathbf{F}}(\vec{\mathbf{X}}) = \left\{ \begin{array}{c} \dot{m}_2(h_{t3} - h_{t2}) + P_{TO}/\eta_{mP} - \dot{m}_4(h_{t4} - h_{t5}) \cdot \eta_m \\ \dot{m}_{c2} - \dot{m}_{c4}/(1+f) \cdot (P_{t4}/P_{t2}) \cdot \frac{T_{t4}}{T_{t2}} \\ \dot{m}_{c4} - \dot{m}_{c8}(P_{t5}/P_{t4})\sqrt{T_{t4}/T_{t5}} \end{array} \right\} = \vec{\mathbf{0}} \tag{C.4}$$

Thus the state vector is

$$\vec{\mathbf{X}} = \{\pi_c, \pi_t, (\%N_c)\}^T \tag{C.5}$$

The Jacobian is calculated as

$$\left[\frac{\partial F}{\partial X}\right] = \left\{ \begin{array}{ccc} \frac{\partial f_1}{\partial \pi_c} & \frac{\partial f_1}{\partial \pi_t} & \frac{\partial f_1}{\partial (\%N_c)} \\ \frac{\partial f_2}{\partial \pi_c} & \frac{\partial f_2}{\partial \pi_t} & \frac{\partial f_2}{\partial (\%N_c)} \\ \frac{\partial f_3}{\partial \pi_c} & \frac{\partial f_3}{\partial \pi_t} & \frac{\partial f_3}{\partial (\%N_c)} \end{array} \right\} \tag{C.6}$$

Finally, the residual vector is defined as

$$\vec{R} = \left[\frac{\pi_c}{\pi_{c,r}}, \ \frac{\pi_t}{\pi_{t,r}}, \ \frac{(\%N_c)}{(\%N_c^r)}\right]^T \tag{C.7}$$

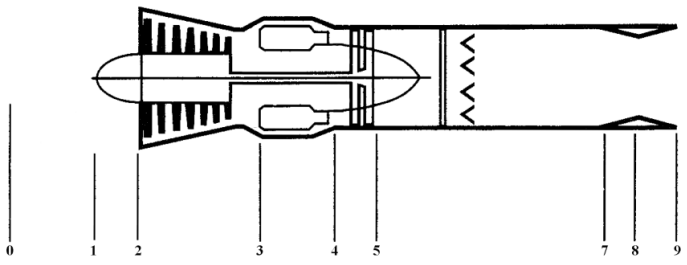

Figure C.2: Single spool turbojet scheme

Appendix D

The dual-spool turbojet

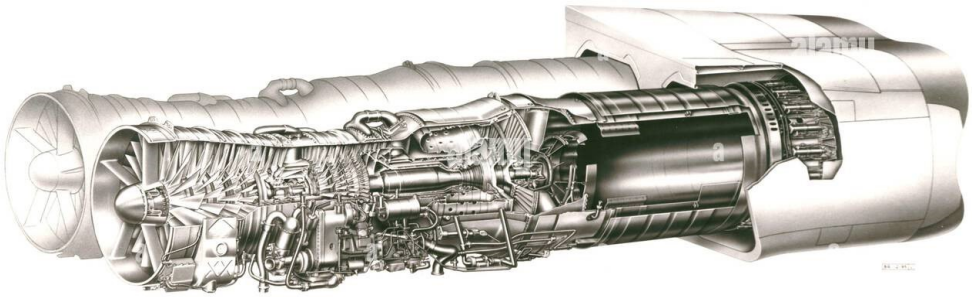

Figure D.1: The Olympus

In this section, the no afterburning dual-spool turbojet balancing equations, the related state vector, and the Jacobian matrix are reported, the procedure to find the solution of the non-linear system of equations is the same as the Turbofan Mixed flows described in Sec. 4.5. This particular engine is quite similar to the turbofan engine, however, the absence of the mixer and of the bypass change the balancing equations.

Referring to the engine scheme reported in Fig. D.2, the first balancing equation is related to the low-pressure shaft power balancing

$$\dot{m}_3(h_{t2.5} - h_{t2}) + P_{TOL}/\eta_{mPL} = \dot{m}_{4.5}(h_{t4.5} - h_{t5}) \cdot \eta_{mL} \tag{D.1}$$

The second refers to the high-pressure spool power balance

$$\dot{m}_3(h_{t3} - h_{t2.5}) + P_{TOH}/\eta_{mPH} = \dot{m}_{4.1}(h_{t4.1} - h_{t4.4}) \cdot \eta_{mH} \tag{D.2}$$

The third equation refers to the mass flow rate balance between the low-pressure compressor and the high-pressure one

$$\dot{m}_{c2} = \dot{m}_{c2.5} \frac{P_{t2.5}}{P_{t2}} \sqrt{\frac{T_{t2}}{T_{t2.5}}} \tag{D.3}$$

The fourth equation refers to the mass flow rate balance between the low-pressure turbine and the low-pressure compressor

$$\dot{m}_{c4.5} = \dot{m}_{c2} \cdot [(1 - \beta - \varepsilon_1 - \varepsilon_2)(1 + f) + \varepsilon_1 + \varepsilon_2] \sqrt{\frac{T_{t4.5}}{T_{t2}}} \cdot \frac{P_{t2.5}}{P_{t4.5}} \tag{D.4}$$

The fifth equation refers to the mass flow rate balance between the high-pressure compressor and the high-pressure turbine

$$\dot{m}_{c4.1} = \dot{m}_{c2.5} \cdot [(1 - \beta - \varepsilon_1 - \varepsilon_2)(1 + f) + \varepsilon_1] \cdot \sqrt{\frac{T_{t4.1}}{T_{t2.5}}} \cdot \frac{P_{t2.5}}{P_{t4.1}} \tag{D.5}$$

The last equation is related to the flow rate balance between the low-pressure turbine and nozzle

$$\dot{m}_{c4.5} = \dot{m}_{c8} \sqrt{\frac{T_{t4.5}}{T_{t8}}} \cdot \frac{P_{t8}}{P_{t4.5}} \tag{D.6}$$

The final system is

$$\vec{\mathbf{F}}(\vec{\mathbf{X}}) = \left\{ \begin{array}{c} \dot{m}_3(h_{t2.5} - h_{t2}) + P_{TOL}/\eta_{mPL} - \dot{m}_{4.5}(h_{t4.5} - h_{t5}) \cdot \eta_{mL} \\ \dot{m}_3(h_{t3} - h_{t2.5}) + P_{TOH}/\eta_{mPH} - \dot{m}_{4.1}(h_{t4.1} - h_{t4.4}) \cdot \eta_{mH} \\ \dot{m}_{c2} - \dot{m}_{c2.5} P_{t2.5}/P_{t2} \sqrt{T_{t2}/T_{t2.5}} \\ \dot{m}_{c4.5} - \dot{m}_{c2} \cdot [...] \sqrt{T_{t4.5}/T_{t2}} \cdot P_{t2.5}/P_{t4.5} \\ \dot{m}_{c4.1} - \dot{m}_{c2.5} \cdot [...] \cdot \sqrt{T_{t4.1}/T_{t2.5}} \cdot P_{t2.5}/P_{t4.1} \\ \dot{m}_{c4.5} - \dot{m}_{c8} \sqrt{T_{t4.5}/T_{t8}} \cdot P_{t8}/P_{t4.5} \end{array} \right\} = \vec{\mathbf{0}} \tag{D.7}$$

Thus the state vector is

$$\vec{\mathbf{X}} = \{\pi_{cL}, \pi_{cH}, \pi_{tL}, \pi_{tH}, (\%N_{cL}), (\%N_{cH})\}^T \tag{D.8}$$

The Jacobian is calculated as

$$\left[\frac{\partial F}{\partial X}\right] = \begin{Bmatrix} \frac{\partial f_1}{\partial \pi_{cL}} & \frac{\partial f_1}{\partial \pi_{cH}} & \frac{\partial f_1}{\partial \pi_{tL}} & \frac{\partial f_1}{\partial \pi_{tH}} & \frac{\partial f_1}{\partial (\%N_{cL})} & \frac{\partial f_1}{\partial (\%N_{cH})} \\ \frac{\partial f_2}{\partial \pi_{cL}} & \frac{\partial f_2}{\partial \pi_{cH}} & \frac{\partial f_2}{\partial \pi_{tL}} & \frac{\partial f_2}{\partial \pi_{tH}} & \frac{\partial f_2}{\partial (\%N_{cL})} & \frac{\partial f_2}{\partial (\%N_{cH})} \\ \frac{\partial f_3}{\partial \pi_{cL}} & \frac{\partial f_3}{\partial \pi_{cH}} & \frac{\partial f_3}{\partial \pi_{tL}} & \frac{\partial f_3}{\partial \pi_{tH}} & \frac{\partial f_3}{\partial (\%N_{cL})} & \frac{\partial f_3}{\partial (\%N_{cH})} \\ \frac{\partial f_4}{\partial \pi_{cL}} & \frac{\partial f_4}{\partial \pi_{cH}} & \frac{\partial f_4}{\partial \pi_{tL}} & \frac{\partial f_4}{\partial \pi_{tH}} & \frac{\partial f_4}{\partial (\%N_{cL})} & \frac{\partial f_4}{\partial (\%N_{cH})} \\ \frac{\partial f_5}{\partial \pi_{cL}} & \frac{\partial f_5}{\partial \pi_{cH}} & \frac{\partial f_5}{\partial \pi_{tL}} & \frac{\partial f_5}{\partial \pi_{tH}} & \frac{\partial f_5}{\partial (\%N_{cL})} & \frac{\partial f_5}{\partial (\%N_{cH})} \\ \frac{\partial f_6}{\partial \pi_{cL}} & \frac{\partial f_6}{\partial \pi_{cH}} & \frac{\partial f_6}{\partial \pi_{tL}} & \frac{\partial f_6}{\partial \pi_{tH}} & \frac{\partial f_6}{\partial (\%N_{cL})} & \frac{\partial f_6}{\partial (\%N_{cH})} \end{Bmatrix} \tag{D.9}$$

Finally, the residual vector is defined as

$$\vec{R} = \left[\frac{\pi_{cL}}{\pi_{cL,r}}, \frac{\pi_{cH}}{\pi_{cH,r}}, \frac{\pi_{tL}}{\pi_{tL,r}}, \frac{\pi_{tH}}{\pi_{tH,r}}, \frac{(\%N_{cL})}{(\%N_{cL}^r)}, \frac{(\%N_{cH})}{(\%N_{cH}^r)}\right]^T \tag{D.10}$$

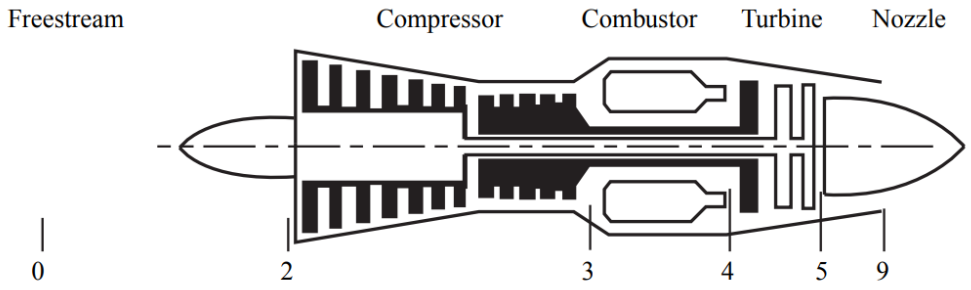

Figure D.2: The dual-spool turbojet scheme

Appendix E

The dual-spool Turbofan with Separated flows

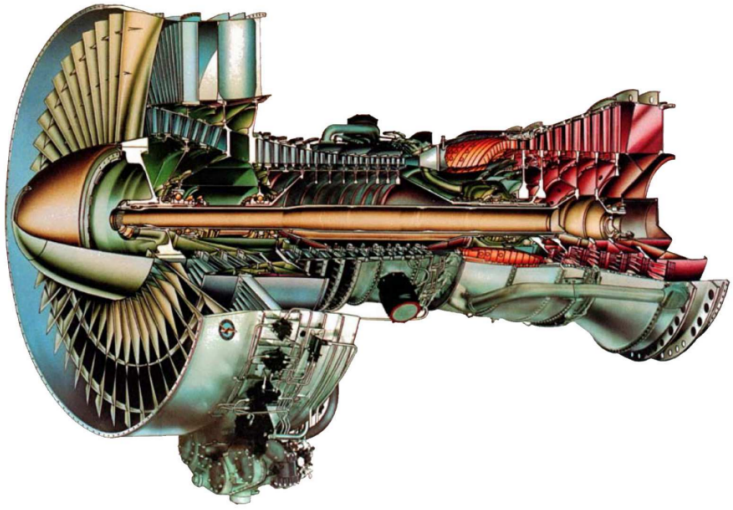

Figure E.1: The JT9D engine

In this section, the no dual-spool turbofan with separated exhausts balancing equations, the related state vector, and the Jacobian matrix are reported, the procedure to find the solution of the non-linear system of equations is the same as the Turbofan Mixed flows described in Sec. 4.5. This particular engine is quite similar to the turbofan engine, however, the absence of the mixer and of the

presence of two exhausts (cold and hot streams) change the balancing equations.

Referring to the engine scheme reported in Fig. E.2, the first balancing equation is related to the low-pressure shaft power balancing

$$\dot{m}_2(1+\alpha)(h_{t13}-h_{t2})+\dot{m}_2(h_{t2.5}-h_{t1.3})+P_{TOL}/\eta_{mPL}=\dot{m}_{4.5}(h_{t4.5}-h_{t5})\cdot\eta_{mL} \quad \text{(E.1)}$$

The second refers to the high-pressure spool power balance

$$\dot{m}_3(h_{t3}-h_{t2.5})+P_{TOH}/\eta_{mPH}=\dot{m}_{4.1}(h_{t4.1}-h_{t4.4})\cdot\eta_{mH} \quad \text{(E.2)}$$

The third equation refers to the mass flow rate balance between the low-pressure compressor and the high-pressure one

$$\dot{m}_{c2}=\dot{m}_{c2.5}(1+\alpha)\frac{P_{t2.5}}{P_{t2}}\sqrt{\frac{T_{t2}}{T_{t2.5}}} \quad \text{(E.3)}$$

The fourth equation refers to the mass flow rate balance between the low-pressure turbine and the low-pressure compressor

$$\dot{m}_{c4.1}=\dot{m}_{c2.5}\cdot[(1-\beta-\varepsilon_1-\varepsilon_2)(1+f)+\varepsilon_1+\varepsilon_2]\sqrt{\frac{T_{t4.5}}{T_{t2}}}\cdot\frac{P_{t2.5}}{P_{t4.5}}\cdot\frac{P_{t2.5}}{P_{t4.1}}\cdot\frac{T_{t4.1}}{T_{t2.5}} \quad \text{(E.4)}$$

The fifth equation refers to the mass flow rate balance between the

$$\dot{m}_{c4.5}=\dot{m}_{c2}\cdot\frac{[(1-\beta-\varepsilon_1-\varepsilon_2)(1+f)+\varepsilon_1+\varepsilon_2]}{(1+\alpha)}\sqrt{\frac{T_{t4.5}}{T_{t2}}}\cdot\frac{P_{t2.5}}{P_{t4.5}} \quad \text{(E.5)}$$

The sixth equation refers to the mass flow rate balance between the high-pressure compressor and the high-pressure turbine

$$\dot{m}_{c13}=\dot{m}_{c2}\cdot\frac{\alpha}{\alpha+1}\cdot\sqrt{\frac{T_{t13}}{T_{t2}}}\cdot\frac{P_{t2}}{P_{t13}} \quad \text{(E.6)}$$

The last equation is related to the flow rate balance between the low-pressure turbine and nozzle

$$\dot{m}_{c8}=\dot{m}_{c4.5}\cdot\sqrt{\frac{T_{t5}}{T_{t4.5}}}\cdot\frac{P_{t4.5}}{P_{t5}} \quad \text{(E.7)}$$

The final system is

$$\vec{\mathbf{F}}(\vec{\mathbf{X}}) = \left\{ \begin{array}{c} P_{cf} + P_{cL} + P_{TOL}/\eta_{mPL} - P_{tL} \cdot \eta_{mL} \\ P_{cH} + P_{TOH}/\eta_{mPH} - P_{tH} \cdot \eta_{mH} \\ \dot{m}_{c2} - \dot{m}_{c2.5}(1+\alpha) P_{t2.5}/P_{t2}\sqrt{T_{t2}/T_{t2.5}} \\ \dot{m}_{c4.1} - \dot{m}_{c2.5} \cdot [...]\sqrt{T_{t4.5}/T_{t2}} \cdot P_{t2.5}/P_{t4.5} \cdot P_{t2.5}/P_{t4.1} \cdot T_{t4.1}/T_{t2.5} \\ \dot{m}_{c4.5} - \dot{m}_{c2} \cdot [...]/(1+\alpha)\sqrt{T_{t4.5}/T_{t2}} \cdot P_{t2.5}/P_{t4.5} \\ \dot{m}_{c13} - \dot{m}_{c2} \cdot \alpha/(\alpha+1) \cdot \sqrt{T_{t13}/T_{t2}} \cdot P_{t2}/P_{t13} \\ \dot{m}_{c8} - \dot{m}_{c4.5} \cdot \sqrt{T_{t5}/T_{t4.5}} \cdot P_{t4.5}/P_{t5} \end{array} \right\} = \vec{\mathbf{0}} \tag{E.8}$$

Thus the state vector is

$$\vec{\mathbf{X}} = \{\pi_f, \pi_{cL}, \pi_{cH}, \pi_{tL}, \pi_{tH}, (\%N_{cL}), (\%N_{cH})\}^T \tag{E.9}$$

The Jacobian is calculated as

$$\left[\frac{\partial F}{\partial X}\right] = \left\{ \begin{array}{ccccccc} \frac{\partial f_1}{\partial \pi_f} & \frac{\partial f_1}{\partial \pi_{cL}} & \frac{\partial f_1}{\partial \pi_{cH}} & \frac{\partial f_1}{\partial \pi_{tL}} & \frac{\partial f_1}{\partial \pi_{tH}} & \frac{\partial f_1}{\partial (\%N_{cL})} & \frac{\partial f_1}{\partial (\%N_{cH})} \\ \frac{\partial f_2}{\partial \pi_f} & \frac{\partial f_2}{\partial \pi_{cL}} & \frac{\partial f_2}{\partial \pi_{cH}} & \frac{\partial f_2}{\partial \pi_{tL}} & \frac{\partial f_2}{\partial \pi_{tH}} & \frac{\partial f_2}{\partial (\%N_{cL})} & \frac{\partial f_2}{\partial (\%N_{cH})} \\ \frac{\partial f_3}{\partial \pi_f} & \frac{\partial f_3}{\partial \pi_{cL}} & \frac{\partial f_3}{\partial \pi_{cH}} & \frac{\partial f_3}{\partial \pi_{tL}} & \frac{\partial f_3}{\partial \pi_{tH}} & \frac{\partial f_3}{\partial (\%N_{cL})} & \frac{\partial f_3}{\partial (\%N_{cH})} \\ \frac{\partial f_4}{\partial \pi_f} & \frac{\partial f_4}{\partial \pi_{cL}} & \frac{\partial f_4}{\partial \pi_{cH}} & \frac{\partial f_4}{\partial \pi_{tL}} & \frac{\partial f_4}{\partial \pi_{tH}} & \frac{\partial f_4}{\partial (\%N_{cL})} & \frac{\partial f_4}{\partial (\%N_{cH})} \\ \frac{\partial f_5}{\partial \pi_f} & \frac{\partial f_5}{\partial \pi_{cL}} & \frac{\partial f_5}{\partial \pi_{cH}} & \frac{\partial f_5}{\partial \pi_{tL}} & \frac{\partial f_5}{\partial \pi_{tH}} & \frac{\partial f_5}{\partial (\%N_{cL})} & \frac{\partial f_5}{\partial (\%N_{cH})} \\ \frac{\partial f_6}{\partial \pi_f} & \frac{\partial f_6}{\partial \pi_{cL}} & \frac{\partial f_6}{\partial \pi_{cH}} & \frac{\partial f_6}{\partial \pi_{tL}} & \frac{\partial f_6}{\partial \pi_{tH}} & \frac{\partial f_6}{\partial (\%N_{cL})} & \frac{\partial f_6}{\partial (\%N_{cH})} \\ \frac{\partial f_7}{\partial \pi_f} & \frac{\partial f_7}{\partial \pi_{cL}} & \frac{\partial f_7}{\partial \pi_{cH}} & \frac{\partial f_7}{\partial \pi_{tL}} & \frac{\partial f_7}{\partial \pi_{tH}} & \frac{\partial f_7}{\partial (\%N_{cL})} & \frac{\partial f_7}{\partial (\%N_{cH})} \end{array} \right\} \tag{E.10}$$

Finally, the residual vector is defined as

$$\vec{R} = \left[\frac{\pi_f}{\pi_{f,r}}, \frac{\pi_{cL}}{\pi_{cL,r}}, \frac{\pi_{cH}}{\pi_{cH,r}}, \frac{\pi_{tL}}{\pi_{tL,r}}, \frac{\pi_{tH}}{\pi_{tH,r}}, \frac{(\%N_{cL})}{(\%N_{cL}^r)}, \frac{(\%N_{cH})}{(\%N_{cH}^r)}\right]^T \tag{E.11}$$

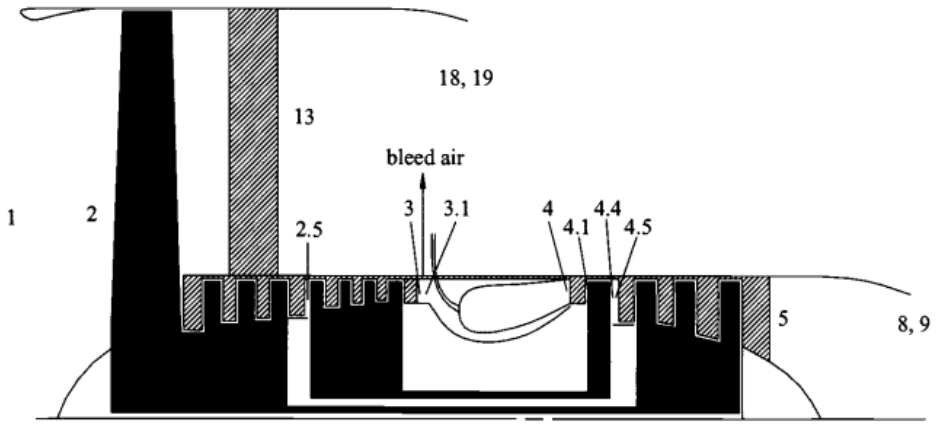

Figure E.2: The dual-spool Turbofan with separated flows scheme

Bibliography

[1] Egbert Torenbeek. *Essentials of supersonic commercial aircraft conceptual design*. John Wiley & Sons, 2020 (cit. on p. 3).

[2] J.D. Mattingly. *Aircraft Engine Design*. AIAA Education Series. American Institute of Aeronautics & Astronautics, 2002. ISBN: 9781600860164. URL: https://books.google.it/books?id=2Wy5rpdm3DMC (cit. on pp. 7, 8, 11, 13, 14, 32, 48, 49, 53, 55, 57, 59, 63, 70, 77, 78, 82, 93, 97).

[3] J Kurzke. *GasTurb 12-Design and Off-Design Performance of Gas Turbines-Manual*. 2014 (cit. on pp. 11, 38).

[4] GSP Development Team. *GSP11, User Manual*. National Aerospace Laboratory NLR Anthony Fokkerweg 2 1006 BM Amsterdam The Netherlands, September 2009. URL: https://www.gspteam.com/Files/manuals/UM/GSP_UM_11.pdf (cit. on pp. 11, 32, 108).

[5] Sanford Gordon and Bonnie J McBride. *Computer program for calculation of complex chemical equilibrium compositions and applications. Part 1: Analysis*. Tech. rep. 1994 (cit. on pp. 13, 88).

[6] J.D. Mattingly. *Elements of Gas Turbine Propulsion*. AIAA education series. American Institute of Aeronautics and Astronautics, 2005. ISBN: 9781563477782. URL: https://books.google.it/books?id=vA98AAAACAAJ (cit. on pp. 17, 30, 60, 63, 64, 77).

[7] Tarek Nada. «Performance characterization of different configurations of gas turbine engines». In: *Propulsion and Power Research* 3.3 (2014), pp. 121–132 (cit. on pp. 20, 21).

[8] J Mattingly and W Heiser. «Performance estimation of the mixed flow, afterburning, cooled, two-spool turbofan engine with bleed and power extraction». In: (1757), p. 1757 (cit. on p. 20).

[9] Gregorio Stiuso. «Tecnica di simulazione numerica delle prestazioni stazionarie e transitorie di turbomotori». MA thesis. Torino: Politecnico di Torino, 2019 (cit. on pp. 20, 63, 72, 75, 76).

[10] J. Kurzke and I. Halliwell. *Propulsion and Power: An Exploration of Gas Turbine Performance Modeling*. Springer International Publishing, 2018. ISBN: 9783319759791. URL: https://books.google.it/books?id=fL5dDwAAQBAJ (cit. on pp. 32, 49).

[11] Joachim Kurzke. *GasTurb 11, user manual*. 2007 (cit. on p. 32).

[12] Joachim Kurzke. «How to Get Component Maps for Aircraft Gas Turbine Performance Calculations». In: (1996). URL: https://api.semanticscholar.org/CorpusID:58614919 (cit. on pp. 32, 33).

[13] F Deidewig, A Döpelheuer, and M Lecht. «Methods to assess aircraft engine emissions in flight». In: *ICAS PROCEEDINGS*. Vol. 20. 1996, pp. 131–141 (cit. on p. 38).

[14] Dimitri Papamoschou and Marco Debiasi. «Conceptual development of quiet turbofan engines for supersonic aircraft». In: *Journal of propulsion and power* 19.2 (2003), pp. 161–169 (cit. on p. 63).

[15] Timo Schlette and Stephan Staudacher. «Preliminary Design and Analysis of Supersonic Business Jet Engines». In: *Aerospace* 9.9 (2022), p. 493 (cit. on pp. 66, 82).

[16] Renjun Qian, Benwei Li, Hanqiang Song, Qing Dong, and Yonghua Wang. «Aerodynamic Thermodynamic Modeling and Simulation of Turbofan Engine». In: 685.1 (2019), p. 012024 (cit. on pp. 72, 75).

[17] AJ Fawke and HIH Saravanamuttoo. «Digital computer simulation of the dynamic response of a twin-spool turbofan with mixed exhausts». In: *The Aeronautical Journal* 77.753 (1973), pp. 471–478 (cit. on pp. 72, 75).

[18] Aria Tahmasebi. «Turbofan Engine Modeling - For The Fighter Aircraft of The Future». MA thesis. Linköpings University | Department of Management and Engineering - 581 83 Linköping, Svezia: Linköpings University | Department of Management and Engineering, 2022 (cit. on p. 72).

[19] MATLAB. *version: 9.14.0.2239454 (R2023a) Update 1*. Natick, Massachusetts: The MathWorks Inc., 2023 (cit. on p. 76).

[20] Venedikt Kuz'michev, Ilia Krupenich, Evgeny Filinov, and Yaroslav Ostapyuk. «Comparative Analysis of Mathematical Models for Turbofan Engine Weight Estimation». In: *MATEC Web of Conferences*. Vol. 220. EDP Sciences. 2018, p. 03012 (cit. on p. 82).

[21] Noorakmal Noorashid and Nurul Musfirah Mazlan. «Computational Study of Biofuels Effect on Pressure and Temperature Changes Across Two-spool High Bypass Turbofan Engine Components at Various Engine Rotational Speeds». In: *Journal of Advanced Research in Fluid Mechanics and Thermal Sciences* 92.2 (2022), pp. 138–156 (cit. on p. 88).

[22] Riccardo Biasco. «Emissions analysis routine for subsonic aircrafts using biofuel». MA thesis. Torino: Politecnico di Torino, 2021 (cit. on p. 89).

[23] Bonnie J McBride. *Computer program for calculation of complex chemical equilibrium compositions and applications*. Vol. 2. NASA Lewis Research Center, 1996.

[24] Vivek Sanghi, BK Lakshmanan, and V Sundararajan. «Digital simulator for steady-state performance prediction of military turbofan engine». In: *Journal of Propulsion and Power* 14.1 (1998), pp. 74–81.

[25] Francesco Piccionello, Grazia Piccirillo, and Nicole Viola. «Performance Assessment of Low-By-Pass Turbofan Engines for Low-Boom Civil Supersonic Aircraf». In: *AIDAA XXVII Congress, Padua, 4-7 September 2023* (2023).

[26] Giacomo Richiardi. «Low-Boom Supersonic Business Jet: Aerodynamic Analysis and Mission Simulation towards a CO2 Emission Standard». MA thesis. Torino: Politecnico di Torino, 2023.

[27] USAF Ionio Q. Andrus Captain. «Comparative Analysis of a High Bypass Turbofan Using a Pulsed Detonation Combustor». MA thesis. AIR FORCE INSTITUTE OF TECHNOLOGY Wright-Patterson Air Force Base, Ohio: DEPARTMENT OF THE AIR FORCE AIR UNIVERSITY, 2007.

[28] Team DESIGN TOPIC 1. *DESIGN TOPIC 1: LOW BOOM SUPERSONIC BUSINESS JET*. Relazione tecnica. Politecnico di Torino, 2023.

[29] Dr. Chen Min Yingjun Guo Minghao 'I&' Hu Yu. *CJ-3000 Turbofan Engine Design Proposal*. Engine Request of Proposal. Beihang University, 2008.